

TY FORM 602

(ACCESSION NUMBER)

(THRU)

(PAGES)

83
NASA-CR-123580 SHUTTLE REENTRY
AERODYNAMIC HEATING TEST Interim Report,
1971 J.E. Pond, et al (Lockheed Missiles
and Space Co.) Dec. 1971 83 p CSCI 20M

N72-20928

Unclas
23894



Reproduced by
NATIONAL TECHNICAL
INFORMATION SERVICE
U S Department of Commerce
Springfield VA 22151

Lockheed

HUNTSVILLE RESEARCH & ENGINEERING CENTER

LOCKHEED MISSILES & SPACE COMPANY

A GROUP DIVISION OF LOCKHEED AIRCRAFT CORPORATION

HUNTSVILLE, ALABAMA

83 PE
80

LOCKHEED MISSILES & SPACE COMPANY
HUNTSVILLE RESEARCH & ENGINEERING CENTER
HUNTSVILLE RESEARCH PARK
4800 BRADFORD DRIVE, HUNTSVILLE, ALABAMA

SHUTTLE REENTRY AERODYNAMIC
HEATING TEST

INTERIM REPORT

December 1971

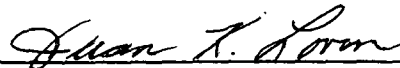
Contract NAS8-26359

Prepared for National Aeronautics and Space Administration
Marshall Space Flight Center, Alabama 35812

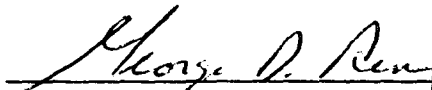
by

J. E. Pond
P. O. McCormick
S. D. Smith


APPROVED:



Juan K. Lovin, Supervisor
Thermal Environment Section



George D. Reny, Manager
Aeromechanics Dept.



for J. S. Farrior
Resident Director

FOREWORD

This Interim Report summarizes the results of work performed by Lockheed's Huntsville Research & Engineering Center, Inc., under Contract NAS8-26359, "Shuttle Reentry Aerodynamic Heating Tests," for the Aero-Astroynamics Laboratory of Marshall Space Flight Center during the 1971 calendar year. The NASA-MSFC technical monitor for this contract is Mr. J. Alan Forney, S&E-AERO-AT.

CONTENTS

Section		Page
	FOREWORD	ii
1	INTRODUCTION AND SUMMARY	1
2	AERODYNAMIC HEATING EXPERIMENTAL PROGRAMS	3
	2.1 Low Reynolds Number Windward Side Heating Test	3
	2.2 Base and Leeward Heating and High Reynolds Number Heating Test	4
	2.3 Results	10
3	ANALYTICAL TOOLS AND METHODOLOGY DEVELOPMENT	30
	3.1 Entropy Swallowing and Streamline Divergence by Semi-Empirical Methods	30
	3.2 Windward Side Aeroheating by Analytic Streamline Divergence	44
	3.3 Flight Environment from Data (FED)	48
	3.4 Thermal Environment Optimization Program (TEOP)	56
	3.5 A Small Thermal Analyzer with Simplified Input	58
4	APPLICATION OF ANALYTIC TOOLS TO PREDICTING THERMAL ENVIRONMENTS	62
	4.1 LOX-RP1 Trajectory Tradeoff Analysis	62
	4.2 Effects of Surface Radiation Interchange	69
	REFERENCES	78

Section 1
INTRODUCTION AND SUMMARY

During the past year Lockheed-Huntsville has conducted several studies, both experimental and analytical, that were directly involved with determining the Space Shuttle aerothermal environment. A large amount of this work has been documented in separate reports, however, a general discussion is presented herein. This discussion is grouped in three sections: (1) experimental work; (2) analytic development; and (3) application of analytic and test data in generating thermal environments.

The experimental work involved the fabrication of six Stycast models of the NASA-MSFC 437 Booster configuration and the subsequent testing of these models to determine the heating rates to be expected on the windward side, leeward side and on the base region. Some of the results of the oilflow data from these tests were used in the entropy swallowing analysis to define the streamline patterns. Utilizing these oilflow data, a series of centerline heating rates was calculated. These data were compared to the data that were taken by Lockheed-Huntsville. The success of this semi-empirical technique prompted an investigation of theoretical methods for predicting streamline divergence. The analytic technique also produced impressive results.

One of the most rewarding tasks undertaken under this contract was the development of the Thermal Environment Optimization Program (to be documented) which in one computer run, calculates the heating rate and sizes the thermal protection system (TPS) for a given configuration. This program has found many applications and has proved to be a valuable design and trade study tool. The basic technique for calculating the aerodynamic heating for this program was devised separately and is documented as the Flight Environment from Data (FED) Program (Ref. 1).

With the many and varied requirements for a thermal analyzer program within the scope of thermal environment prediction, a small thermal analyzer was written that suited the particular needs of predicting the thermal environment. This program (whose primary advantage is its simplicity) has found many applications, which are discussed later. One of the most important uses of the thermal analyzer is in the TEOP program.

In summary, there has been a wide variety of work performed under this contract during the last year: From manufacturing thermal test models to analytical prediction of streamline divergence; from developing a huge and complex TPS sizing program to writing a small, simple thermal analyzer. The tools and techniques that were developed were also used in producing thermal environments and TPS weights in response to the need of the NASA-MSFC Contracting Officer's Representative.

Section 2

AERODYNAMIC HEATING EXPERIMENTAL PROGRAMS

During the past year two major aerodynamic heating tests were conducted in which phase change paint techniques were used. Both tests were conducted at Langley Research Center, Hampton, Virginia. Their purpose was to help define the aerothermal environment about the then-current NASA-MSFC Space Shuttle booster configuration. The detailed results of these tests are presented in Refs. 2 and 3 and only a token representation of the data obtained is contained in this report.

2.1 LOW REYNOLDS NUMBER WINDWARD SIDE HEATING TEST

Heat transfer tests were performed on the NASA-MSFC Space Shuttle booster configuration in the Hypersonic Continuous Flow Tunnel at Langley Research Center. The test results are contained in Ref. 2. The tests were conducted at a nominal Mach number of 10 with the freestream unit Reynolds number approximately 1 million per foot. Heat transfer data were obtained by coating 0.0035-scale plastic models of the MSFC booster with a material which melts at a known temperature and recording the phase-change patterns on movie film. Data reduction consisted of measuring the time required for the surface to reach a known temperature as indicated by the phase change and calculating the corresponding heat transfer rates by the semi-infinite slab transient heat conduction equation. This technique was developed by Langley and is used by several facilities.

Flow visualization data were obtained by the oilflow technique. Various mixtures of silicone oil and zinc oxide were used to obtain oilflow patterns at all angles of attack. Black and white still photographs were made showing top, bottom and side patterns.

The MSFC booster heat transfer models were fabricated in the laboratory facilities at Lockheed's Huntsville Research & Engineering Center at Huntsville, Alabama. Two identical test models and one set-up model were made from Stycast, a 600°F castable plastic. Detachable sting adapters were made for 0, 30 and 55 degrees. These models and adapters are shown in Fig. 1. Each model was instrumented with two chromel-alumel thermocouples imbedded at a depth of 1/8 inch below the surface for monitoring the model temperature before each run. Figure 2 shows an example of the data obtained during this test. The lines on Fig. 2 are lines of constant heating rate and the values assigned to the lines are the corresponding ratios of local film coefficient to the film coefficient at the stagnation point of a one-foot radius sphere scaled down to model dimensions. The bottom centerline film coefficient ratios are shown in Fig. 3 as a function of body station for all angles of attack tested. As anticipated, the entire bottom centerline remained laminar for all angles of attack listed.

Typical results of the oilflow visualization tests are shown in Figs. 4 and 5. These flow visualization data contributed significantly to a later analysis of entropy swallowing. They are presented in more detail in Section 3.1.

2.2 BASE AND LEEWARD HEATING AND HIGH REYNOLDS NUMBER HEATING TEST

Heat transfer tests were performed on the NASA-MSFC Space Shuttle booster configuration in the Mach 8 Variable Density Tunnel at Langley Research Center. These tests were conducted at a nominal Mach number of 8 with the freestream unit Reynolds number varying from 0.60 to 6.2 million per foot. Heat transfer data were obtained by coating 0.0035-scale plastic models of the MSFC booster with a material which melts at a known temperature and recording the phase-change patterns on movie film. The results of this test are documented in detail in Ref. 3.

Flow visualization data were obtained by the oilflow technique. Various mixtures of 60-weight motor oil, STP oil treatment, and zinc oxide were used

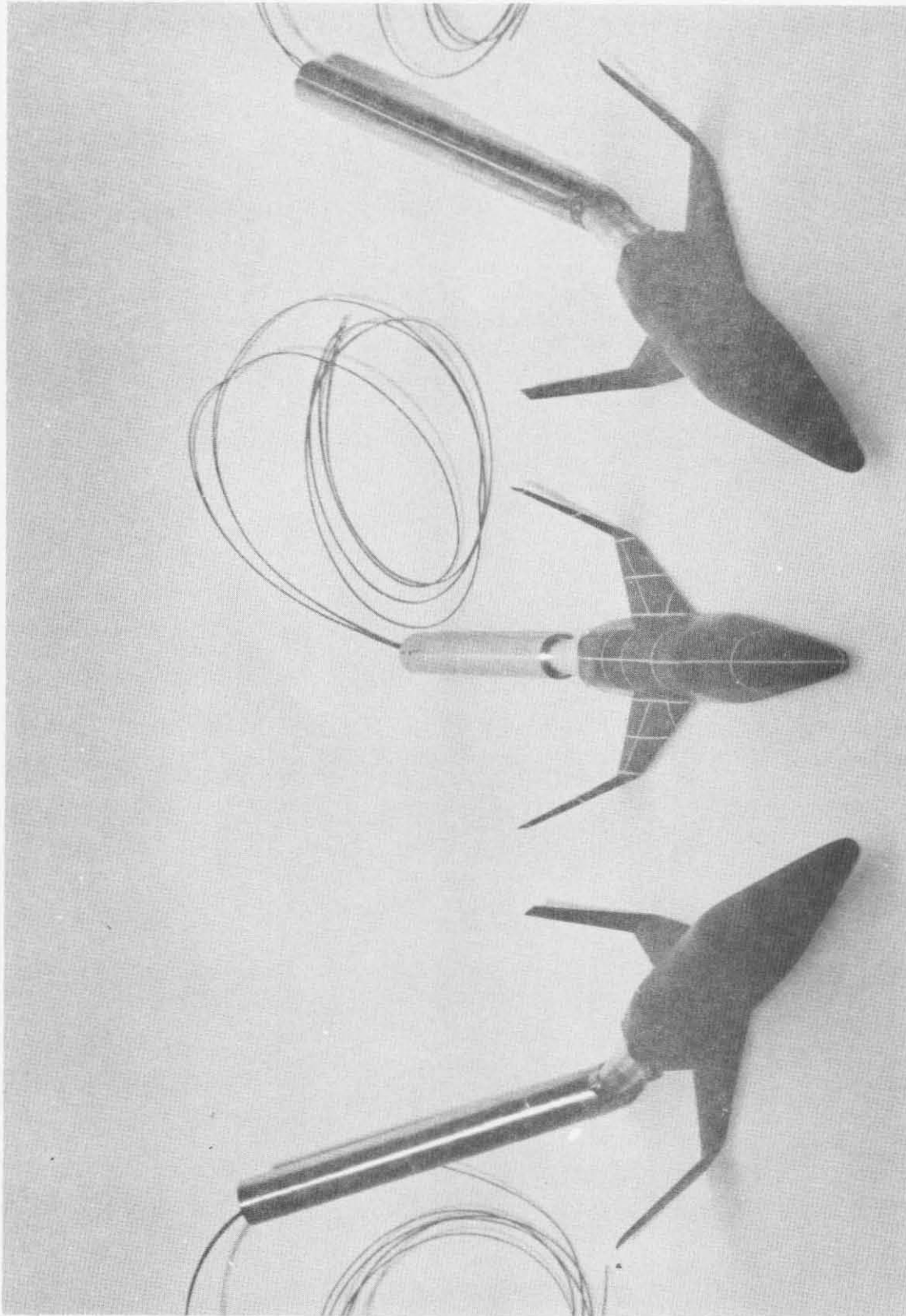


Fig. 1 - NASA-MSFC Booster Test Models

Run 1 Bottom View
 Alpha = 55° $T_{pc} = 350^{\circ}\text{F}$
 $R_n = 1.18 \times 10^6$

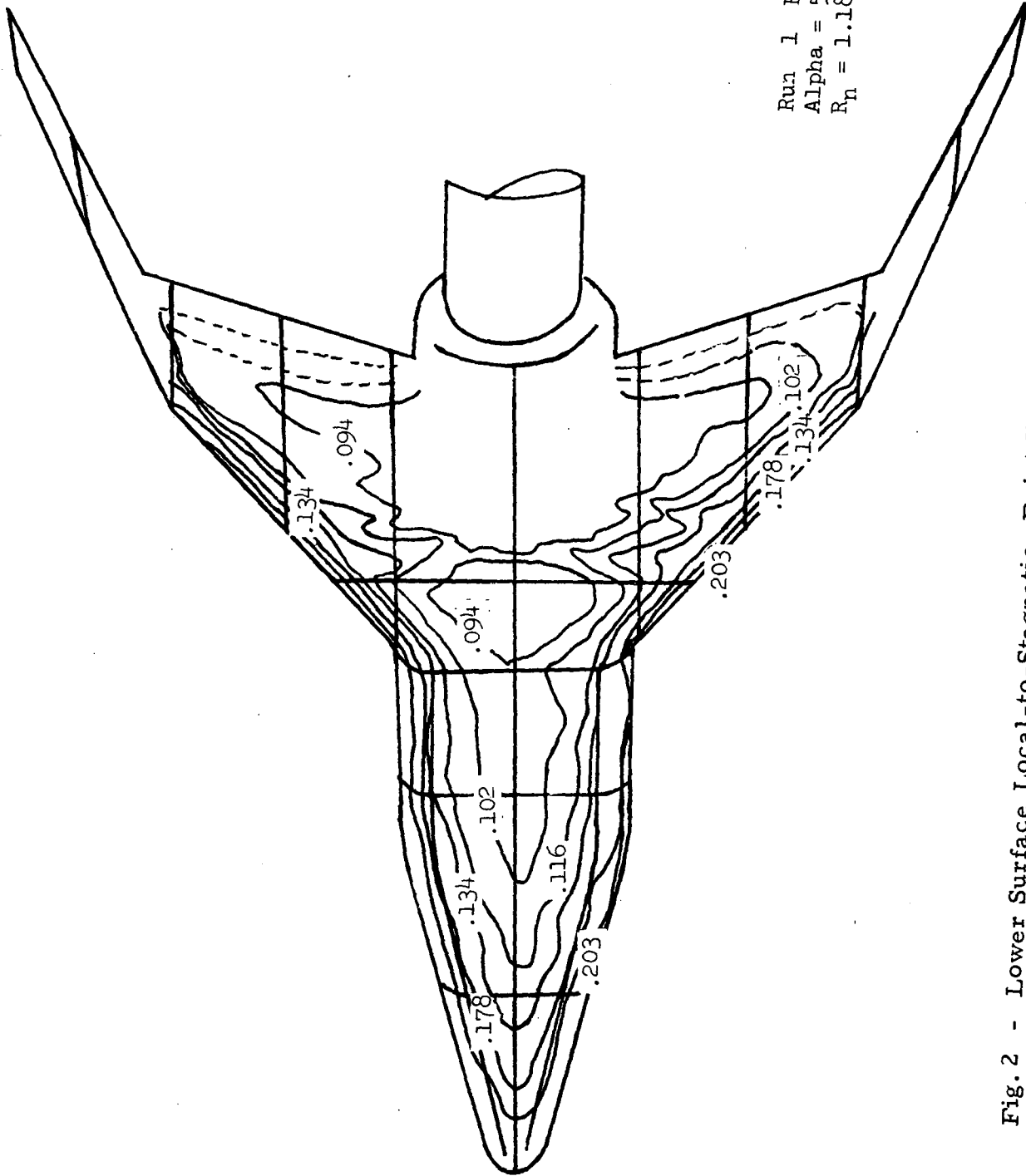


Fig. 2 - Lower Surface Local-to-Stagnation Point Heat Transfer Coefficients

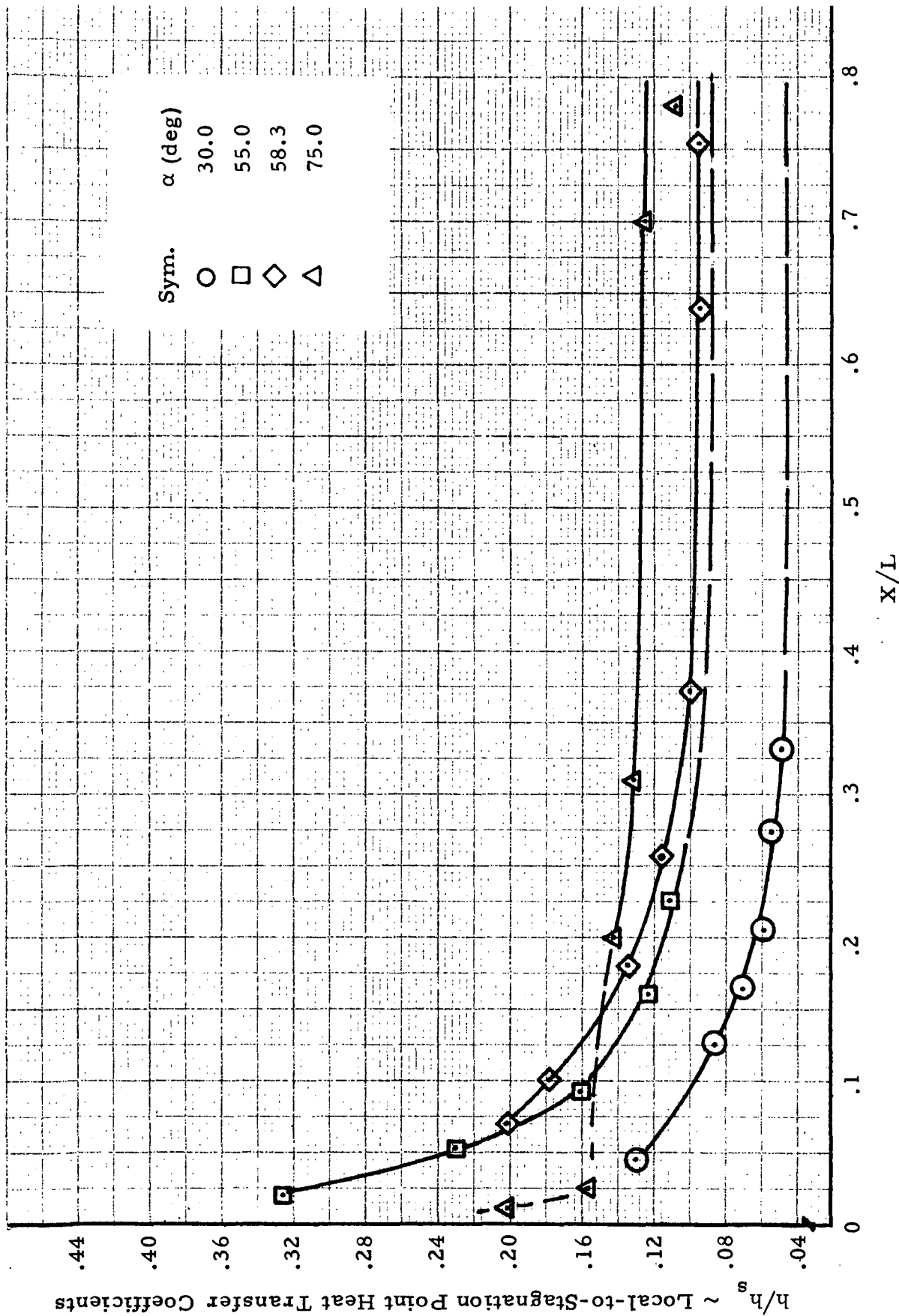


Fig. 3 - Bottom Center Line Local-to-Stagnation Point Heat Transfer Coefficients

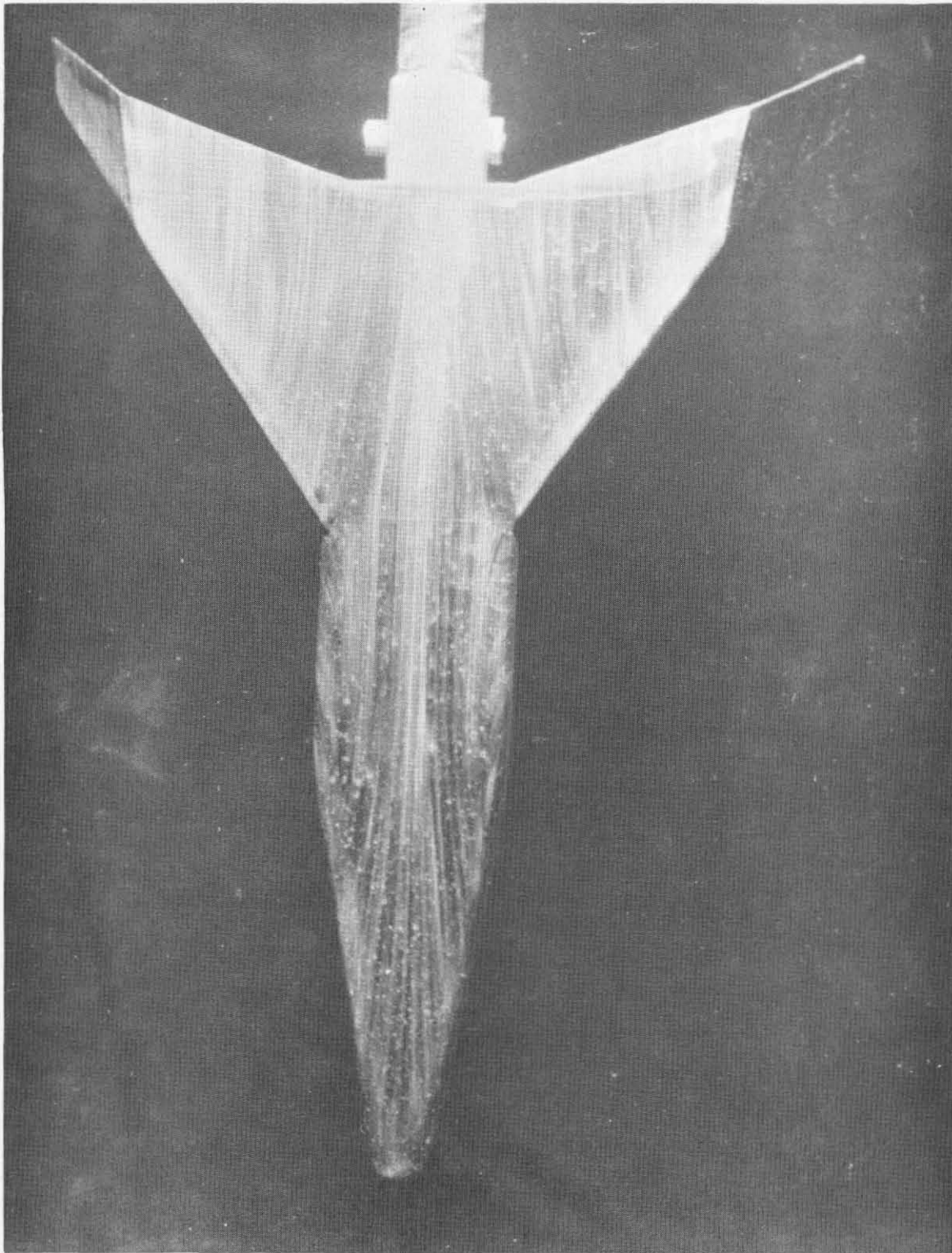


Fig. 4 - Oilflow Visualization for Bottom View at $\text{Alpha} = 10 \text{ deg}$

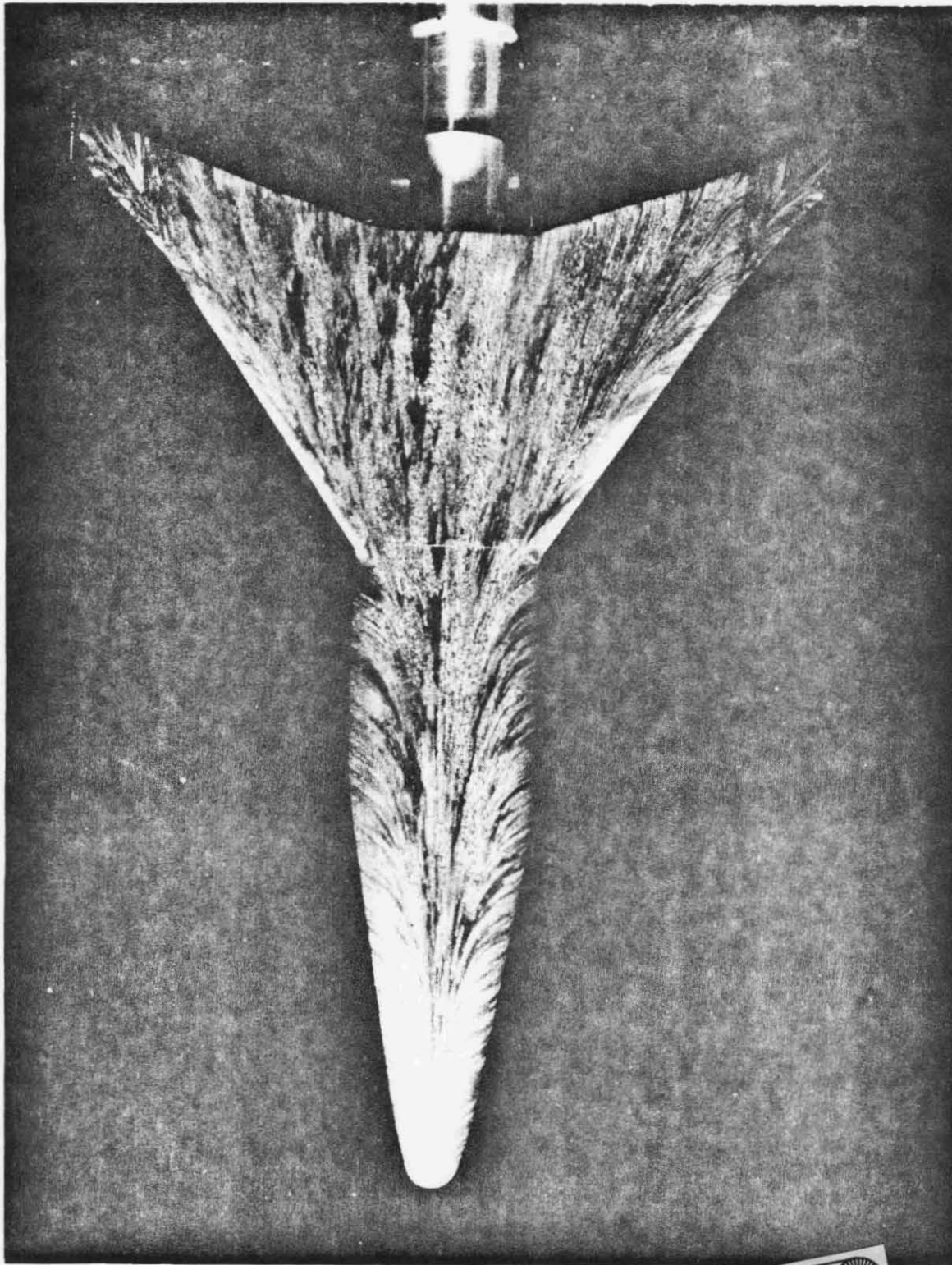


Fig. 5 - Oilflow Visualization for Bottom View at $\text{Alpha} = 55^\circ$

to obtain oilflow patterns at various angles of attack and Reynolds numbers. Black and white photographs were made showing windward (bottom) side patterns. Also schlieren photographs were taken for a number of runs.

The MSFC booster heat transfer models were fabricated at Lockheed's Huntsville Research & Engineering Center, Inc., at Huntsville, Alabama. Three models previously fabricated and tested (Ref. 2) were used in these tests. These models were used only for a limited number of runs at 45 and 55-degree angles of attack. Three additional models were fabricated with adjustable top sting mounts. The models were identical except for the base regions. Figure 6 shows the TSJ (top-mounted sting-engine nozzle attached) model with simulated rocket nozzles in the base region. The McDonnell Douglas straight wing orbiter nozzle designs were used for fabrication and placement of engines and test models. This model was used as a grid to provide vehicle surface locations during most of the tests. The grid was then removed and the model tested. Figure 7 shows the top-mounted sting-hole in base) (TSH) model with a 0.720-inch diameter hole, 0.25-inch deep, located in the base region. The center of the hole was located 0.60 inches from the base lip.

Figure 8 shows the top-mounted sting-smooth base (TBS) model with a clean base region and thickened wings and fins. This model was fabricated so as to validate all semi-infinite slab assumptions for data reduction.

2.3 RESULTS

Through use of a Telereadax machine at NASA-MSFC, melt contours of all runs were drawn. Each contour represents an isotherm of constant heat transfer coefficient. These data were presented as ratios of local heat transfer to the spherical stagnation point heat transfer coefficient based on the stagnation conditions for that run using a nose radius of 1 ft scaled to 0.0035 ft.

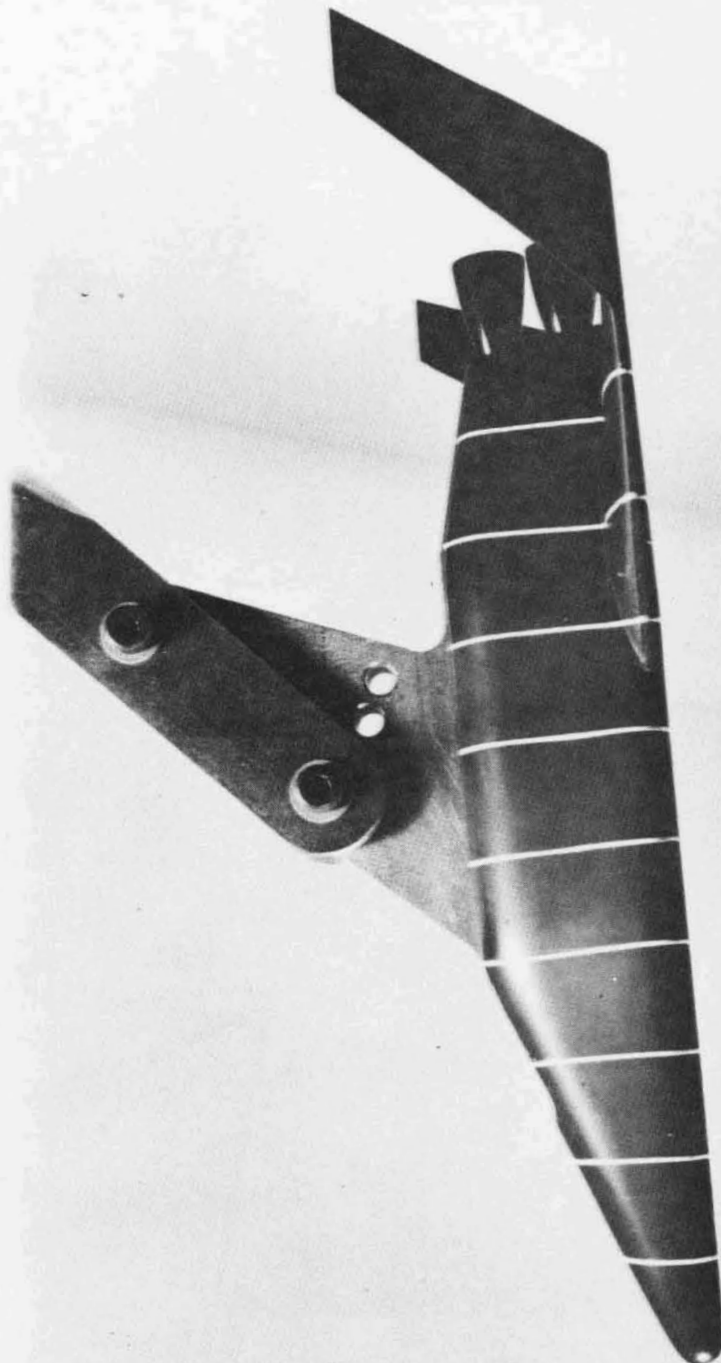


Fig. 6 - NASA-MSFC Booster Stycast TSJ Model

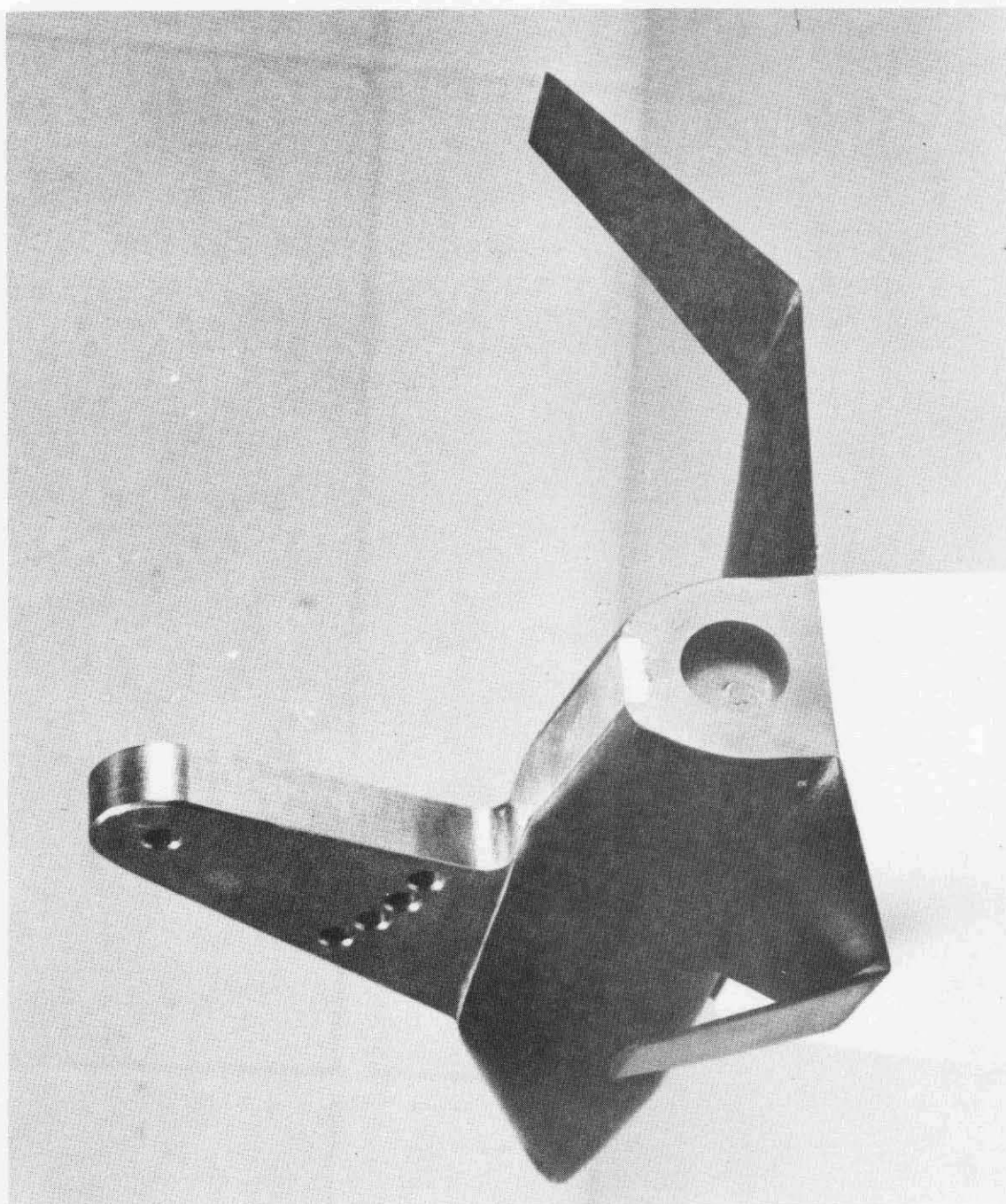


Fig. 7 - NASA-MSFC Booster Stycast TSH Model

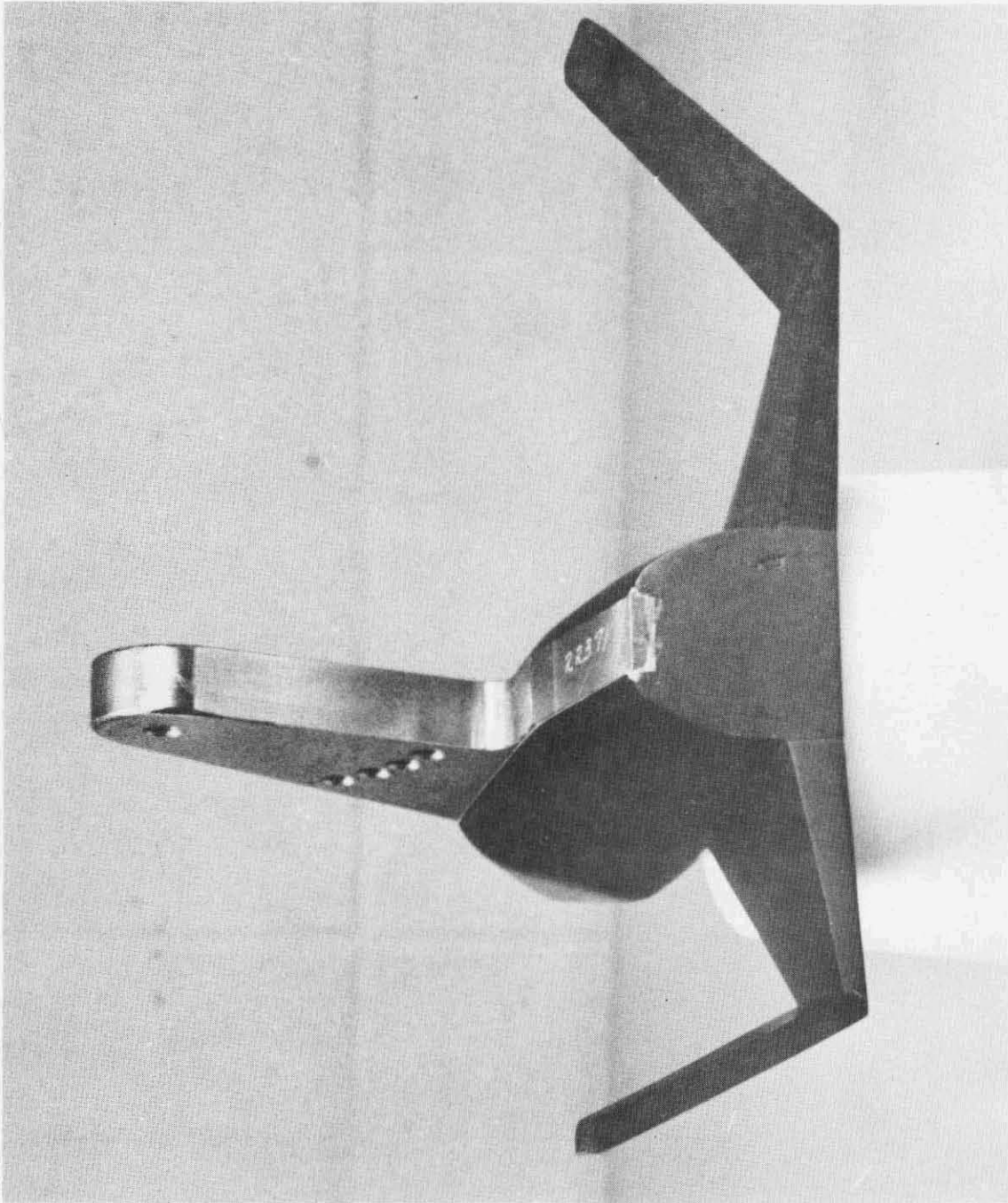


Fig.8 - NASA-MSFC Booster Stycast TSB Model

Figures 9, 10 and 11 show representations of heating data on the three different base configurations. Figure 12 shows some of the results of the leeward heating tests. Run conditions used to reduce each set of data are presented in the table on the right of each figure.

Figure 13 presents an average base heating value for the TSH model over a range of angles of attack and Reynolds number. These numbers were taken from those figures where actual melting due to convective heating is evident. Contours in the model base regions as shown in Figs. 9 through 11 are not necessarily due to convection, indeed most are due to conduction. The heating rates were very low in the base region and test times were prolonged in attempts to obtain the desired data.

Figures 14 and 15 present centerline distributions for two different Reynolds numbers. A preliminary evaluation of the data presented indicates that the models were too large at these high angles of attack for the low Reynolds number cases. The tunnel test core increases with Reynolds number from approximately 5 to 10 inches in diameter. Therefore, it is possible that the nosetips of the models were submerged in the tunnel boundary layer and produced incorrect data.

Selected off-centerline data are shown in Figs. 16 and 17 for two different angles of attack. The shape of the body at this station is typical of many orbiter and booster configurations. Note that on the sides of the vehicle the heat transfer coefficients were practically independent of Reynolds number (with the exception of the 1 million per foot case which is suspected of being in the tunnel boundary layer) and Mach number indicating that the heating in such separated regions is, in general, independent of the centerline heating.

Very good oilflow and schlieren photographs were obtained during this test. Several of these photographs are presented in Figs. 18 through 23.

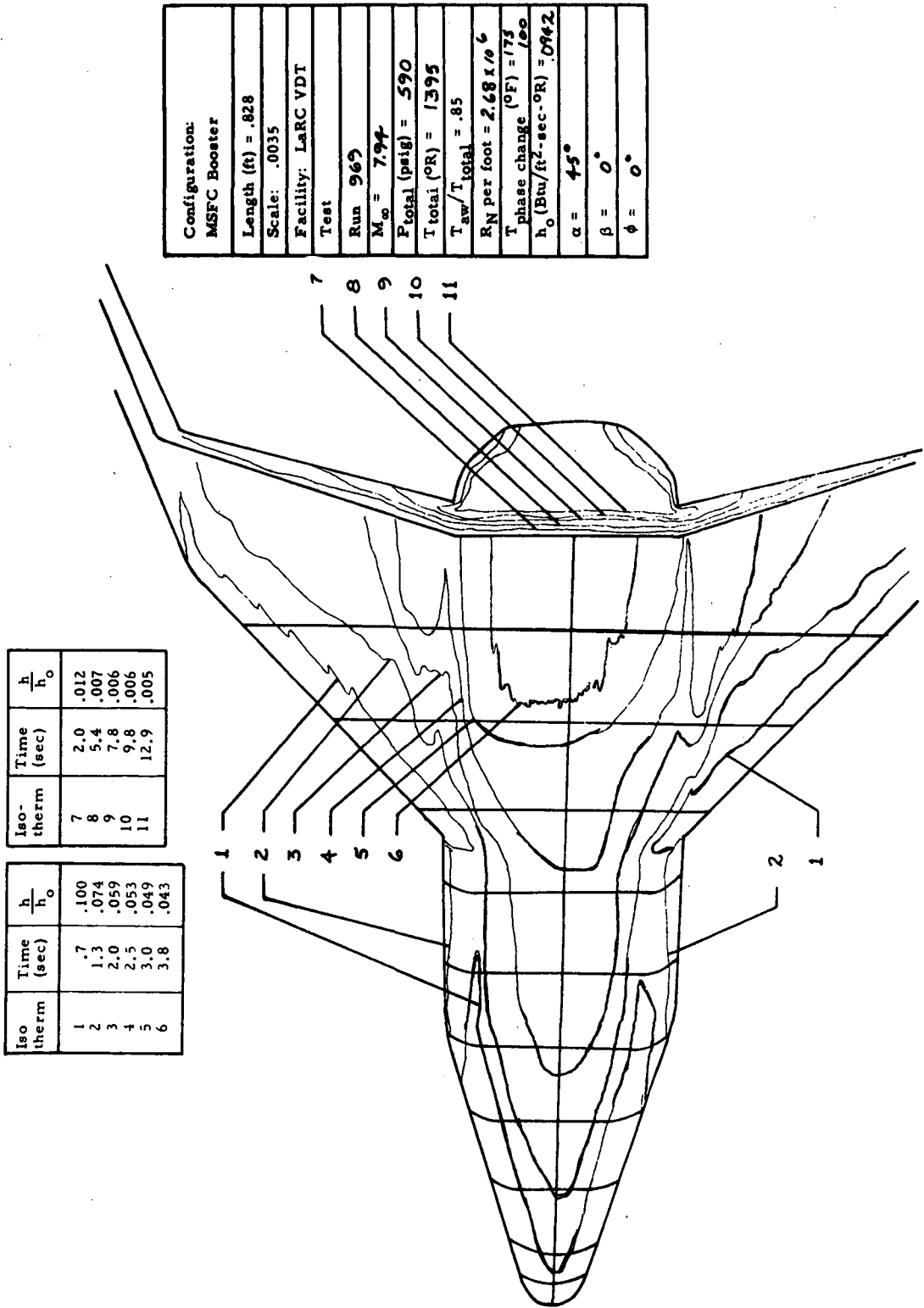
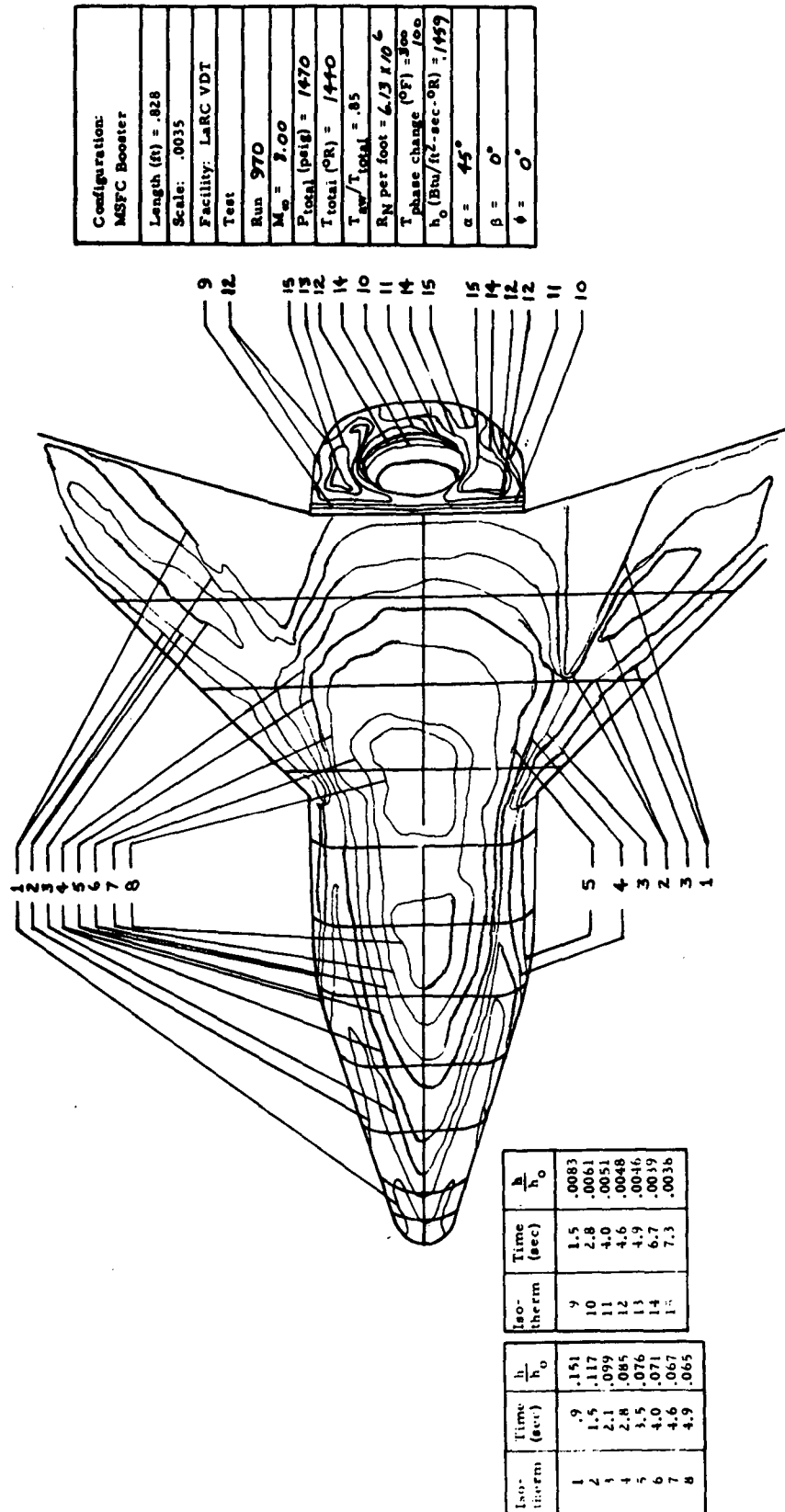
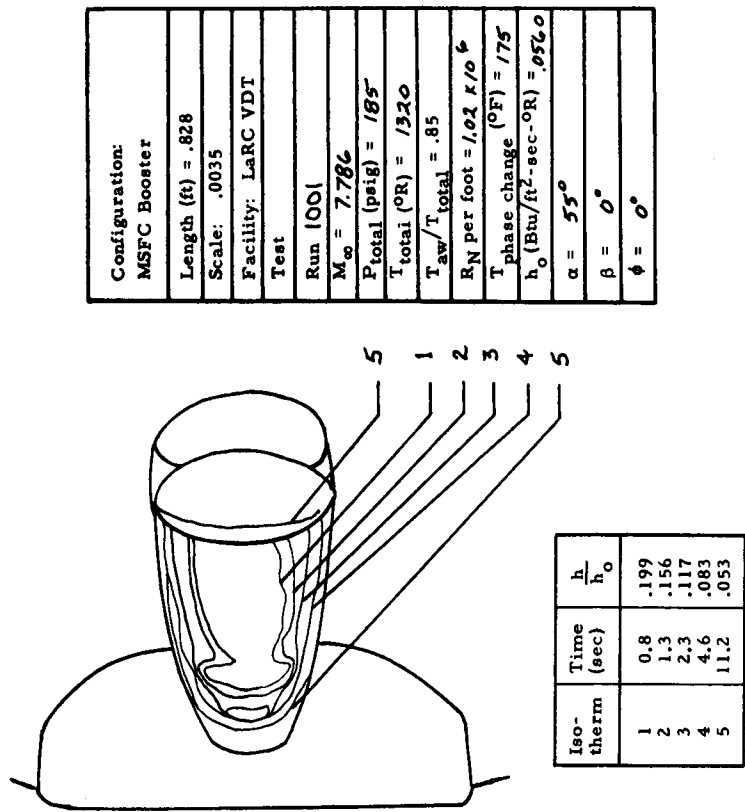


Fig. 9 - Lower Surface Local to Stagnation Point Heat Transfer Coefficient for Run 969



Configuration:	MSFC Booster
Length (ft)	.828
Scale:	.0035
Facility:	LARC VDT
Test:	
Run	970
M_∞	3.00
P_{Total} (psig)	1470
T_{Total} (°R)	1440
$T_{\text{aw}}/T_{\text{Total}}$.85
RN per foot	6.13 K/ft
$T_{\text{Phase change}}$ (°F)	300
h_0 (Btu/ft ² -sec-°R)	100
h_0 (Btu/ft ² -sec-°R)	1459
α	45°
β	0°
ϕ	0°

Fig. 10 - Lower Surface Local to Stagnation Point Heat Transfer Coefficients for Run 970 (Ref. 5)



Configuration: MSFC Booster
Length (ft) = .828
Scale: .0035
Facility: LaRC VDT
Test
Run 1001
$M_{\infty} = 7.786$
$P_{total} (psig) = 185$
$T_{total} (^{\circ}R) = 1320$
$T_{aw}/T_{total} = .85$
R_N per foot = 1.02×10^6
T phase change ($^{\circ}F$) = 175
h_o (Btu/ft ² -sec- $^{\circ}R$) = $.0560$
$\alpha = 55^{\circ}$
$\beta = 0^{\circ}$
$\phi = 0^{\circ}$

Fig. 11 - Engine Surface Local to Stagnation Point Heat Transfer Coefficients for Run 1001

Configuration: MSFC Booster
Length (ft) = .828
Scale: .0035
Facility: LaRC VDT
Test
Run 1008
$M_\infty = 9.00$
$P_{\text{total}} (\text{psig}) = 1450$
$T_{\text{total}} (^{\circ}\text{R}) = 1430$
$T_{\text{aw}}/T_{\text{total}} = .85$
$R_N \text{ per foot} = 6.12 \times 10^6$
$T \text{ phase change } (^{\circ}\text{F}) = 100$
$h_o (\text{Btu/ft}^2\text{-sec-}^{\circ}\text{R}) = .1447$
$\alpha = 45^{\circ}$
$\beta = 0^{\circ}$
$\phi = 0^{\circ}$

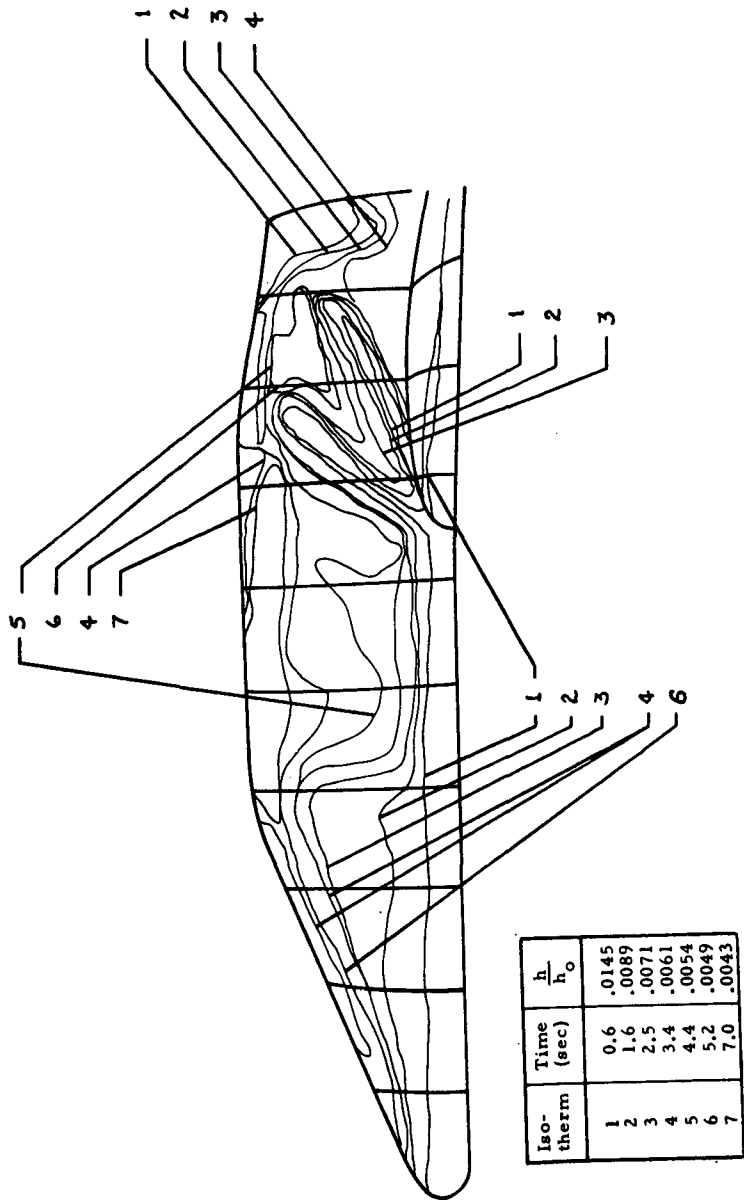


Fig. 12 - Side Panel Local to Stagnation Point Heat Transfer Coefficients for Run 1008

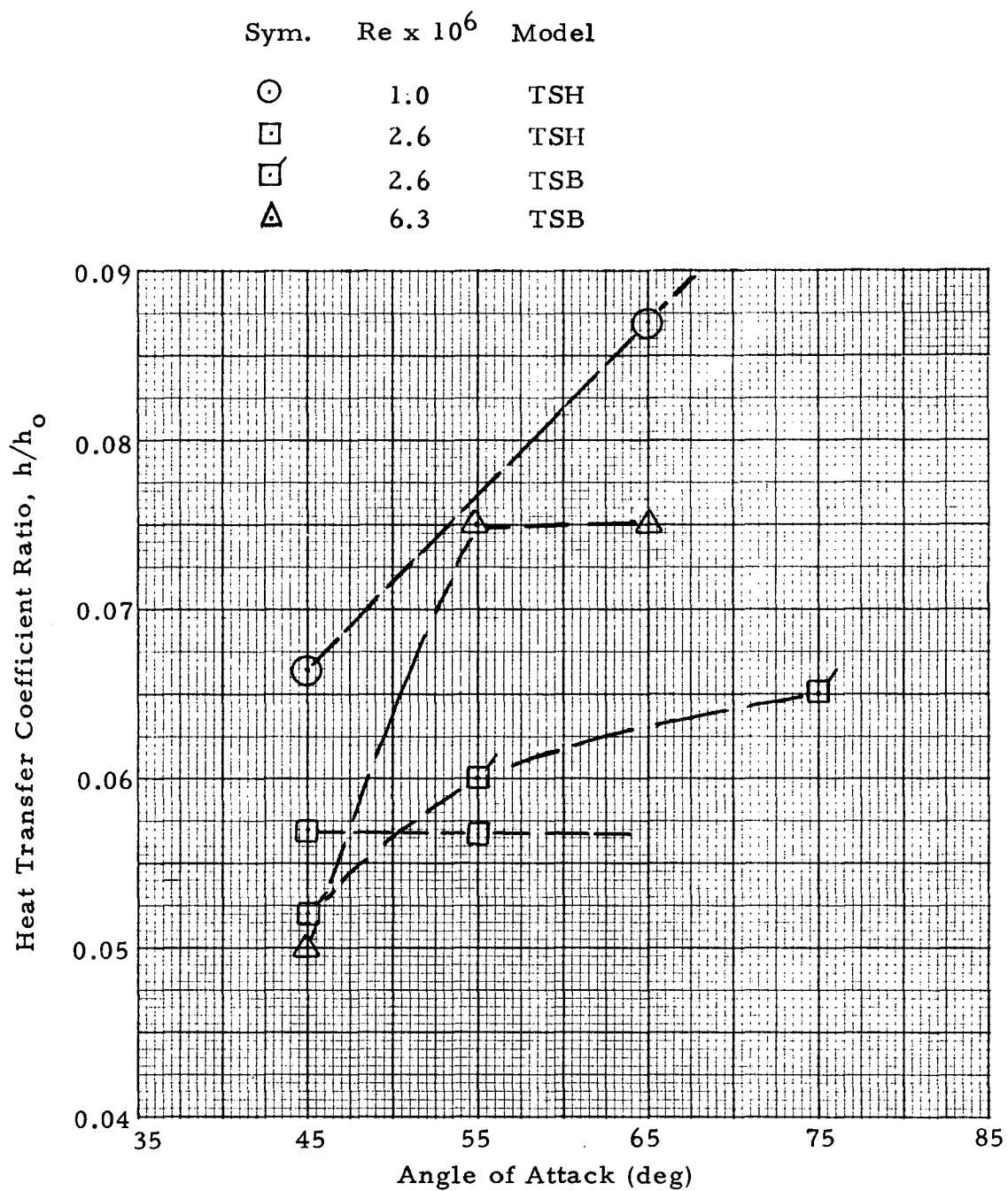


Fig. 13 - Average Base Heating as a Function of Reynolds Number and Angle of Attack

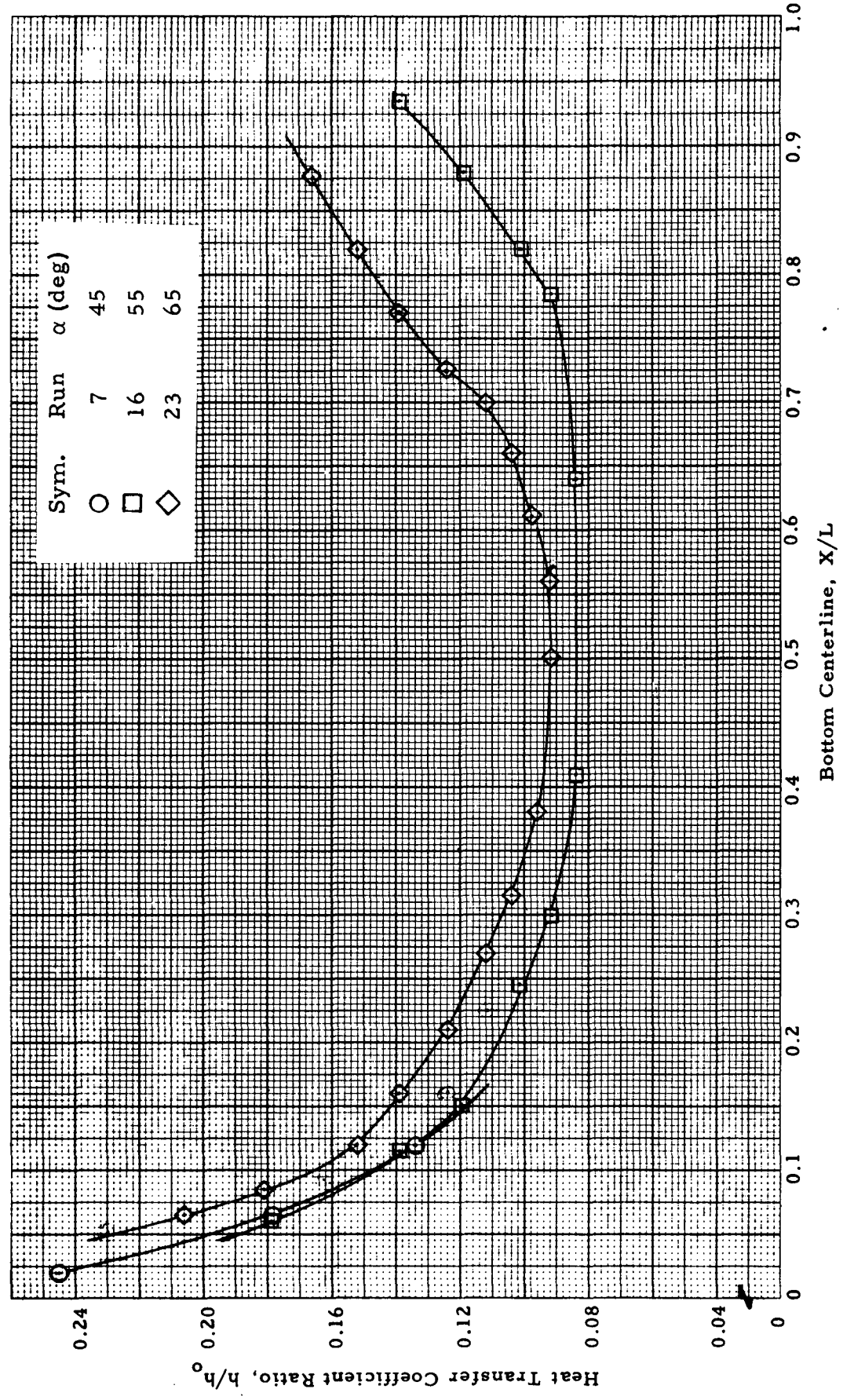


Fig. 14 - Bottom Centerline Heat Transfer Distribution for Angle of Attack Variation at a Reynolds Number $\approx 6.3 \times 10^6$, TSB Model

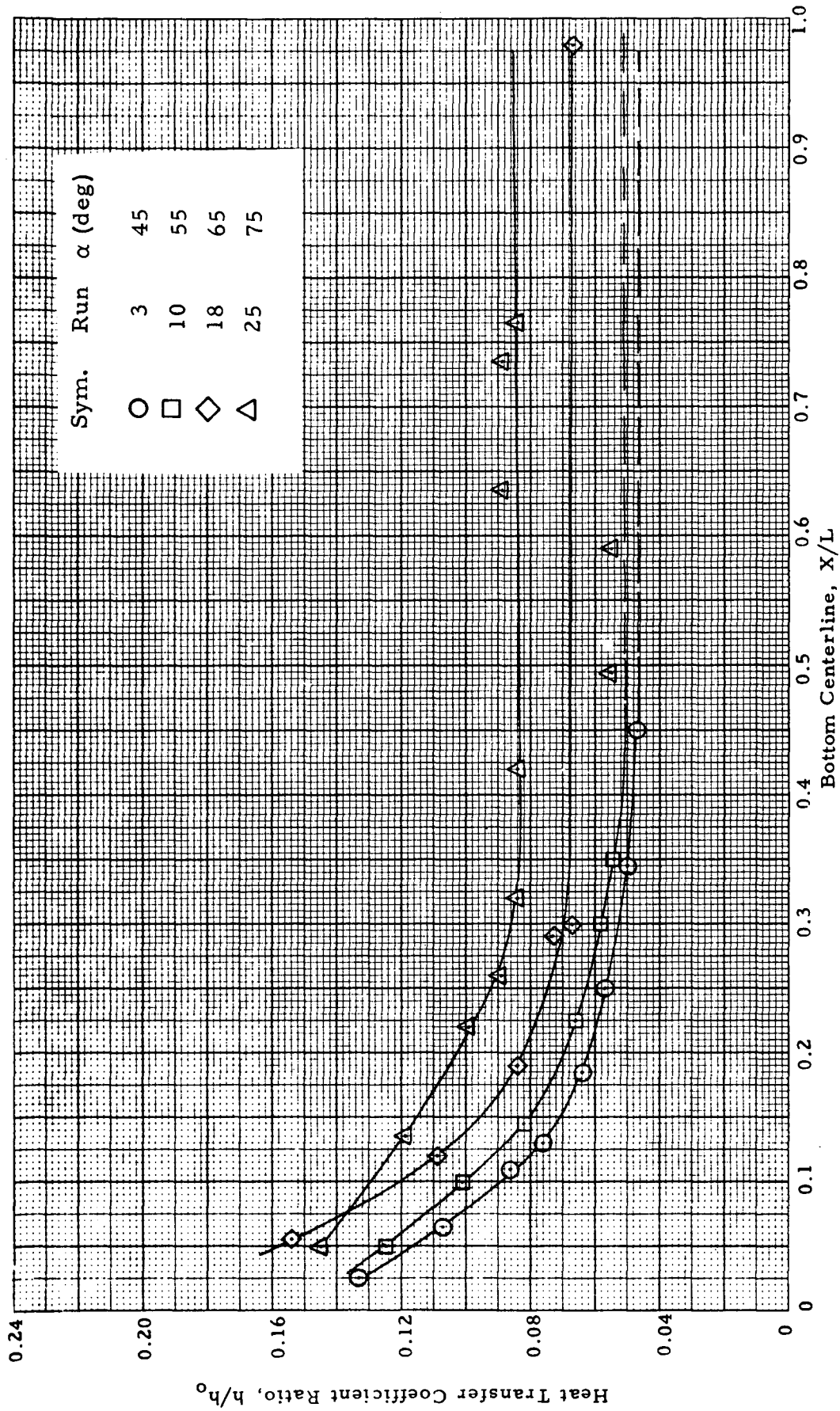


Fig. 15 - Bottom Centerline Heat Transfer Distribution for Angle of Attack Variation at a Reynolds Number $\approx 1.05 \times 10^6$, TSH Model

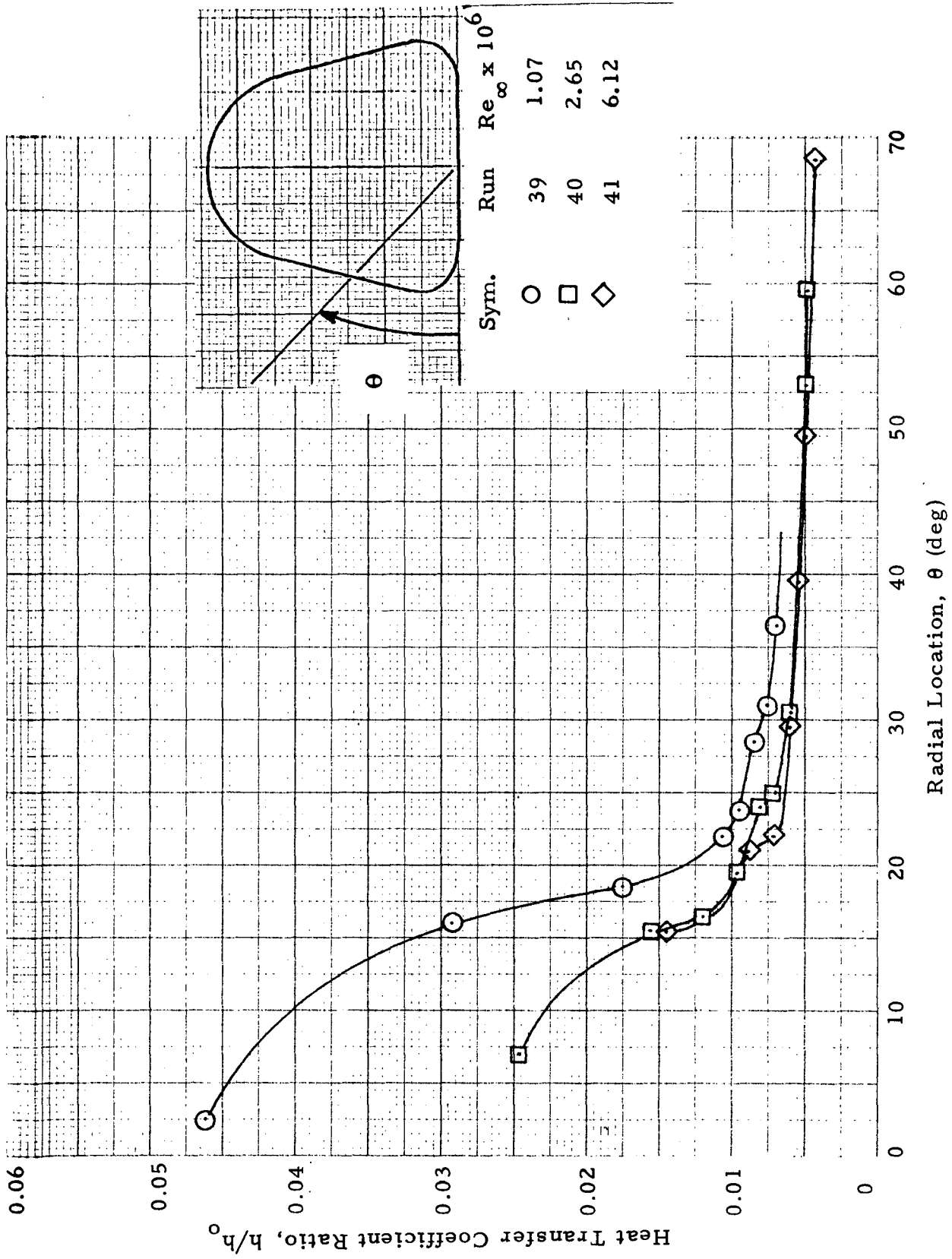


Fig. 16 - Side Panel Heat Transfer Distribution at Body Location $X/L = 0.5$ and Angle of Attack = 45 Degrees

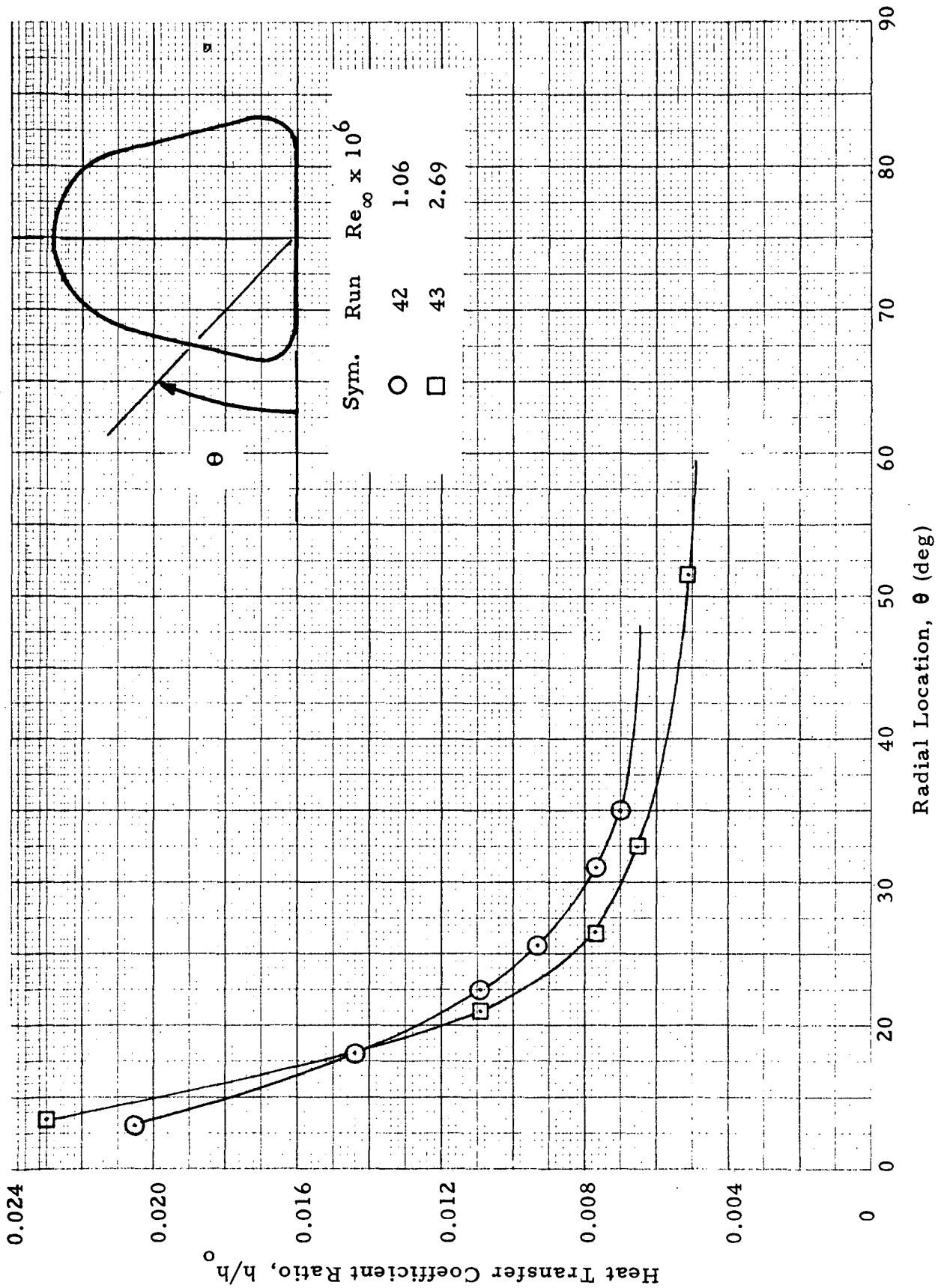


Fig. 17 - Side Panel Heat Transfer Distribution at Body Location $X/L = 0.5$ and Angle of Attack = 55

Reproduced from
best available copy.

1024

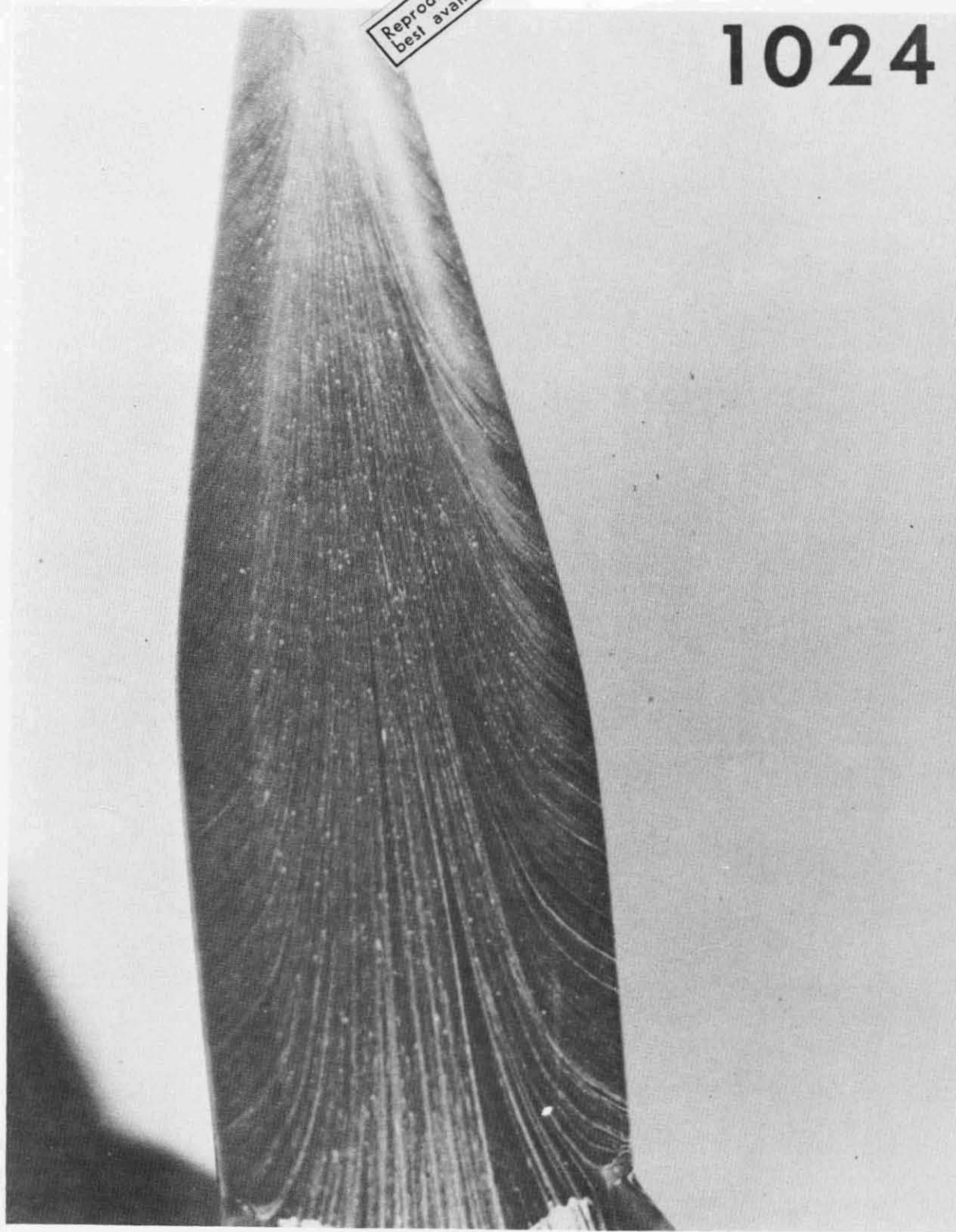


Fig. 18 - Oilflow Visualization for $\alpha = 45$ Degrees, $Re/ft = 2.7 \times 10^6$

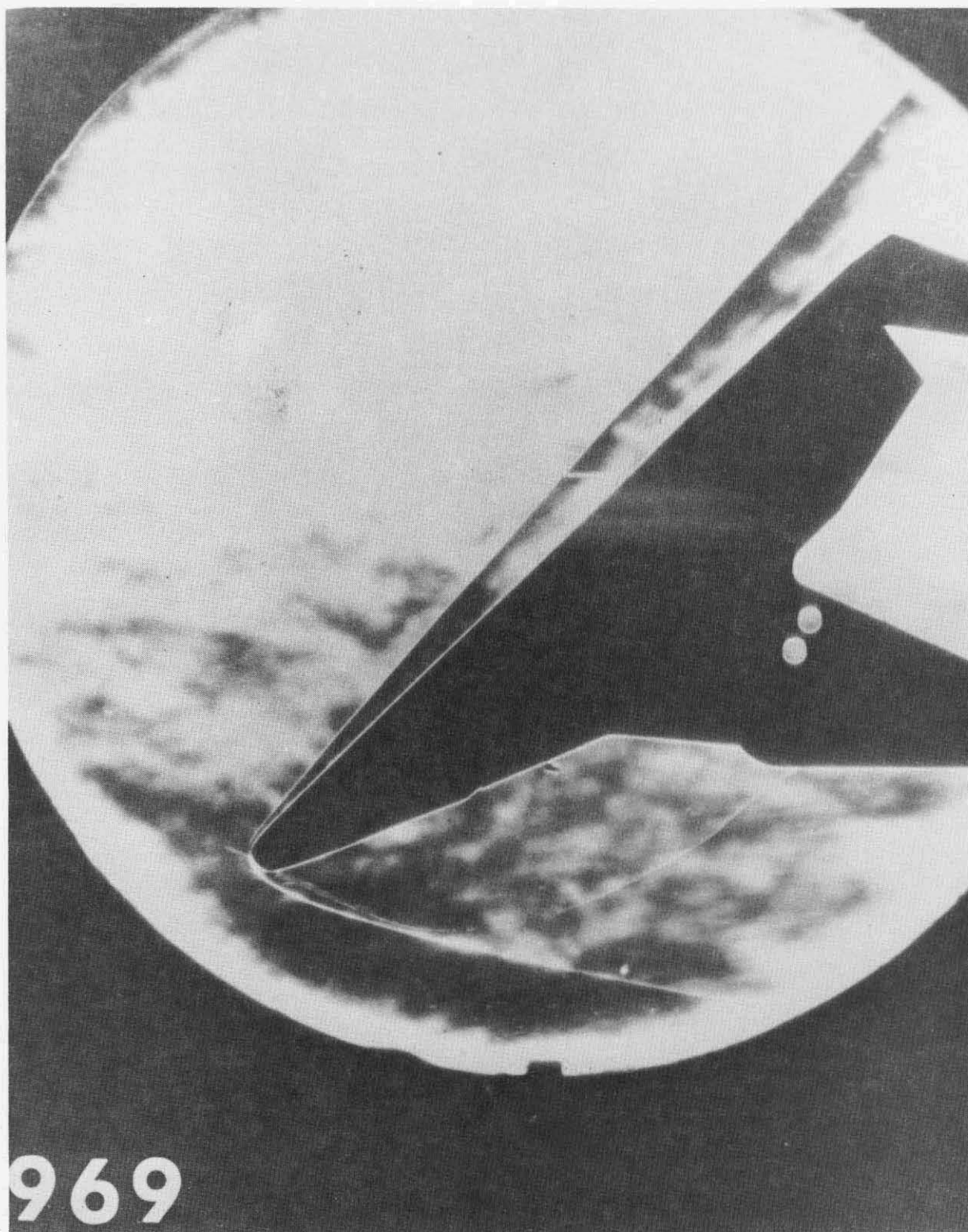


Fig. 19 - Schlieren Photograph of Run 969, $\alpha = 45$ Degrees, $Re/ft = 2.68 \times 10^6$

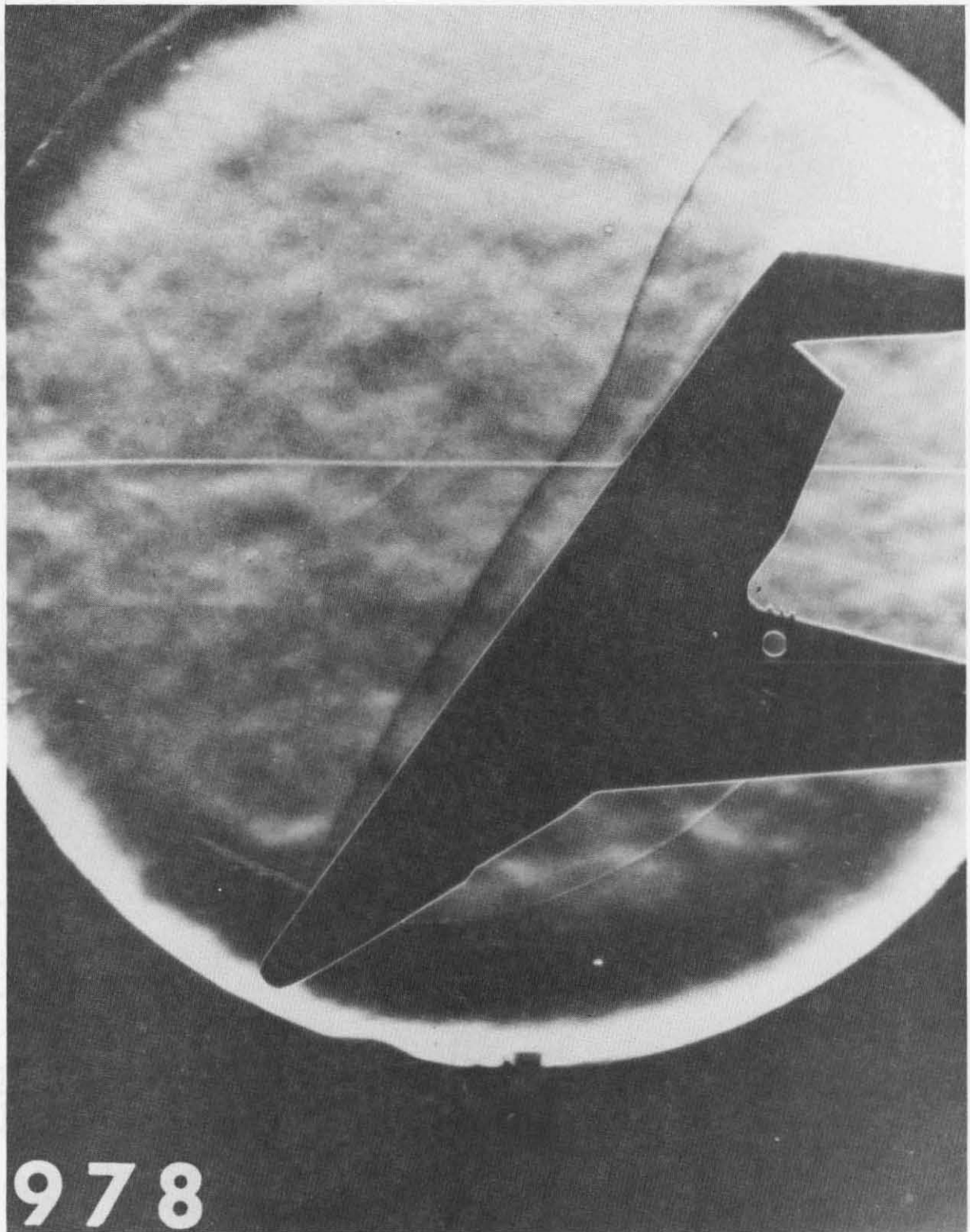


Fig.20 - Schlieren Photograph for Run 978, $\alpha = 55$ Degrees, $Re/ft = 0.60 \times 10^6$

Reproduced from
best available copy.

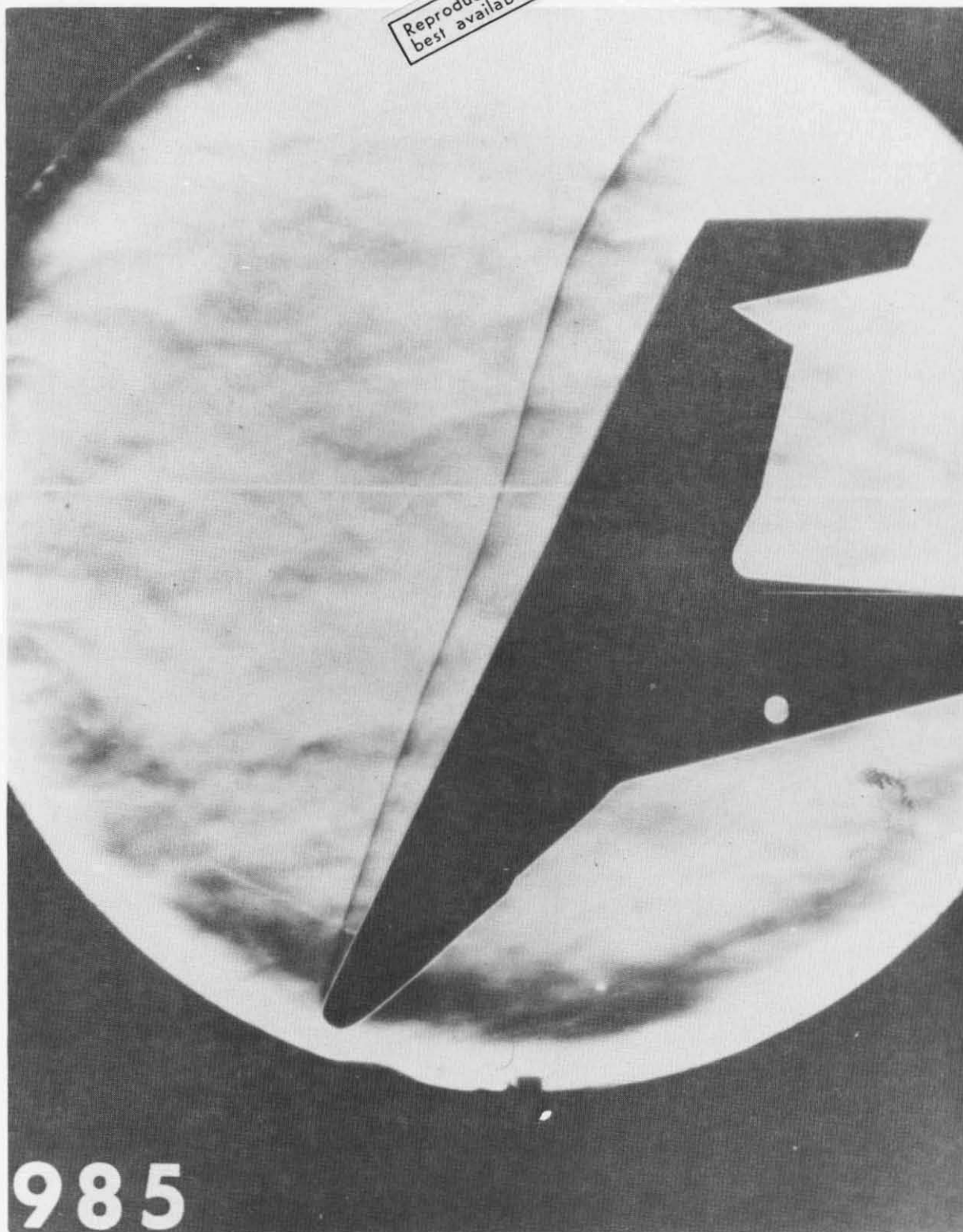


Fig.21 - Schlieren Photograph for Run 985, $\alpha = 65$ Degrees, $Re/ft = 1.05 \times 10^6$

Reproduced from
best available copy.

LMSC-HREC D225535

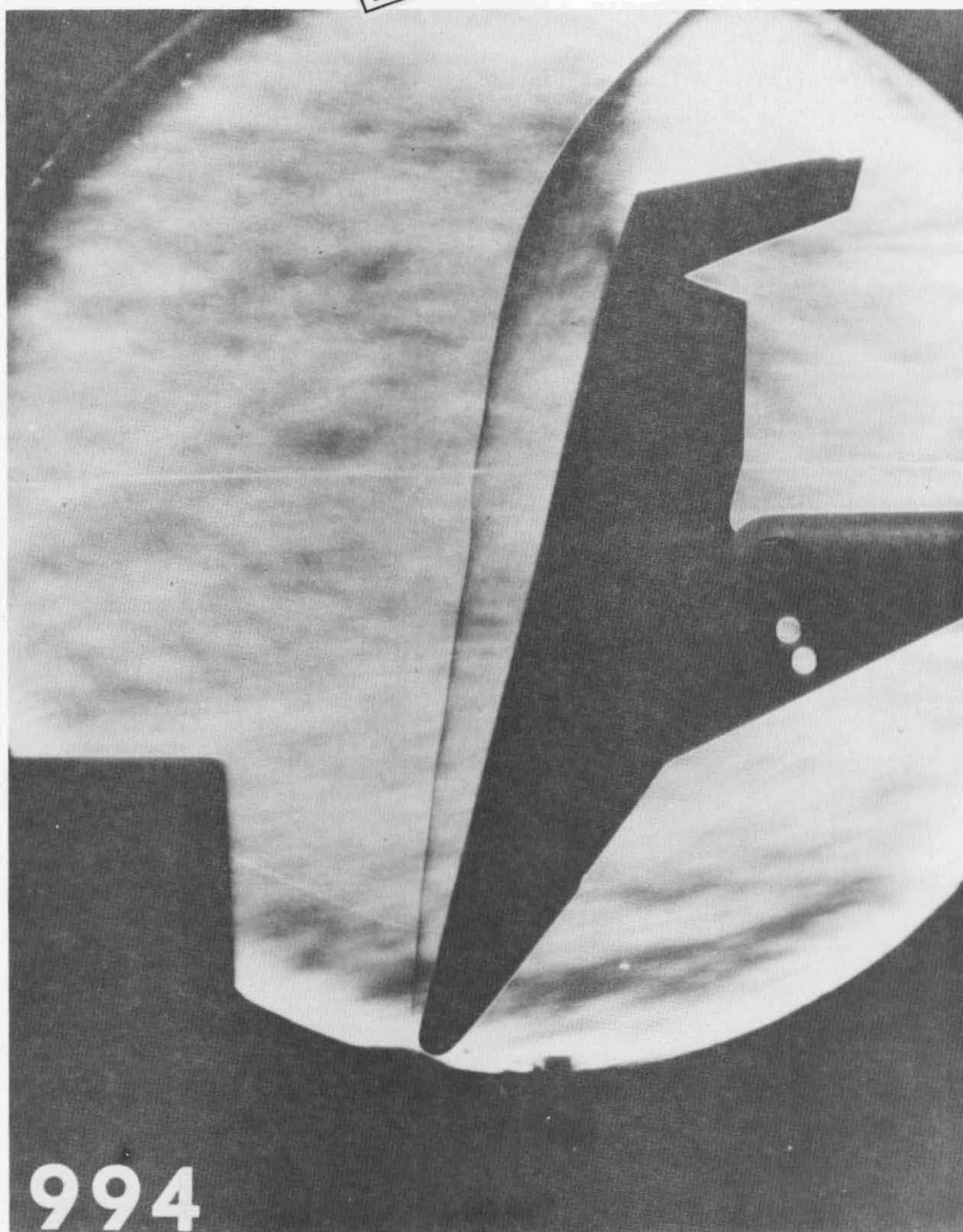


Fig. 22 - Schlieren Photograph for Run 994, $\alpha = 75$ Degrees, $Re/ft = 2.65 \times 10^6$

Reproduced from
best available copy.

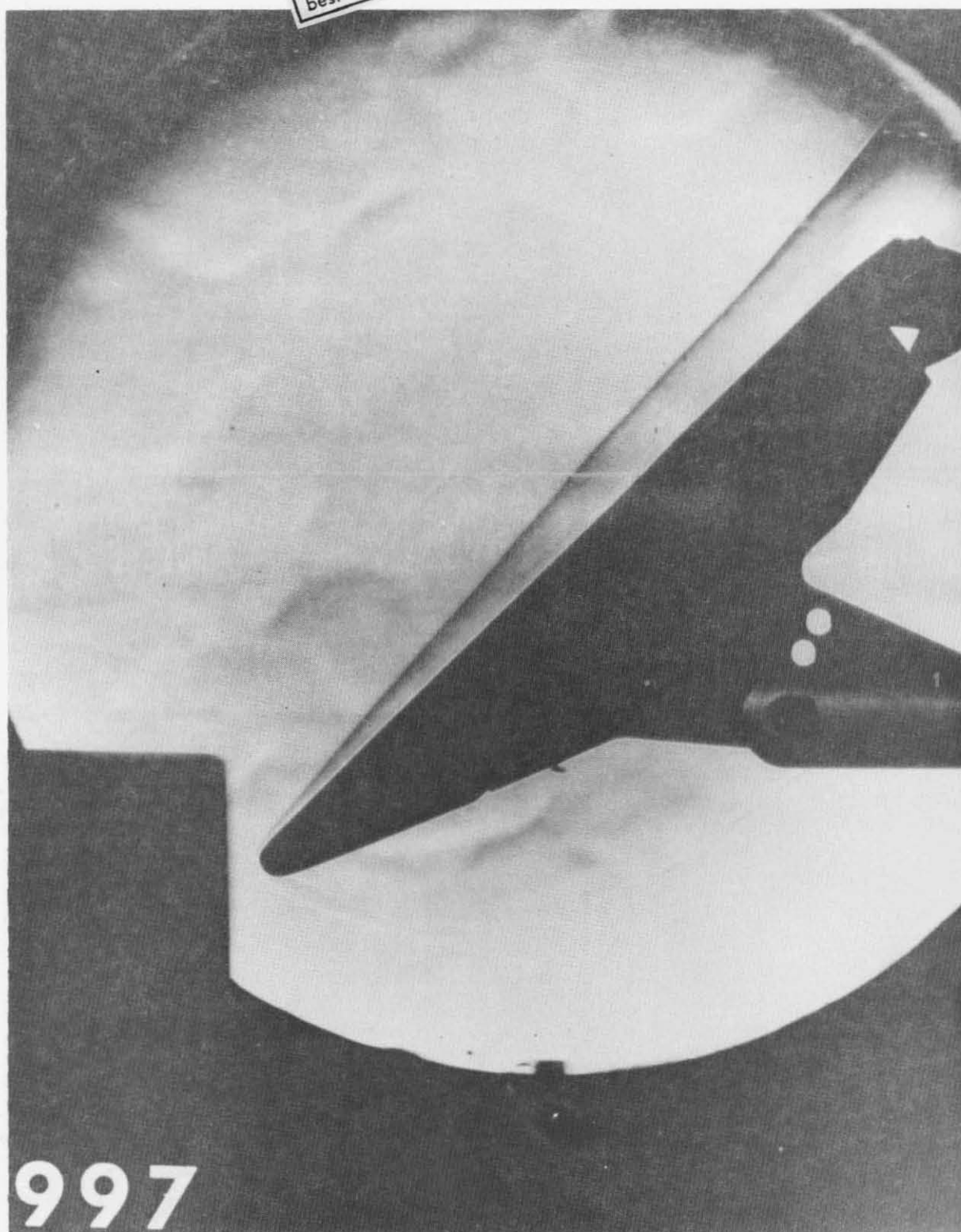


Fig. 23 - Schlieren Photograph for Run 997, $\alpha = 45$ Degrees, $Re/ft = 0.99 \times 10^6$

Section 3

ANALYTICAL TOOLS AND METHODOLOGY DEVELOPMENT

During the past year several significant studies were performed that provide insight into the problem of aerodynamic heating and in particular information about the local mass entrained in the boundary layer. Local pressure in the boundary layer does not seem to be affected by whether or not the flow goes through a strong or weak shock, but obviously the entropy is strongly affected. Since these two state variables (along with total enthalpy) are normally used to determine the local flow properties for any heating calculation, it is easy to see how significant errors in local flow properties and heating rates can result. Another aspect of the problem which was investigated is the effect that the flow path over the surface has on the local heating rate. This effect was investigated both analytically and semi-empirically.

This section contains a brief discussion of five tasks, four of which are documented separately. The first two tasks are primarily concerned with streamline divergence and the resulting effect on aerodynamic heating. The first task (Section 3.1) discusses a semi-empirical approach to streamline divergence while the second (Section 3.2) is concerned with a strictly analytical method. Sections 3.3 and 3.4 are basically two similar applications of the semi-empirical streamline divergence method with a few additional capabilities that will be discussed later. The final section (3.5) concerns a thermal analyzer program that is extremely versatile and is used in many applications, including the TEOP program discussed in Section 3.4.

3.1 ENTROPY SWALLOWING AND STREAMLINE DIVERGENCE BY SEMI-EMPIRICAL METHODS

A first-order investigation of the entropy swallowing of the boundary layer of a space shuttle vehicle was made and is documented in Ref.4.

Utilizing oilflow streamline data about the NASA-MSFC 437 booster configuration, the local flow at the edge of the vehicle's centerline boundary layer, at all angles of attack, was shown to be more accurately represented by parallel shock theory than by normal shock or oblique flowfield approximations. During this effort, a computer code was developed by which the interaction of the entropy/boundary layer is carried from the normal shock to parallel shock flow regimes in a step-by-step process from the vehicle's stagnation point, along the centerline of the configuration.

During the study, a streamline divergence analysis was completed to calculate the entropy swallowing; and, as a logical step in analyzing the data, the aerodynamic heating along the vehicle's centerline was predicted. At all angles of attack from 10 to 75 deg, the semi-empirical technique is shown to accurately match data taken by phase-change paint techniques. The test data were taken from the Langley Research Center's Mach 10 wind tunnel (Ref.2). From a knowledge only of streamline geometry and local flow properties, as determined from a first-order (mass conservation) analysis, excellent agreement between analytical data and test data is shown to be attainable without recourse to choosing the shape factors customarily used in theoretical analysis.

3.1.1 Method of Approach

The method discussed herein for determining the properties at the edge of the boundary layer requires both the inviscid and viscous portions of the flow field about the reentry configuration to be considered. This consideration is necessary since mass of the inviscid flow field becomes entrained in the viscous boundary layer as it develops along the vehicle surface. The physical situation can be analyzed exactly by numerical and analytical procedures as in Refs. 5 and 6 for axisymmetric shapes at zero angle of attack. However for the non-axisymmetric space shuttle configurations which are to fly at varying angles of attack, the application of such methods is severely limited. As a consequence, the flow near the centerline of the body is usually calculated by making extremely simplified assumptions; e.g., that the flow

enters the boundary layer after it negotiates a normal, an oblique, or a parallel shock system prior to entering the vehicle-influenced flow field. Depending upon the assumed shock system, the local flow properties vary substantially, with each case only partially fulfilling the true picture of the curved vehicle bow shock which moves from the normal to the oblique, and finally to parallel shock conditions. The purpose of this effort was to demonstrate, at least to the first order, the condition that most accurately matches the actual flow situation.

This was done by applying the entropy-swallowing concept as used in the aforementioned axisymmetric analyses. In this approach, the mass flow entering the flow system is equated to the mass entrainment in the boundary layer along the surface of the vehicle. Since an exact analytical (three-dimensional) flow field is not available for arbitrarily shaped bodies at angle of attack, the inviscid flow field is estimated from a streamtube approach in which the geometry of the oilflow patterns is used to determine the spanwise boundary, and the estimated centerline shock shape (test schlieren) is used as the shock layer boundary of the flow. Figure 24 is a schematic of this streamtube, which shows how it is eventually entrained into the centerline boundary layer profile. The thickness of the centerline boundary layer also relies upon the oilflow streamlines and streamline divergence theory for definition. The location of the centerline point on the vehicle shock system (see Fig. 24) is determined through an iteration procedure in which flow in the inviscid stream tube is equated to the flow in boundary layer where the boundary layer thickness has been corrected for mass outflow. The local flow properties are calculated by knowing the local pressure and the particular entropy level at which the local flow negotiated the curving centerline shock system.

3.1.2 MSFC 437 Space Shuttle Booster Analysis

● Vehicle Configuration and Test Summary

During the latter stages of the Phase A study of the reusable space shuttle vehicle, a booster configuration (Fig. 25) was tested for NASA-Marshall

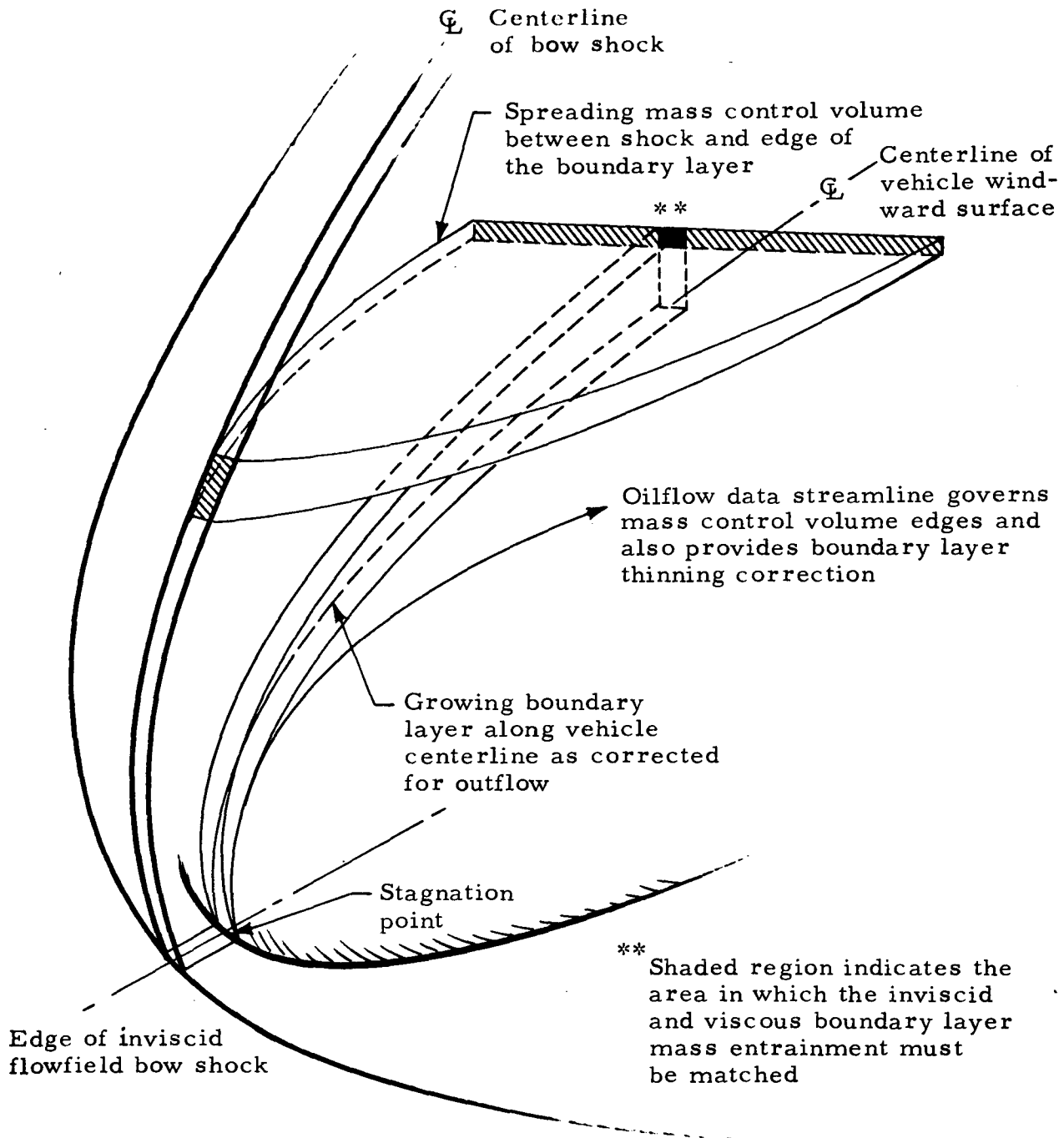


Fig. 24 - Schematic of Inviscid Streamtube and Boundary Layer at Point of First Order Entropy Swallowing Mass Balance

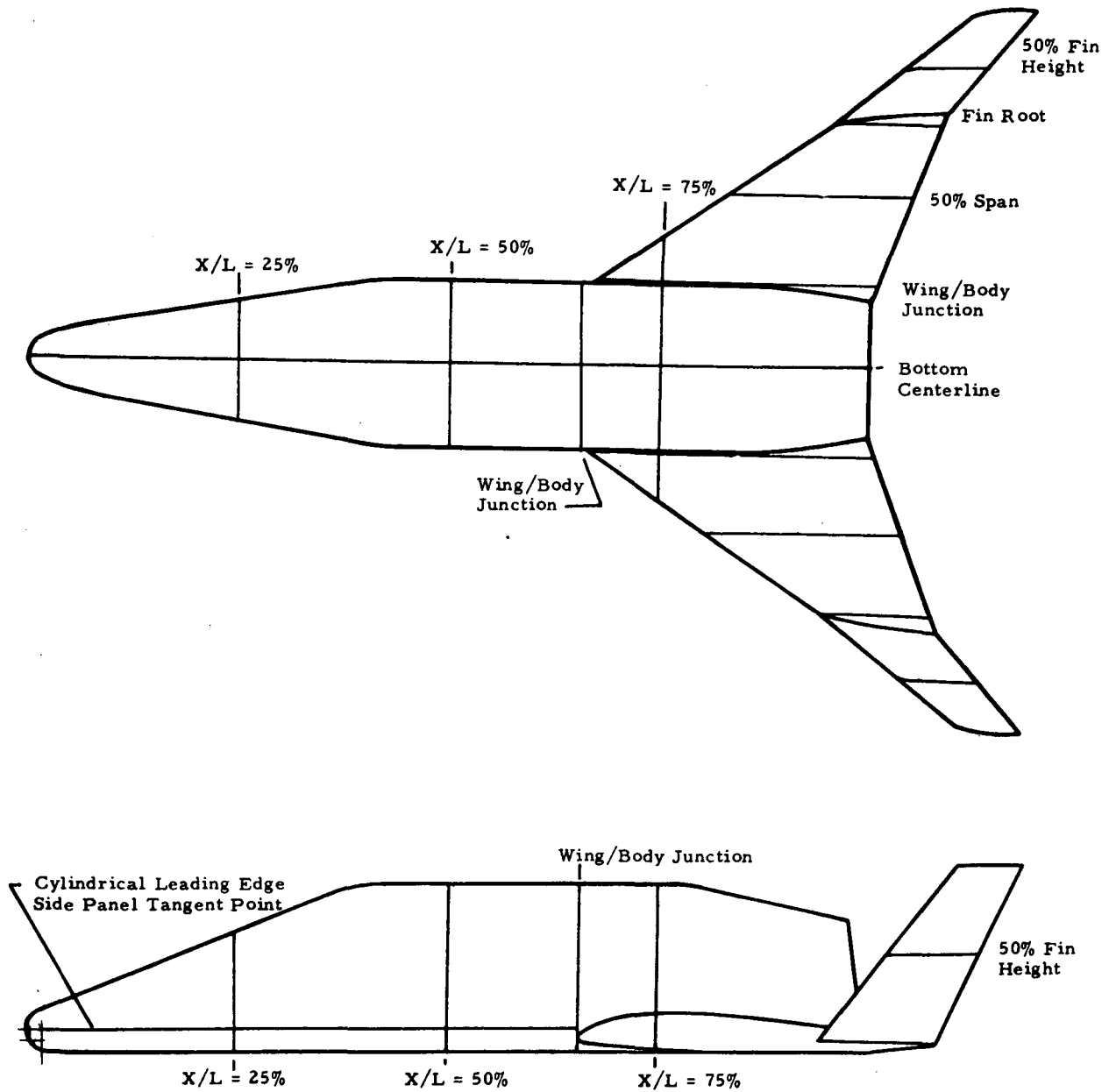


Fig. 25 - Geometry of the MSFC 437 Aerodynamic Heating Data Model

at the NASA-Langley Research Center Mach 10 facility. As reported in Ref. 2, oilflow streamline visualization as well as laminar heat transfer distributions were obtained. Heat transfer data, using Tempilaq testing techniques were obtained at vehicle angles of attack of 10, 30, 55, 58.3 and 75 deg, with oilflow data being generated for the same model attitudes with the exception of the 58.3-deg condition. The primary purpose of this test was to support the delta wing booster design concept in providing pre-Phase B data for use in verifying methods of predicting aerodynamic heating and extrapolating test data to freeflight conditions. These data have proven to be invaluable in performing the entropy swallowing analysis which will also demonstrate the importance of using this type of data (oil flow) in aerodynamic heating analysis. Results of using these data to predict the entropy swallowing and the local heat transfer coefficients along the configuration centerline are now given.

The oilflow data for the MSFC 437 booster are shown for two angles of attack on Figs. 26 and 27 along with the accompanying curve fits for the streamlines at each of the ten segments as analyzed. There were no oilflow data for the 58.3-deg case. However, heat transfer data were available because of a bent test sting which created a misalignment during a 55-deg model paint test run. The curves of crossflow parameters as function of vehicle body station and angle of attack for the cases whose oil-flow was available were plotted and are given in Figs. 28 and 29. From these curves, values of the parameters for non-tested angles of attack can be estimated. Using this reduction of the oilflow data and the results of a shock shape sensitivity study, the local entropy swallowing and centerline heat transfer analysis was completed.

Typical results of the entropy swallowing analysis is visualized in Fig. 30 for the 55-deg angle-of-attack case for the parallel shock standoff distance of 0.025% of the nose radius. As can be seen, the entropy level at the edge of the boundary layer rapidly moves from the normal shock regime to the parallel portion of the bow shock system. Therefore, for this case,

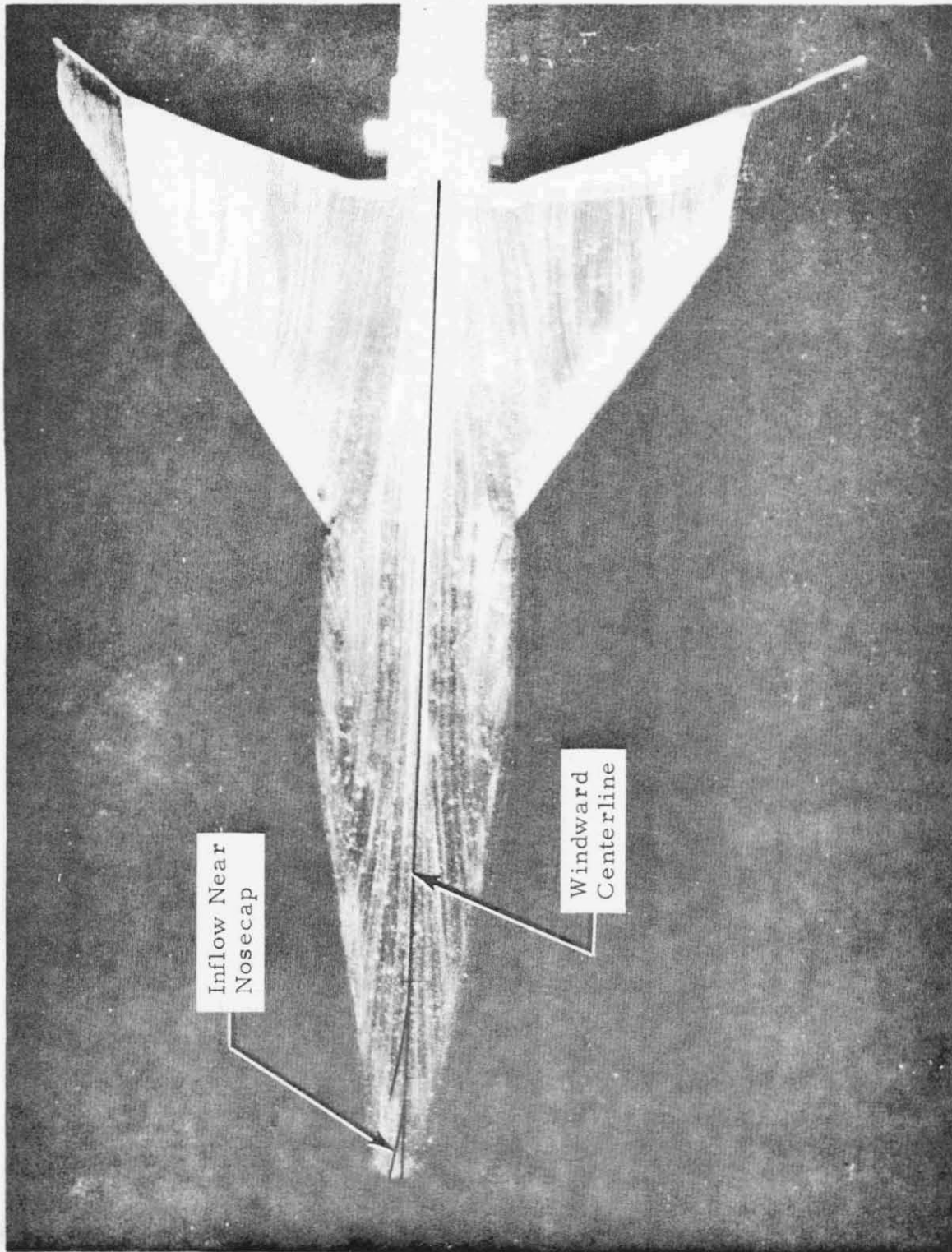


Fig. 26 - Oilflow Curve Fits of Data for MSFC 437 Booster at 10 Degrees Angle of Attack



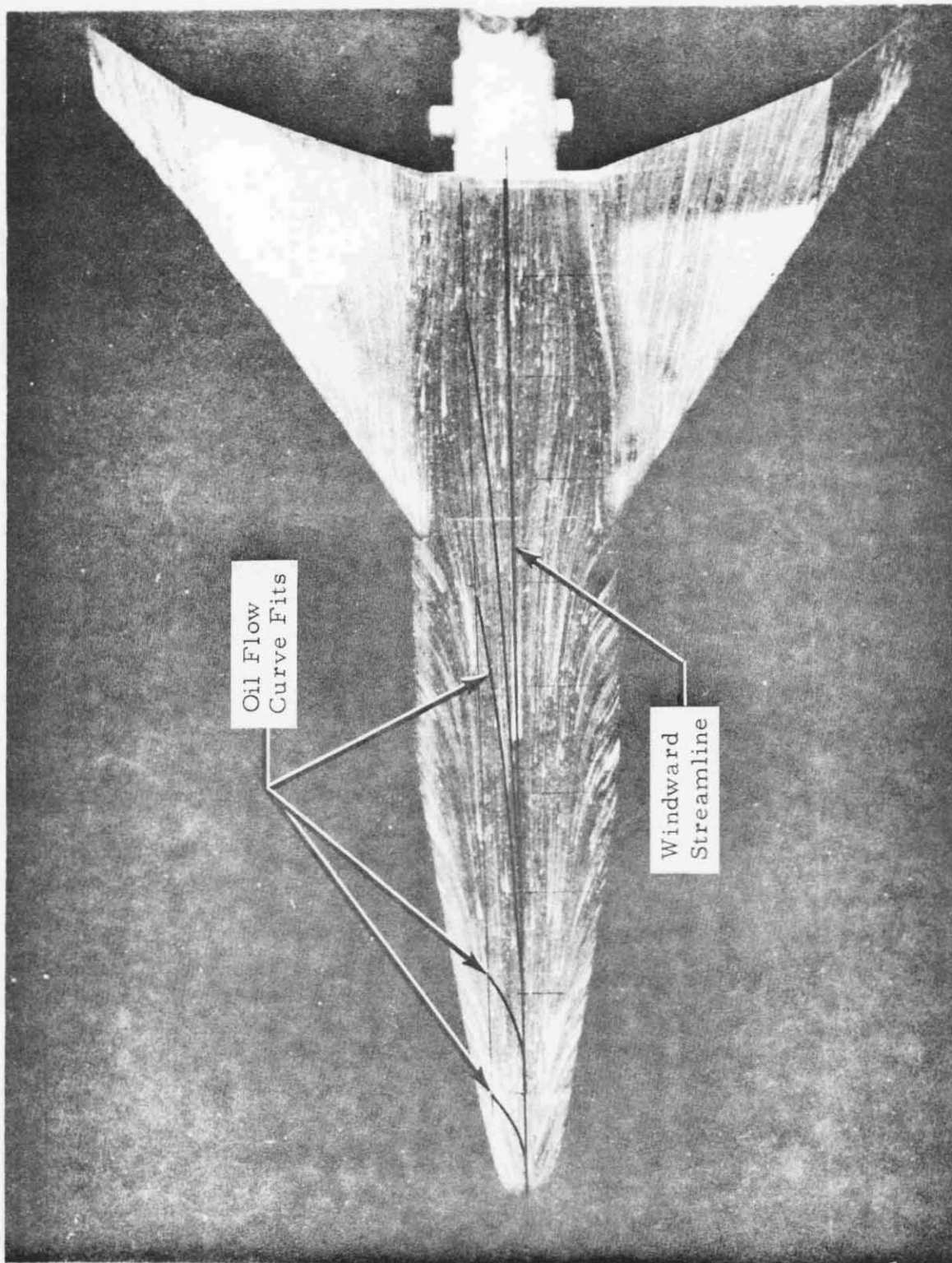


Fig. 27- Curve Fits of Oilflow Data for MSFC 437 Booster at 30-Degree Angle of Attack

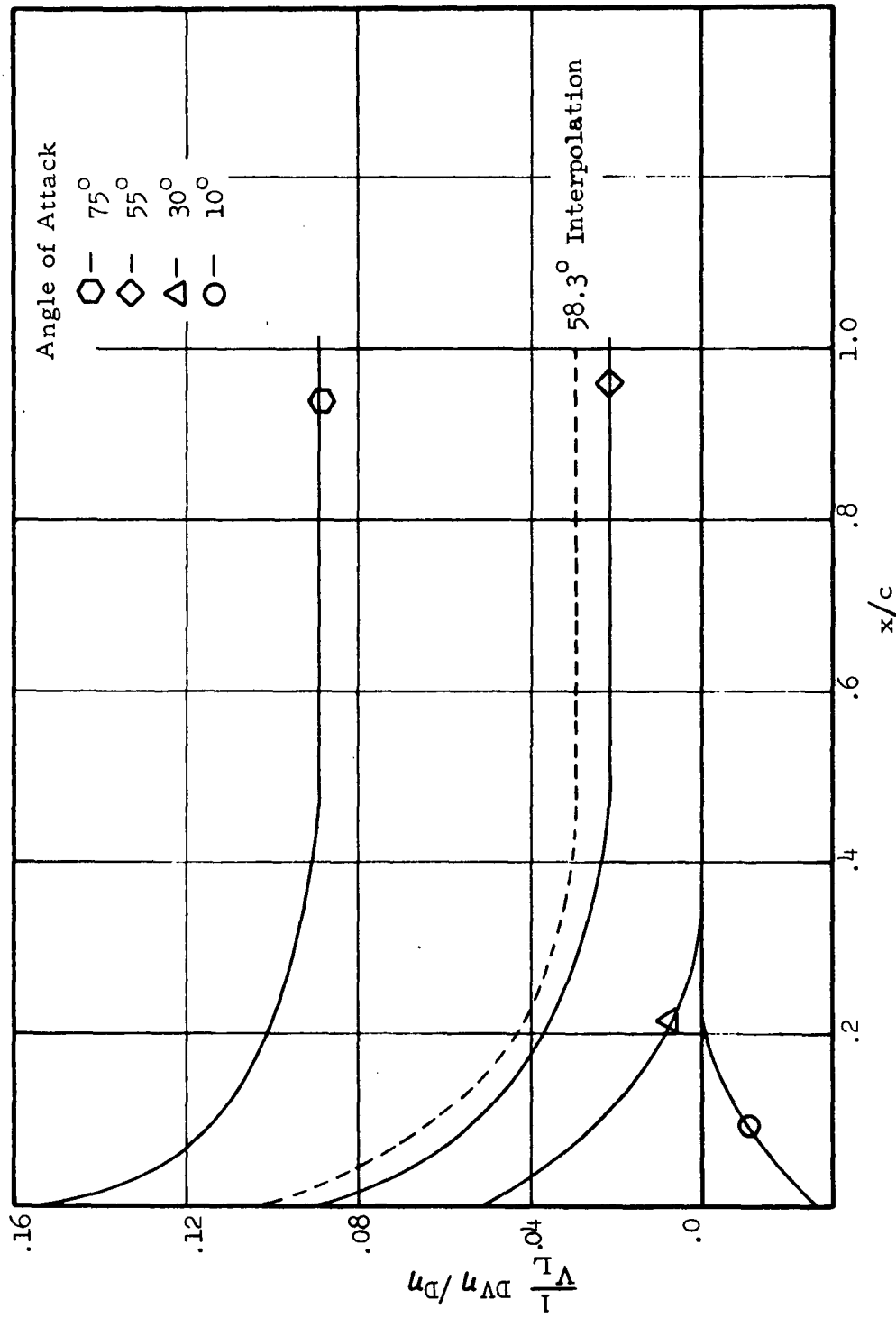


Fig.28 - Crossflow Correction Exponential as a Function of Body Length

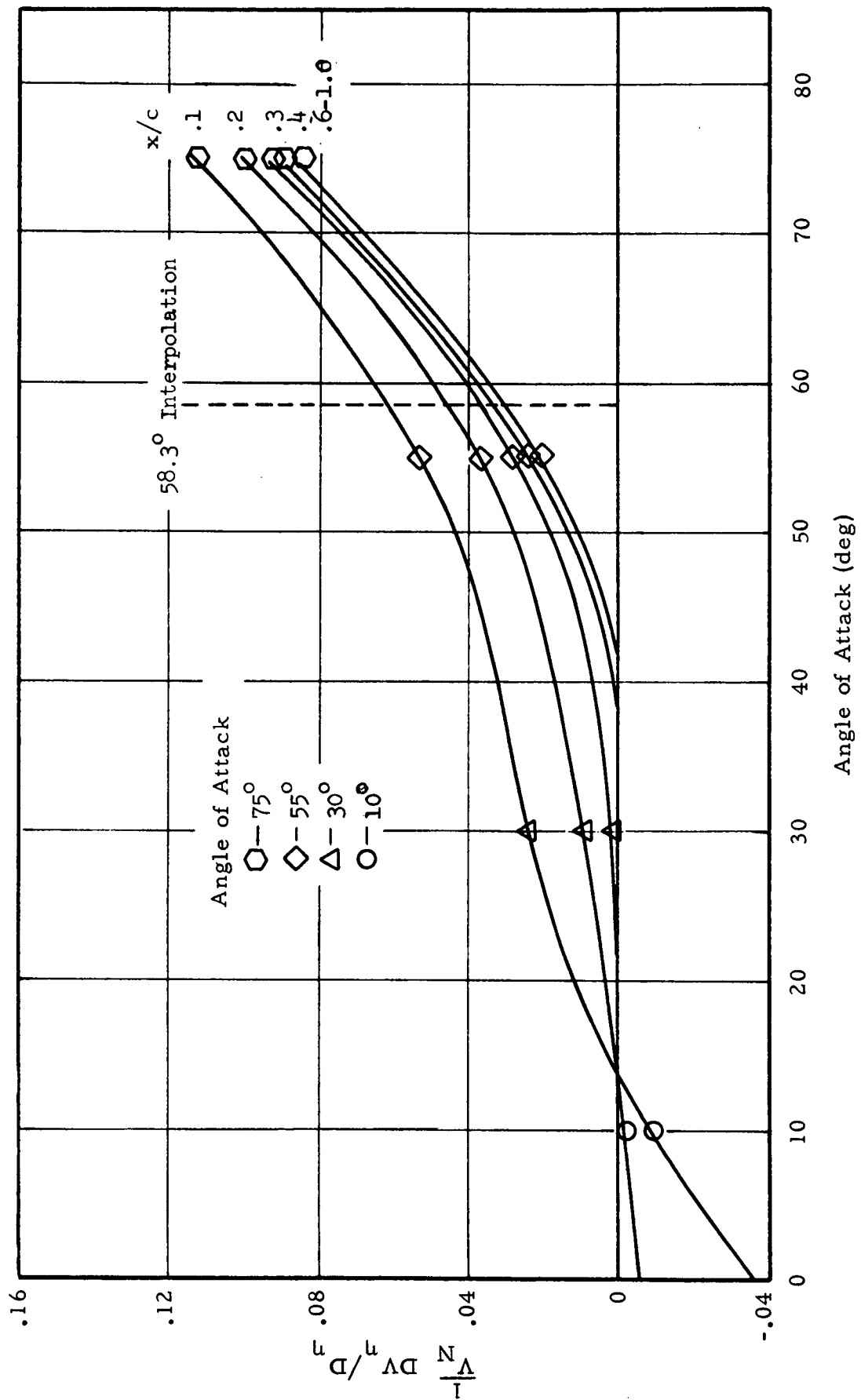


Fig.29 - Crossflow Correction Exponential as a Function of Vehicle Angle of Attack

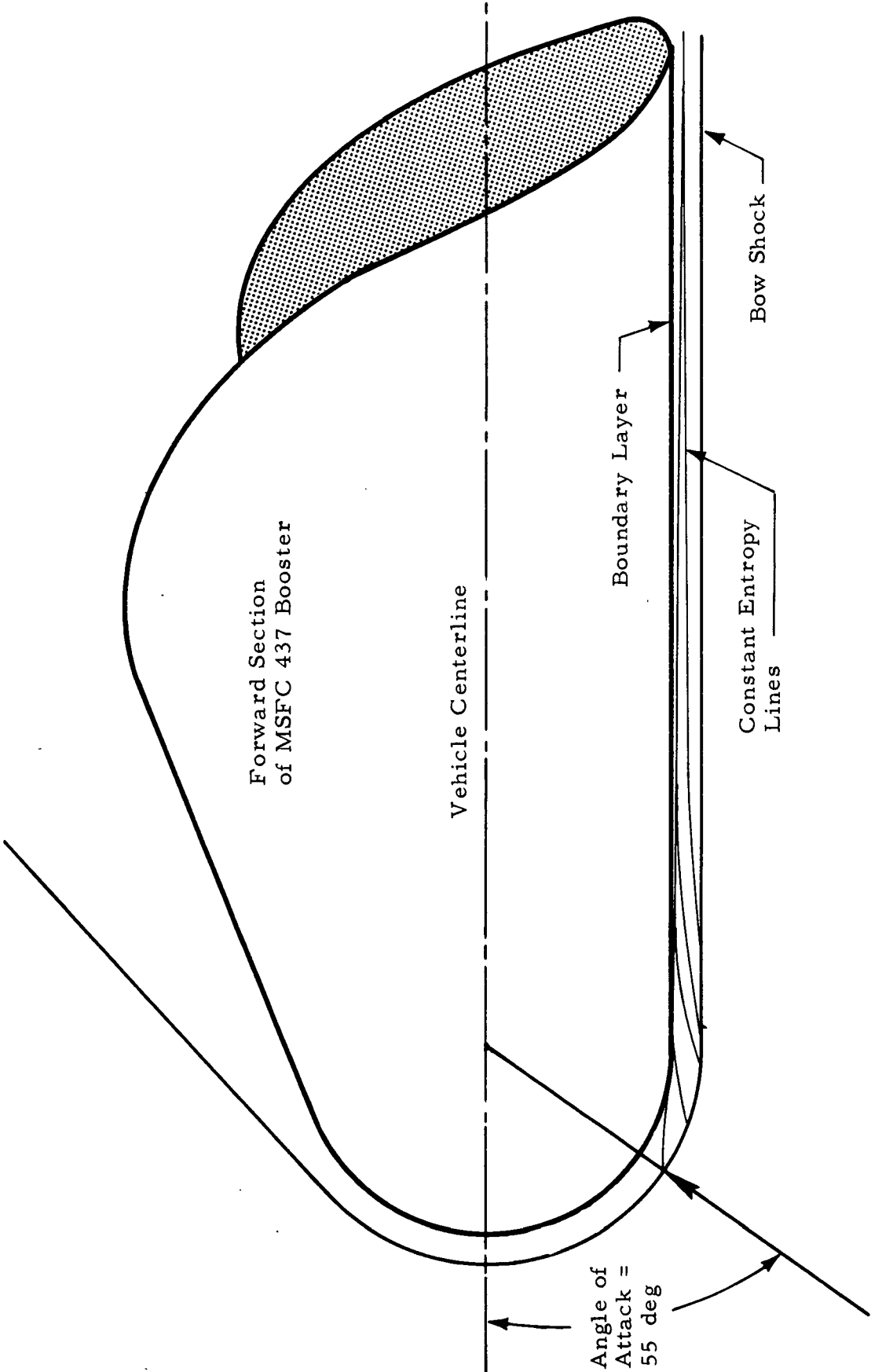


Fig. 30 - Results of Entropy Swallowing Analysis for Close Shock About MSFC 437 Booster

a parallel shock analysis without correction for entropy swallowing would be more appropriate for a simplified analysis of the local flow as opposed to normal shock theory.

Returning to the method of analysis, the values of cross flow as estimated from the oilflow data and entropy swallowing analysis were used in that analysis to provide the local flow properties and the equivalent characteristic length for the boundary layer calculations. The results of using this method for providing the characteristic lengths are shown in Fig. 31 as a function of vehicle angle of attack and actual body station. At the lower angle of attack; namely 10 deg, the characteristic length is somewhat longer than the physical length, while the 30-deg case is nearly the same as the physical length. The oilflow data show the obvious streamlines inflow leading to thickening of the centerline boundary layer for the 10-deg case, while the flow in the 30-deg situation is more nearly parallel, leading to the conclusion that uncorrected flat plate theory would suffice for a rough analysis between 10 and 30 deg angle of attack. From Fig. 29, the angle of attack that would result in no inflow or outflow is about 14 deg.

At the higher angles of attack, the streamline outflow is significant with a corresponding shortening of the equivalent length as compared to the physical length. This indicates a thinning of the boundary layer due to substantial outflow. Consequently, higher heating than that predicted with flat plate theory can be expected. This is indeed the case, with flat plate theory over-predicting (Ref. 7) at the low angle of attack, roughly matching at 30 deg and under-predicting at the higher angles of attack.

However, upon using the crossflow corrected values of the boundary layer characteristic lengths and the heat transfer properties in the flat plate heat transfer grouping evaluated at Eckert's reference enthalpy, the data-theory match is phenomenal. This can be seen in Fig. 32, which compares the analysis results with the paint test data for the vehicle centerline. In all

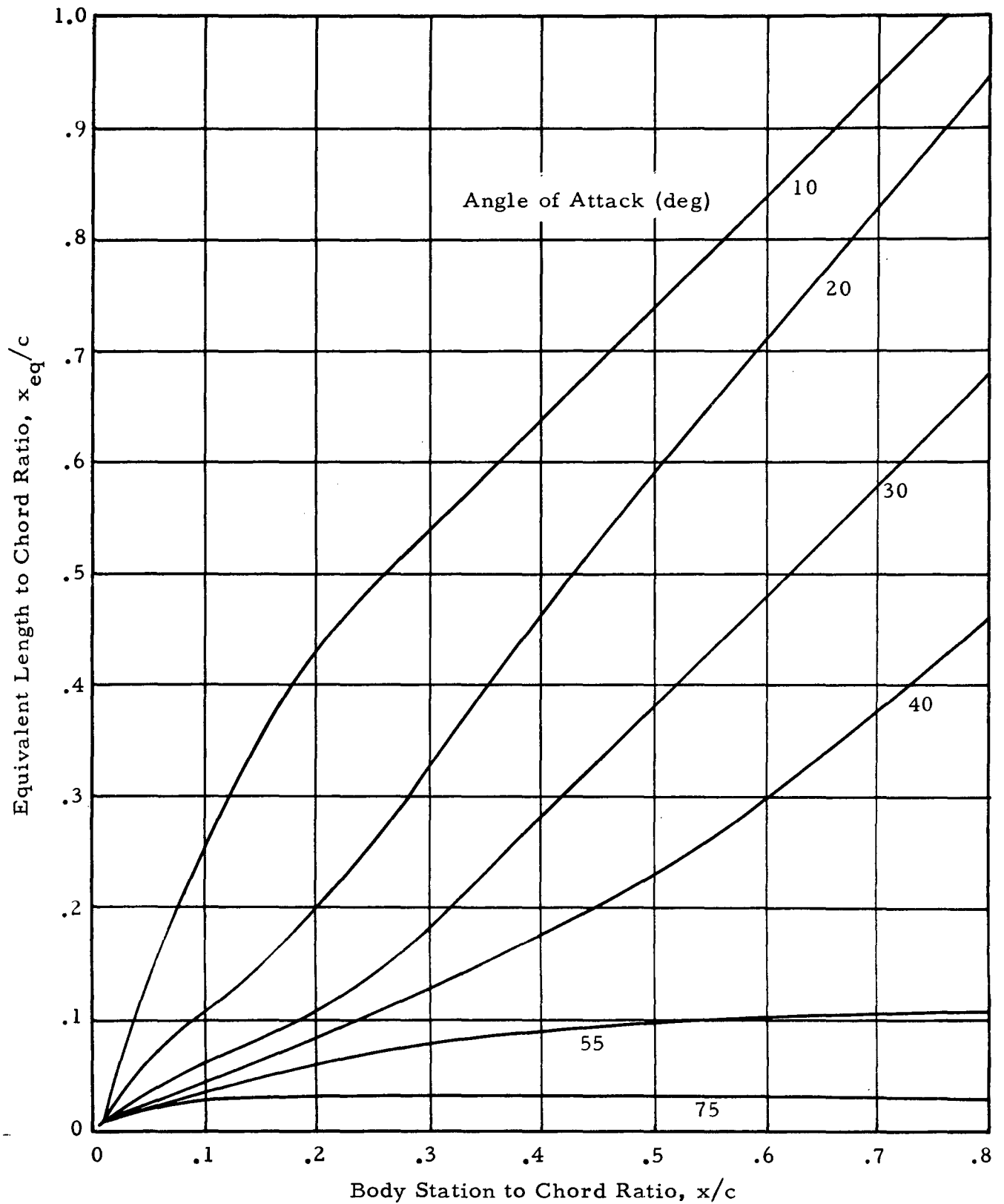


Fig. 31 - Comparison of Actual Length and Boundary Layer Characteristic Length for MSFC 437 Booster

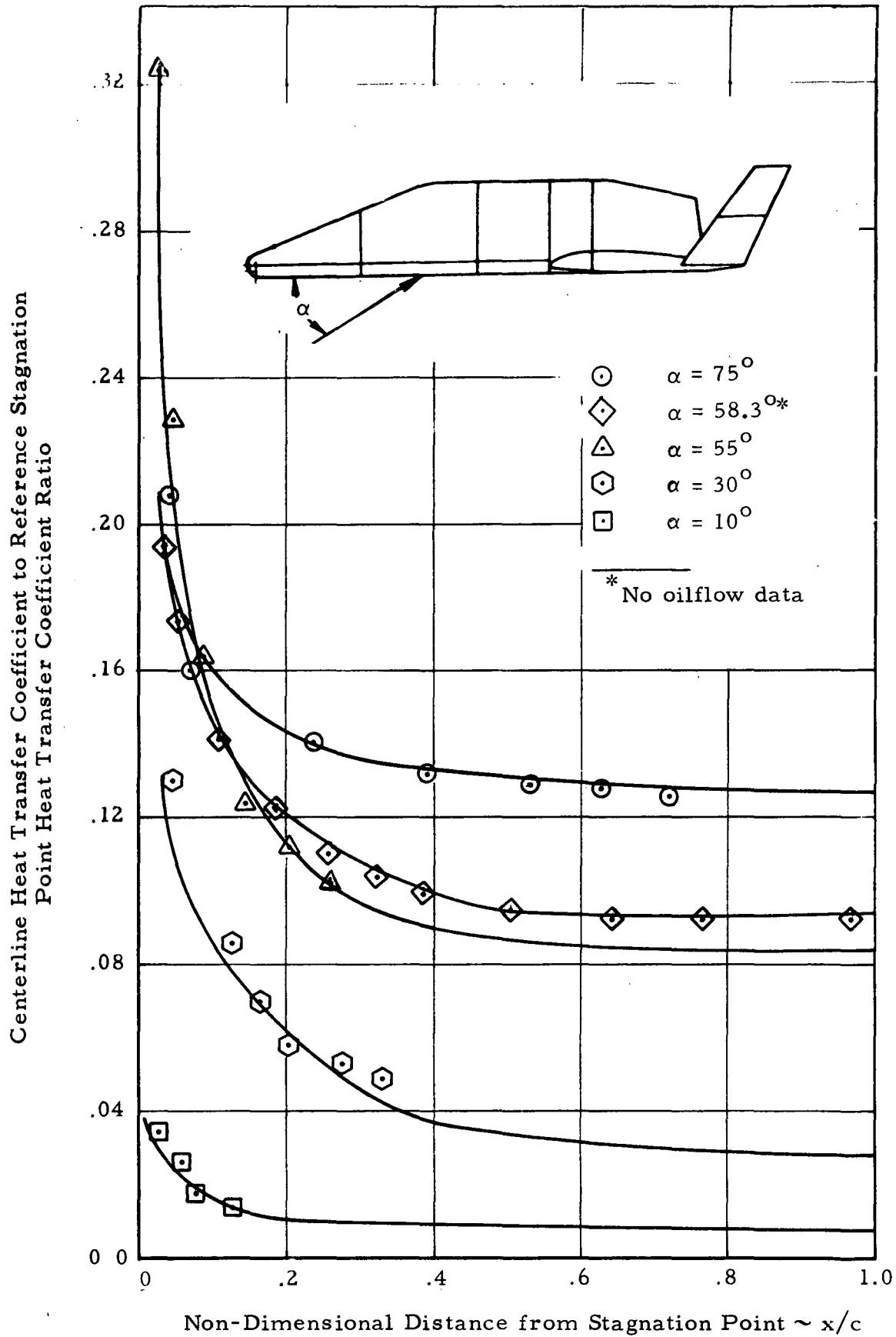


Fig. 32 - Analytic Predictions of Heat Transfer Coefficient Compared to Experimental Phase-Change Data. (Analytic Predictions are based on oil flow data)

cases no prior knowledge of the heat transfer coefficients was known and the analytic results depended solely upon the oilflow streamline data and, to a much lesser extent, upon the entropy swallowing analysis. Finally, the dashed line and the points representing the 58.3 deg angle-of-attack data are shown as an example of confidence to be attributed to the Streamline Divergence method for heat transfer analysis. Although no oilflow data existed at this angle of attack, the data of Fig. 29 were cross plotted to yield an estimate of the crossflow parameter for the 58.3-deg case. As can be seen, the data theory match is also quite good.

3.2 WINDWARD SIDE AEROHEATING BY ANALYTIC STREAMLINE DIVERGENCE

Calculation of the heat transfer to a general three-dimensional body during hypersonic flight is a formidable task. Computing a three-dimensional inviscid flow field and using the results of such a calculation as the edge conditions for a three-dimensional boundary layer study would require a vast amount of effort on the part of the engineer and stretch or surpass present-day computer capabilities. However, if simplifying assumptions are made, one can reduce the problem to a form which can be handled without the extreme complexities of the complete three-dimensional analysis mentioned above. The complexity of a numerical solution to the three-dimensional boundary layer equations (Ref. 8) written in streamline coordinates makes the use of simplifying assumptions quite attractive.

Partial differential equations governing the boundary layer in a three-dimensional situation can be greatly simplified if one assumes that the cross flow velocity term is zero (Ref. 9) or small (Ref. 10). The cross flow is the component of the boundary layer flow normal to the direction of the inviscid streamline and along the body surface. If the cross flow is zero, the three-dimensional boundary layer equations reduce to axisymmetric boundary layer equations, this is termed the axisymmetric analog. If the cross flow term is small the resulting equations are greatly simplified and can be solved using a similar solution (Ref. 10).

In hypersonic flows, bodies are generally considered to have cool walls, i.e., the wall temperature is low compared to the temperature at the edge of the boundary layer. This condition is characterized by relatively low local Mach numbers at the boundary layer edge, a total enthalpy at the boundary layer edge much larger than at the wall, and the density greater at the wall than at the edge. When these conditions are present the zero cross flow assumption is valid and the axisymmetric analog is an applicable method for determining heat transfer to the body (Ref. 11).

The compressible laminar boundary layer for axisymmetric bodies at zero angle of attack has been investigated extensively in the past. Methods for predicting the heat transfer and boundary layer characteristics are well-developed. Solutions are obtained by either similar (Refs. 11 and 12) or integral (Ref. 13) methods. Integration of the axisymmetric boundary layer equations down the streamlines is feasible if velocity, temperature density or enthalpy profiles are desired. Turbulent boundary layers and the problem of transition were not treated at this time.

A detailed derivation of the governing equations for an analytic prediction of streamline divergence is given in Ref. 14, along with a detailed presentation of results. A limited amount of the results is presented here.

3.2.1 Theoretical Streamline Patterns

The streamlines on the windward side of two blunt cone configurations were calculated by integrating the differential equations derived in Section 2.2.3 of Ref. 15. The particular case of a sphere cone was chosen because of the availability of heat transfer data and the ease of describing the geometry of these shapes with analytical expressions. However, any body which has a geometry that can be described with the function $f(x, y)$ could have been chosen. Typical streamline patterns are shown in Figs. 33 and 34. The shapes of these streamlines are somewhat distorted since they are shown as simple projections on the x - y plane in Fig. 33 and the x - z plane in Figs. 34. Streamline angles, β , of 0.001 to 0.300 rad are shown in each of these figures. The

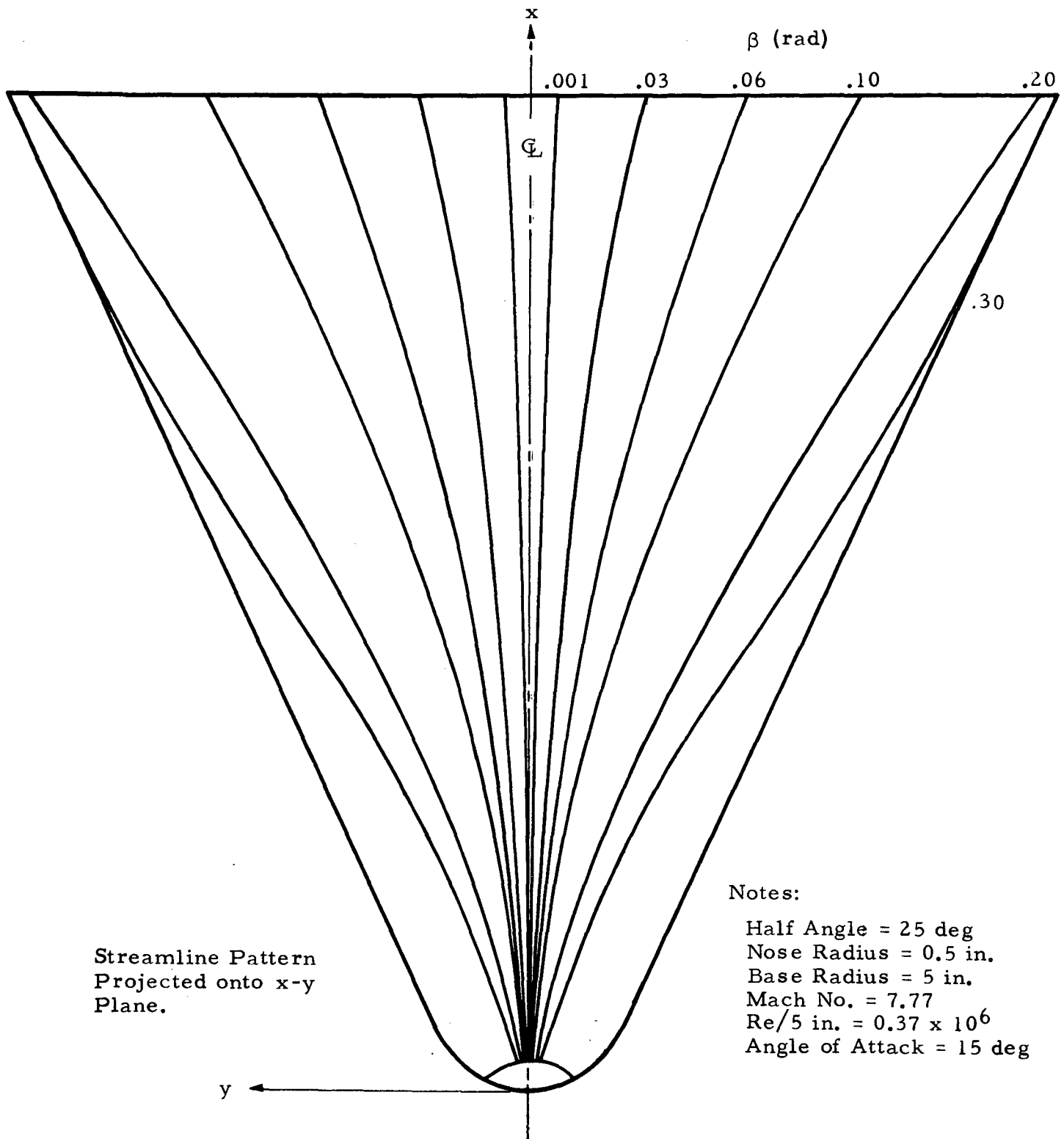


Fig. 33 - Typical Streamline Pattern for Sphere Cone at Angle of Attack

Fig. 34- Typical Streamline Pattern for Sphere Cone at Angle of Attack

effect of the angle of attack on streamline shape is shown in Fig. 35. At zero angle of attack the streamline is a straight line over the conical portion of the cone. As the angle of attack increases the pressure gradient perpendicular to the centerline becomes more negative, bending the streamline outward to the lower pressure region.

3.2.2 Centerline Heat Transfer

The convective heat transfer distribution for two sphere-cone configurations was predicted using the convective heating expression of Lees, Eq. (2.24) of Ref. 14. Agreement with experiment appears to be quite good as is shown in Figs. 36 and 37.

3.3 FLIGHT ENVIRONMENT FROM DATA (FED)

A method of producing flight environments for space shuttle vehicles is presented in detail in Ref. 1. Motivated by the need for a simple design tool and drawing upon the results of several parallel studies, the analysis technique has evolved into the form described herein. Although considerations of simplicity govern the basic concept of the Flight Environment from Data (FED) analytic technique, several other accepted methods can be used to support the analysis. A brief discussion of the FED philosophy is presented here.

In an effort to produce rapid response to thermal environment requirements use is often made of laminar heating distributions ratioed to a stagnation point value to establish local laminar heating rates for the flight environment. Although effective, this method completely ignores the effects of high enthalpy real gas on the distributions which have usually been obtained from relatively low enthalpy (ideal gas) ground test facilities. A comparison of these effects at different altitudes and velocities may be seen on Fig. 38 for the ratio of heat transfer coefficient between the stagnation point and a point on the afterbody of a typical shuttle shape. As can be seen the differences are substantial.

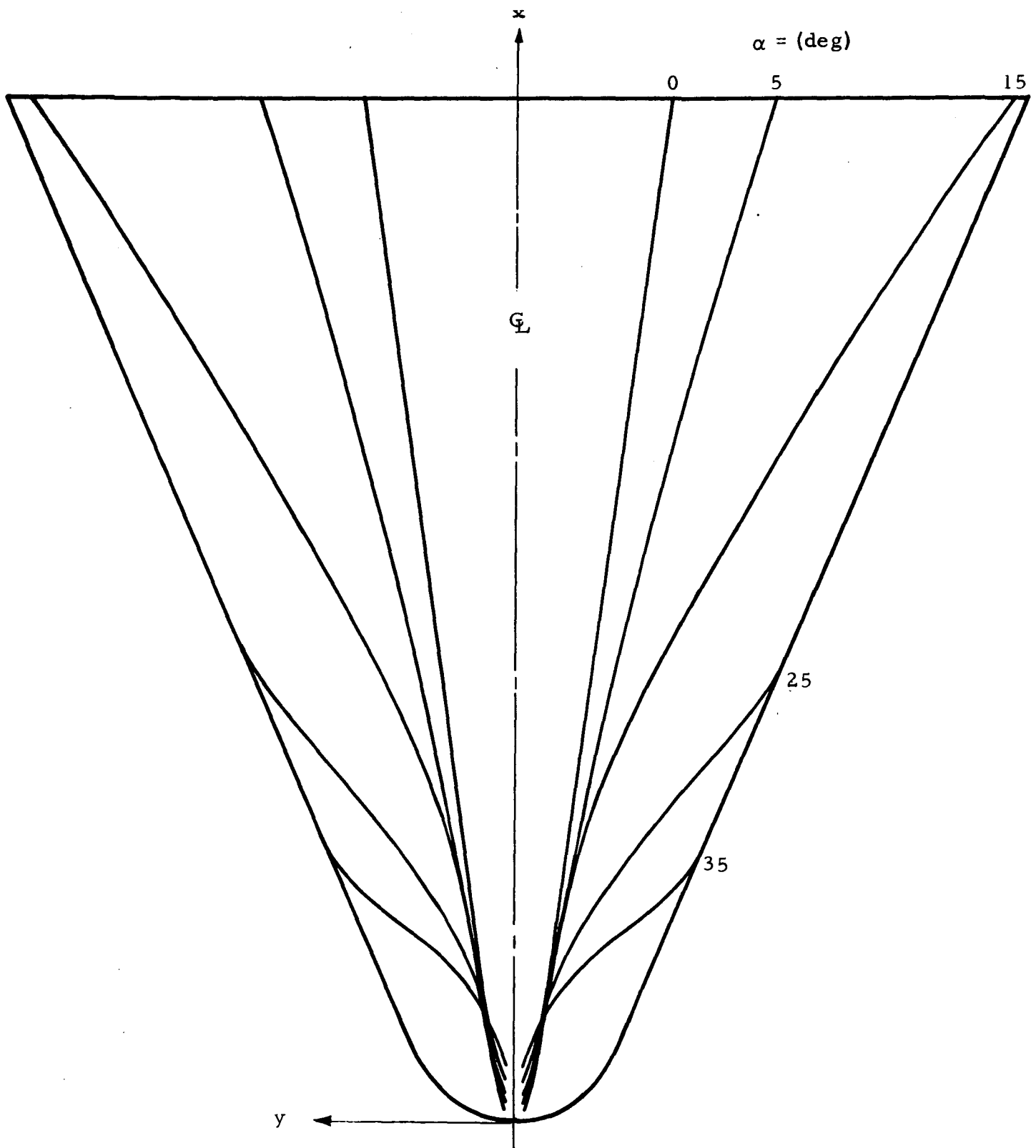
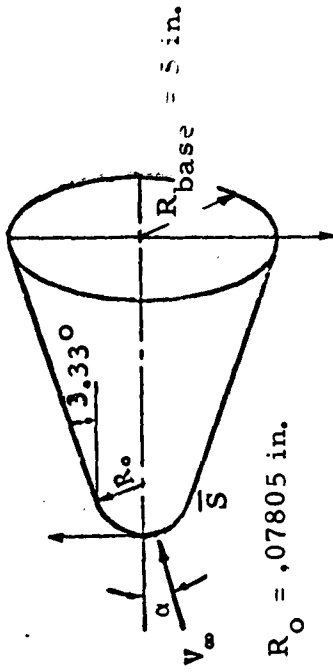


Fig. 35 - Streamline Paths over a Sphere Cone for Several Different Angles of Attack



Notes:

Angle of Attack = 18 deg
Mach Number = 4.8 deg

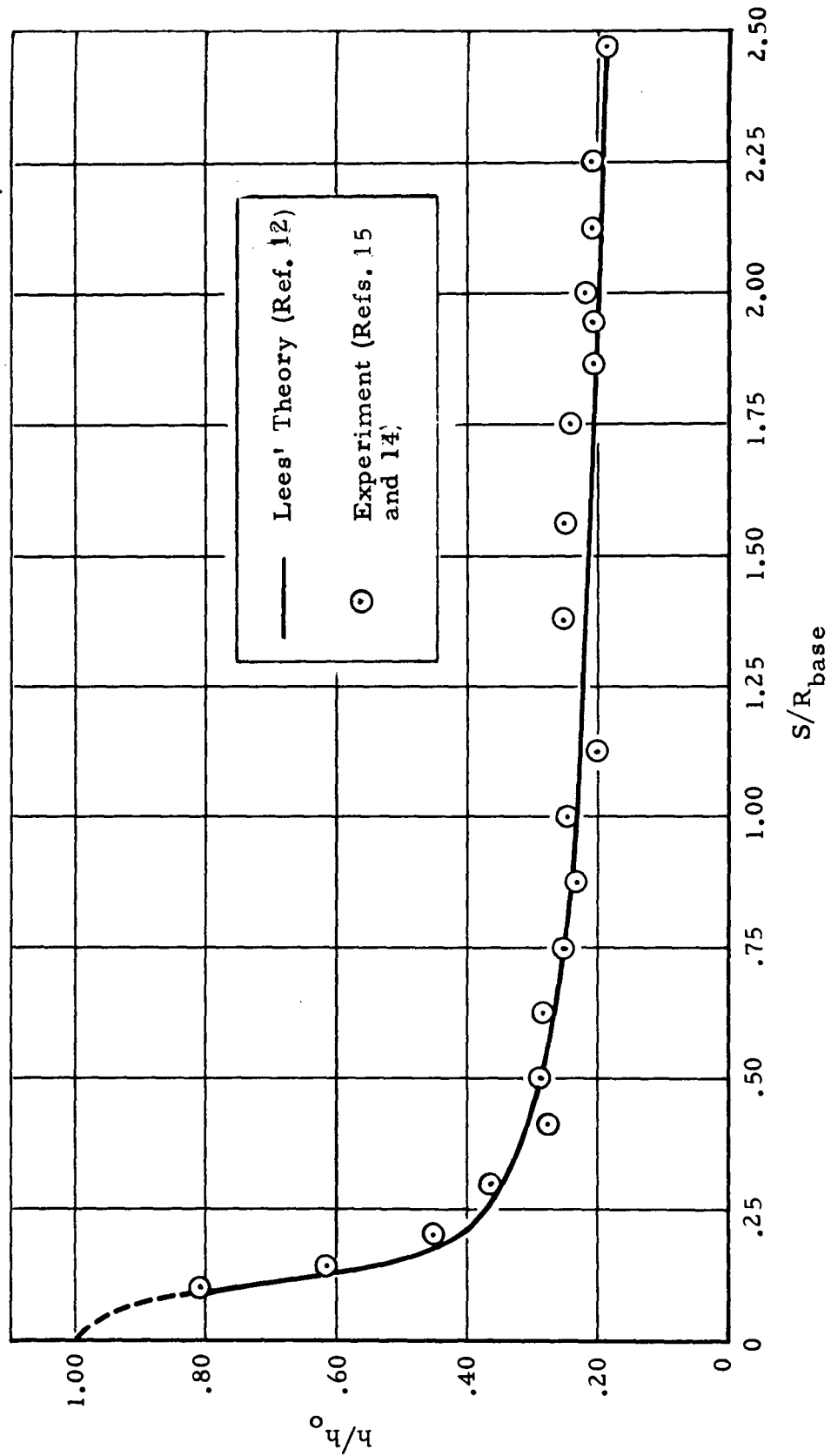
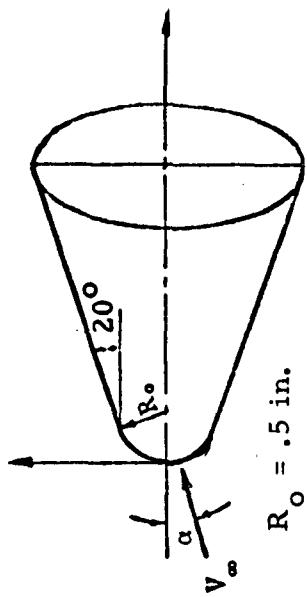


Fig. 36 ~ Windward Centerline Heat Transfer over 13.33-Degree Half Angle Sphere-Cone at Angle of Attack



Notes:
Angle of Attack = 15 deg
Mach Number = 7.77

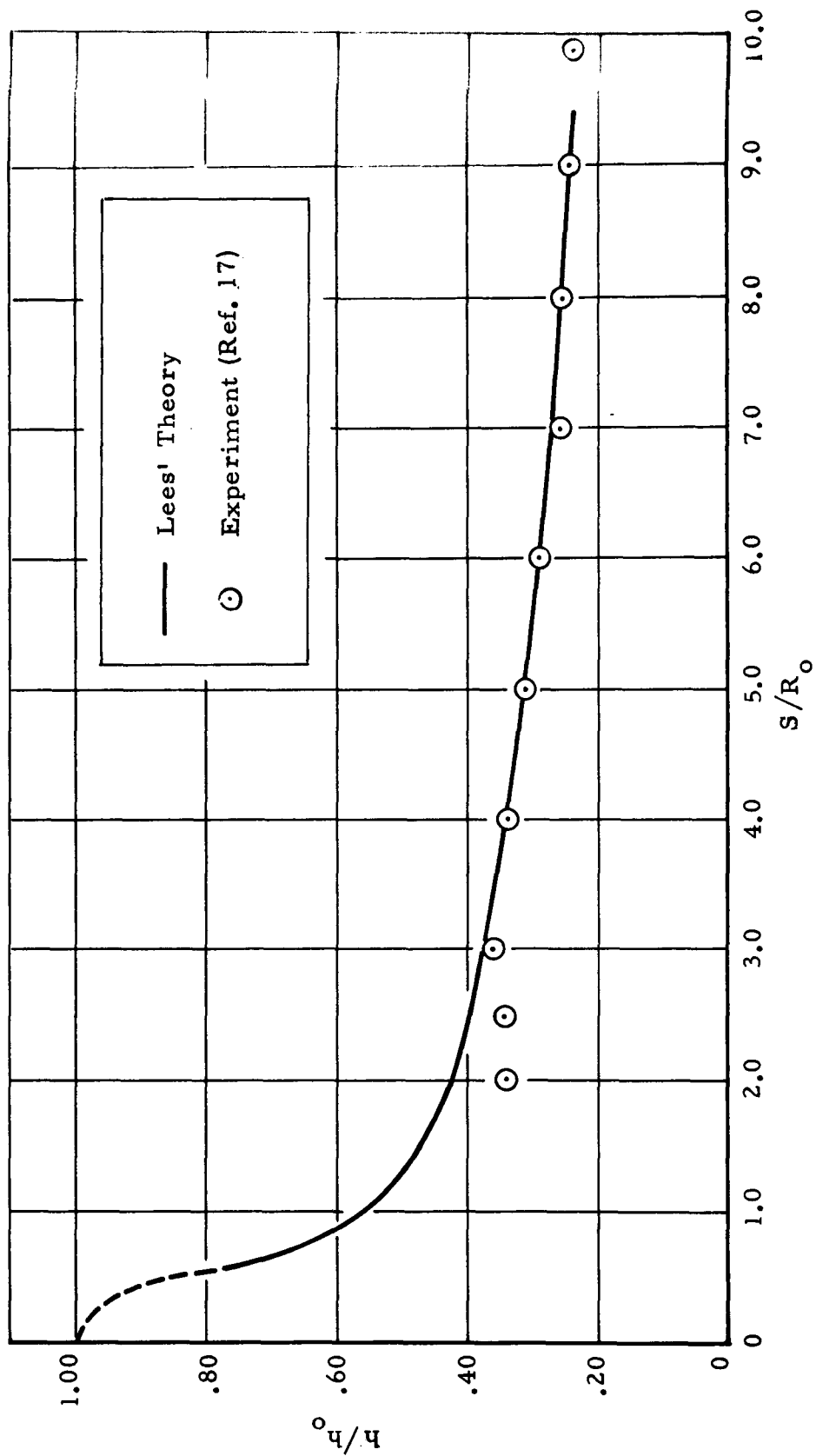


Fig. 37 - Windward Centerline Heat Transfer over 20-Degree Half Angle Cone at Angle of Attack

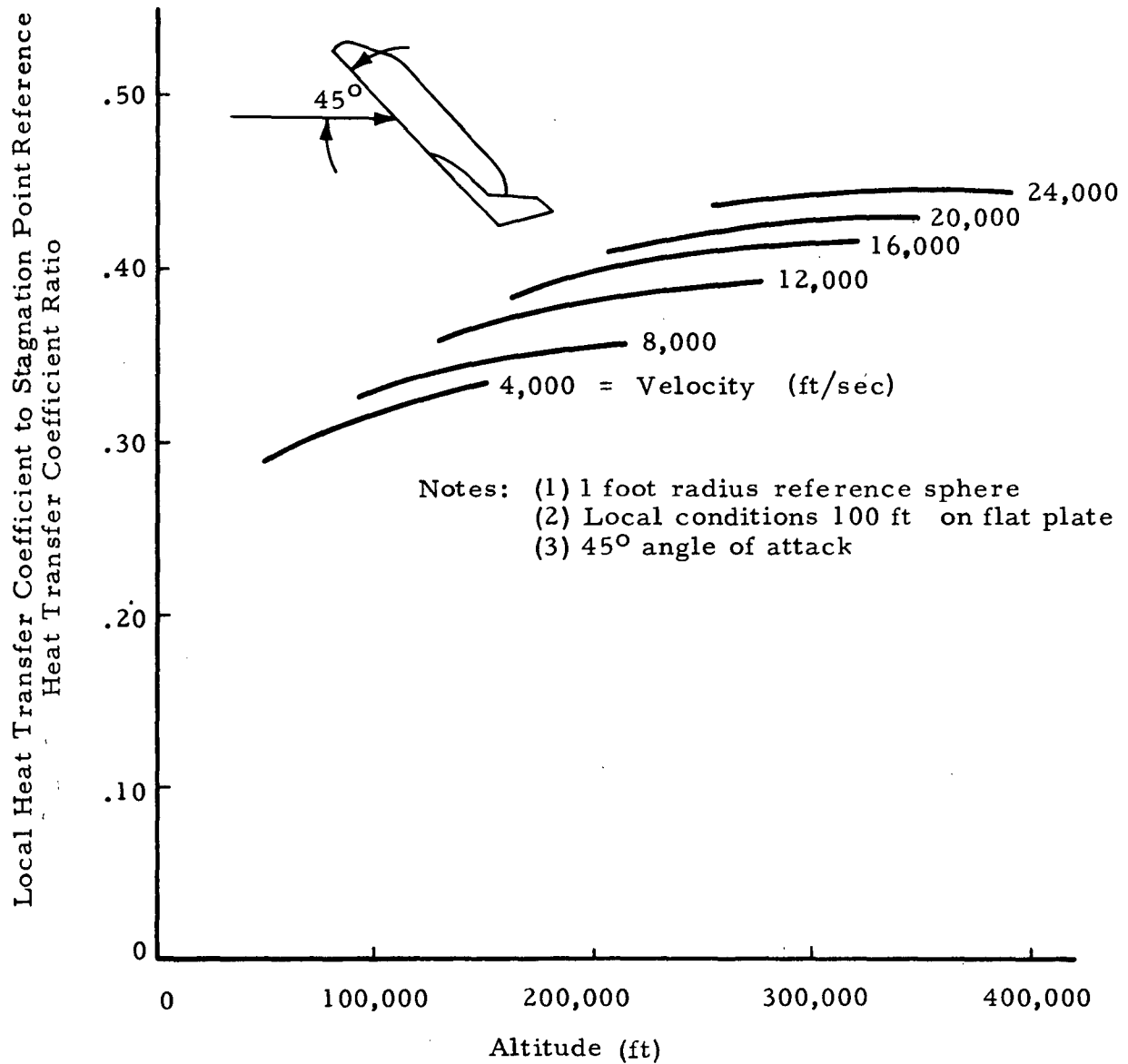


Fig. 38 - Variation of Typical Theoretical Laminar Heat Transfer Coefficient Ratio with Altitude and Velocity

However, the local hypersonic pressure distributions and consequently the streamline divergence parameters affecting the equivalent running lengths in the heating analysis do not vary from investigations of hypersonic flow theory. Therefore, the flight environment from data analysis extracts the equivalent lengths necessary to produce wind tunnel heating distributions directly from analysis of wind tunnel conditions. These pressure distribution driven functions are then used in conjunction with a real gas analysis of the local properties and streamline divergence heating for the trajectory point in the flight environment to give the actual flight heating rates which reflect the full effects of high enthalpy flow. This becomes especially important in situations wherein dissociation exists in the region of the reference stagnation point and due to recombination, does not exist at the local point on the vehicle under analysis.

Although (as shown in Ref. 14) these equivalent lengths may be calculated theoretically with good success; the simplicity in the methods lies in that the equivalent lengths may be directly extracted from the ground test heating distribution data and consequently applied to analysis at the flight conditions. This is done by determining the actual heat transfer coefficient, and then comparing it to a theoretical flat plate value. The difference may be attributed to the equivalent length.

The grouping of parameters affecting the local heating other than the equivalent length are chosen as those used in the customary Eckert Reference Enthalpy method (Ref. 18). These are calculated locally using the real gas normal, oblique, and parallel shock flowfield assumptions. Once the local conditions indicate transition to turbulent flow, a momentum thickness matching technique is used for providing equivalent running lengths in the high Reynolds number flow regimes.

The equivalent length is essentially a measurement of how much a boundary layer has grown as it encounters the various effects of streamwise

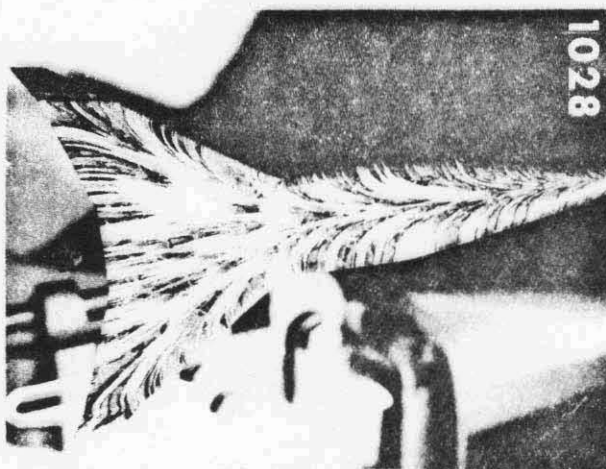
and spanwise pressure gradients. Although the composition of the real gas flow field may change substantially, the local pressures, and consequently pressure gradients which govern the local direction of the flow over the surface, remain similar in distribution throughout the hypersonic flow regime. This is shown by the oilflow photographs of Fig. 39. Therefore the equivalent length is most likely the variable subject to least change during extrapolation of ground test data to the freeflight regime.

Extrapolation of heat transfer coefficients directly to the flight environment is questionable (Fig. 38) due to the influence of real gas effects on the local viscosity, density, velocity, and Prandtl number variables used to establish the stagnation point to local point conditions in the hypersonic flight regime. This ratio varies due to real gas effects. However using the equivalent length, assumed invariant with freeflight flow, and a real gas flat plate analysis at the freeflight conditions, gives a real gas influenced heating rate for design of space shuttle-type vehicles. This relationship is:

$$\dot{q}_{\text{Free Flight}} = \frac{\left[\dot{q}_{\text{Flat Plate at Free Flight Conditions}} \sqrt{X_{\text{eq}}} \right]}{\left[\sqrt{X_{\text{eq}}} \right]_{\text{From Ground Test}}}$$

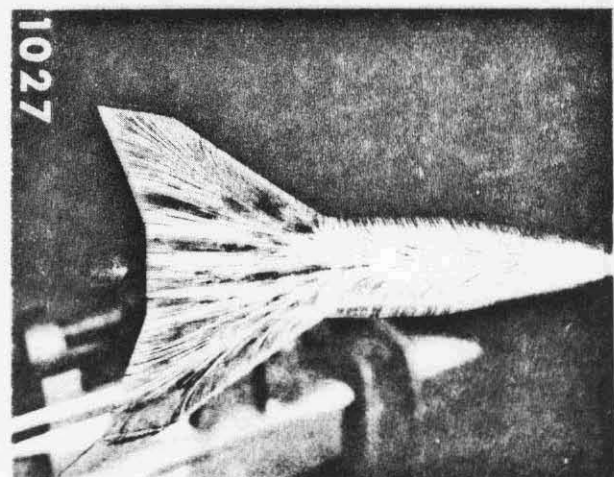
It should be remembered that the equivalent length is determined after careful scrutiny of ground test laminar distributions as analyzed by flat plate methods utilizing the ground test flowfield conditions. In this way the real gas effects of reentry are evaluated by the FED aerodynamic heating computer program.

Using the aeroheating method briefly described above, the flight environment for a shuttle design is prepared in the following sequence of logic. First, laminar flow equivalent lengths along the vehicle centerline are calculated from wind tunnel data and real gas local properties. With the equivalent lengths known, the trajectory information is then entered point by point

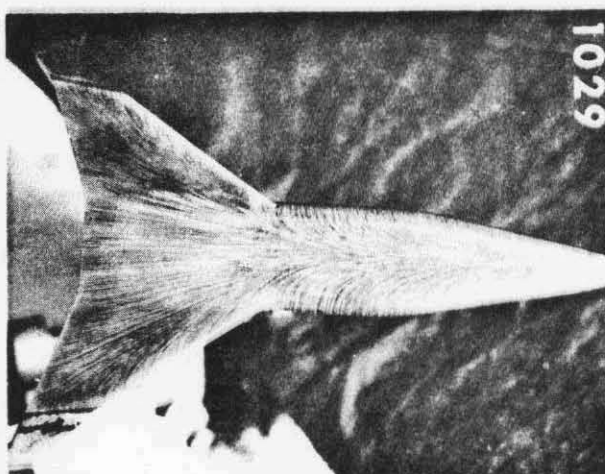


$$\frac{Re}{x} = 1.0 \times 10^6 \text{ 1/ft}$$

Reproduced from
best available copy.



$$\frac{Re}{x} = 2.7 \times 10^6 \text{ 1/ft}$$



$$\frac{Re}{x} = 6.2 \times 10^6 \text{ 1/ft}$$

Fig. 39 - Reynolds Number Effect on Oilflow Patterns ($\alpha = 65^\circ$)

from ascent, through reentry, to the low supersonic flight regime. At each trajectory point of interest, the local properties at each vehicle location on the centerline are calculated by a real gas shock analysis for the particular model atmosphere pre-selected for the study. The laminar local heating parameters are then calculated as well as the transition criteria. If transition is indicated the turbulent and transitional heating parameters are prepared. At present, heating distributions off the centerline are then obtained from the laminar wind tunnel distributions. Hot wall effects in the form of radiation equilibrium temperature or a hot structure heat balance are included in the final analysis. The output of the computer code used for these computations lists the various heating parameters as a function of time for each vehicle location under analysis.

3.4 THERMAL ENVIRONMENT OPTIMIZATION PROGRAM (TEOP)

One of the greatest stumbling blocks in the preliminary design stages of the Space Shuttle programs has been the extremely slow response time for performing a vehicle thermal protection system (TPS) sizing analysis. Using conventional thermal analyzer techniques, optimum TPS weight calculations would require large lag times. The vehicle is often obsolete before realistic weight estimates can be made. In some instances it has been necessary to compare weights of a given configuration flown over several trajectories and with different TPS designs. Again, conventional methodology makes this type of task tedious and time-consuming.

Confronted with several situations similar to the ones described above, Lockheed-Huntsville conceived and wrote a computer program (TEOP), that can in a single computer run, determine the thermal environment, optimize the TPS material or thickness, and determine total vehicle weight. This program is made up basically of three existing programs. The geometry package was lifted from the MDAC Gentry aerodynamics program (Ref. 19). This geometry package divides the body into many flat plates (Fig. 40) and determines areas, direction cosines, and location of each panel. The heating calculations

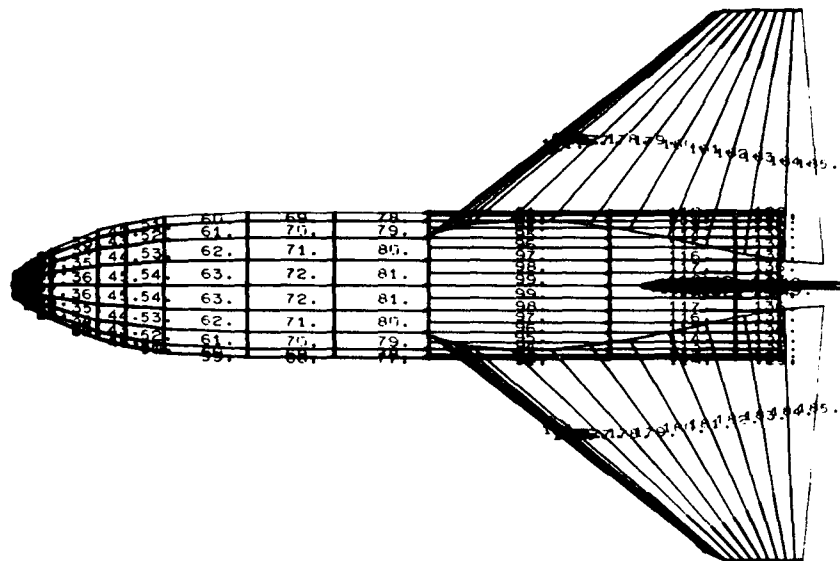


Fig. 40 - S-IC Booster Geometry Representation

are made by using either the FED analysis (Ref. 1) for vehicles where data are available, or some combination of Eckert's flat plate and swept cylinder calculations for the configurations where no test data are available. After the thermal environment is determined, the program then utilizes a version of a thermal analyzer, described in Ref. 20, to determine the backside temperature and from this temperature the program sizes the TPS thickness. The total TPS weight is calculated from the sum of the individual panels and, in the case of re-radiative panels, the insulation weight is added to the panel weights. A discussion of the results of a detailed analysis of the LOX-RP1 booster utilizing this program is presented in Section 4.1.

3.5 A SMALL THERMAL ANALYZER WITH SIMPLIFIED INPUT

Thermal analyzer computer programs (such as Boeing's BETA-I, BETA-II, Lockheed's MARK-5C, and Chrysler's CINDA Refs. 21 through 24) are sometimes difficult to use effectively. From the size and complexity of these programs (e.g., a compiled listing of CINDA requires 370 pages of print on the Univac 1108 computer), one would be led to believe that the heat conduction problem as solved by a finite difference scheme is very difficult. However, the thermal analyzer program is built around only one equation which computes transient temperatures.

From these observations, it appears that the problem has been "over-programmed." As a result, the engineer has lost flexibility, capability and efficiency in solving simple types of problems, and in many cases, has become dependent upon programmer personnel to produce results. To circumvent these problems, a small thermal analyzer package was written.

Recently, the Lockheed program has proven quite useful in solving problems associated with the Space Shuttle TPS. It can be run on the IBM 7094 computer for rapid results in the present system of machine priorities at NASA-MSFC.

Reference 20 contains a description of the heat transfer equations, and the numerical method which was selected for their solution. A discussion of the computer program input and output is made, with two sample problem solutions.

Recently, several Space Shuttle TPS studies were made using this computer code and it was found to be perfectly suited for this type of work. A thermal model was used to determine insulation thickness to maintain 200°F backface temperature. Figure 41 shows some representative results of this study. Figure 42 shows typical temperature histories of several locations in the structure. Because the nature of this study was parametric, the thermal analyzer program was modified somewhat by do-loops to allow different heating rates to be applied for several body locations and angles of attack. This further exemplifies the versatility of a simple engineering aid, which lends itself to rapid changes when new problem variables arise.

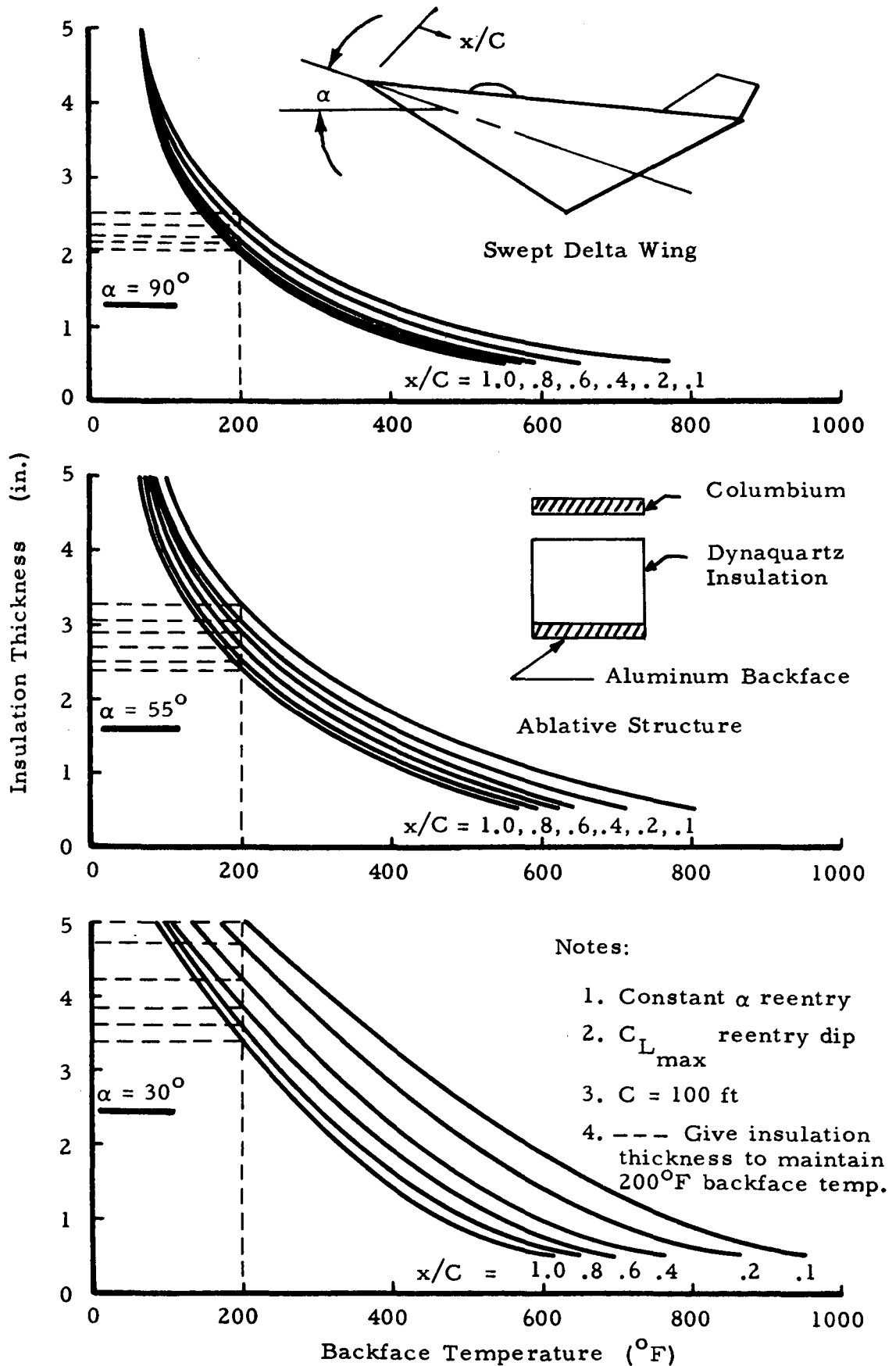


Fig. 41 - Results of Transient Thermal Analysis for Determining Insulation Thickness for 200°F Backface Temperatures

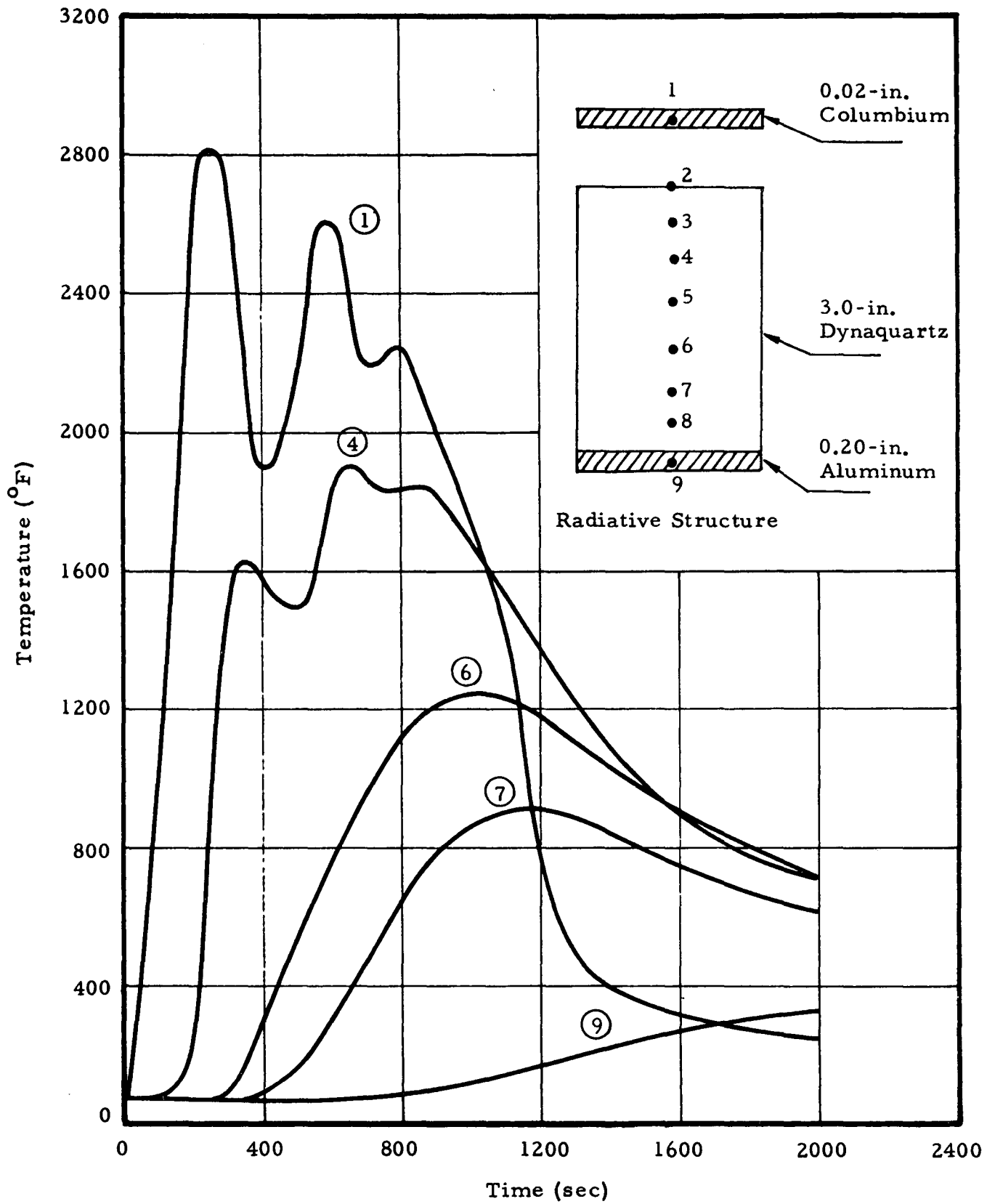


Fig. 42 - Typical Transient Temperatures for Radiative Structure

Section 4

APPLICATION OF ANALYTIC TOOLS TO PREDICTING
THERMAL ENVIRONMENTS

The computer programs and techniques described in Section 3 were prompted by specific tasks, and requirements that have been assigned to Lockheed-Huntsville's Thermal Environment Section. The programs developed would be just computer cards if no use were made of them. The TEOP program, which actually includes the FED and the small thermal analyzer of Ref. 20, has been used in a multitude of tasks since it was originated. It is continually being changed to perform even more sophisticated analyses. A discussion of some of the tasks performed using this program is presented below as well as a short discussion of a radiation blockage problem using the small thermal analyzer.

4.1 LOX-RP1 TRAJECTORY TRADEOFF ANALYSIS

After a computer program has been written, results must be verified. A set of results which are discussed in this section are from a study performed for a Space Shuttle LOX-RP1 booster with a heat sink aluminum and titanium Thermal Protection System (TPS). This vehicle has three different areas of TPS: titanium nose and wing leading edge sections, aluminum panels on the LOX tank and aluminum panels covering the remainder of the vehicle.

After the environment was determined for the entire vehicle throughout the trajectory, a detailed thermal analysis was performed for 18 selected locations on the vehicle. The thermal analysis was performed using a thermal analyzer, which sets up a one-dimensional conduction model for three different panel thicknesses for each of the 18 selected locations on the vehicle. The three panel thicknesses which were used in the thermal models at each vehicle location were calculated internally.

Since three different types of thermal areas make up the LOX-RP1 booster, 18 vehicle locations were chosen such that each area had a representative number of points from which the rest of the vehicle can be thermally sized. For the particular LOX-RP1 booster the 18 vehicle locations for the thermal analyzer were distributed on the vehicle as follows: three locations on the titanium nose, four locations on the LOX tank aluminum panels and eleven locations on the remaining aluminum portion of the vehicle.

The maximum temperatures encountered for each of the three thicknesses at each location are retained in the computer. The resulting thickness versus maximum panel temperature for the 11 aluminum panels of the LOX-RP1 booster are shown in Fig. 41. The same plots of the titanium and aluminum LOX tank panels are similar. From the plots of thickness versus temperature it is possible to determine the panel thickness required to result in a desired maximum panel temperature. For the aluminum panels, this temperature is 760°R . The intersection of a constant 760°R temperature line with the curves of Fig. 43. gives the panel thickness required at the vehicle location. These panel thicknesses are then plotted versus cold wall integrated heating rate for the 11 aluminum panels analyzed with the thermal analyzer. The curves of panel thickness versus coldwall integrated heating rates for the aluminum panels; aluminum LOX tank panels and titanium panels are shown in Figs. 44, 45 and 46 respectively. Depending on the type of panel, the rest of the vehicle is thermally sized using these data and the local cold wall integrated heating rate. This sizing is performed within the program.

A study of the effect of staging velocity on heat sink TPS weight was coordinated along with a trade study which was intended to determine the velocity above which the radiative panel type of TPS would result in less weight than the heat sink. The results of this analysis for the LOX-RP1 booster is shown in Fig. 47.

A study was also conducted to determine the sensitivity of the LOX-RP1 weight to the maximum allowable temperature used for aluminum and titanium.

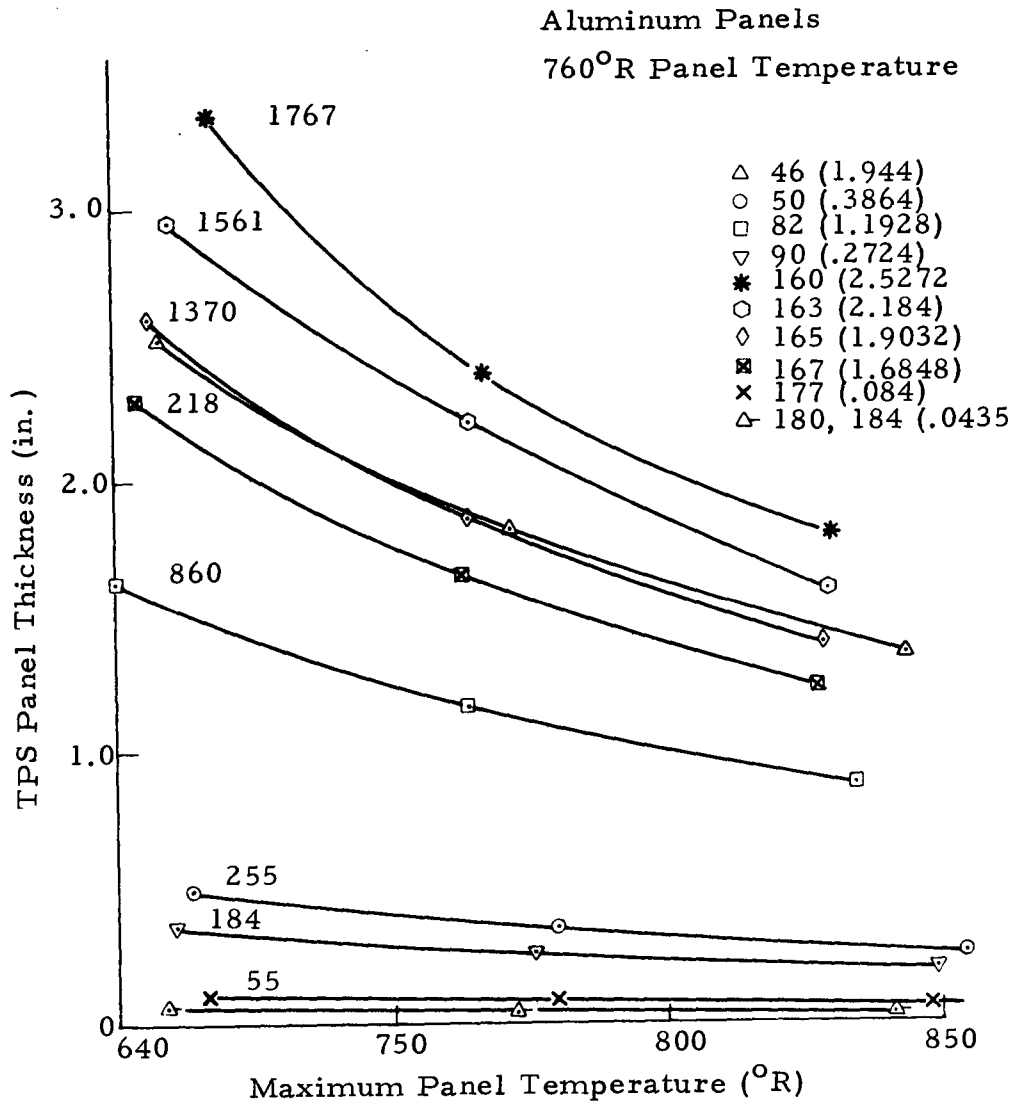


Fig. 43 - Panel Thickness vs Maximum Temperature for LOX-RP1 Booster Aluminum TPS Panels

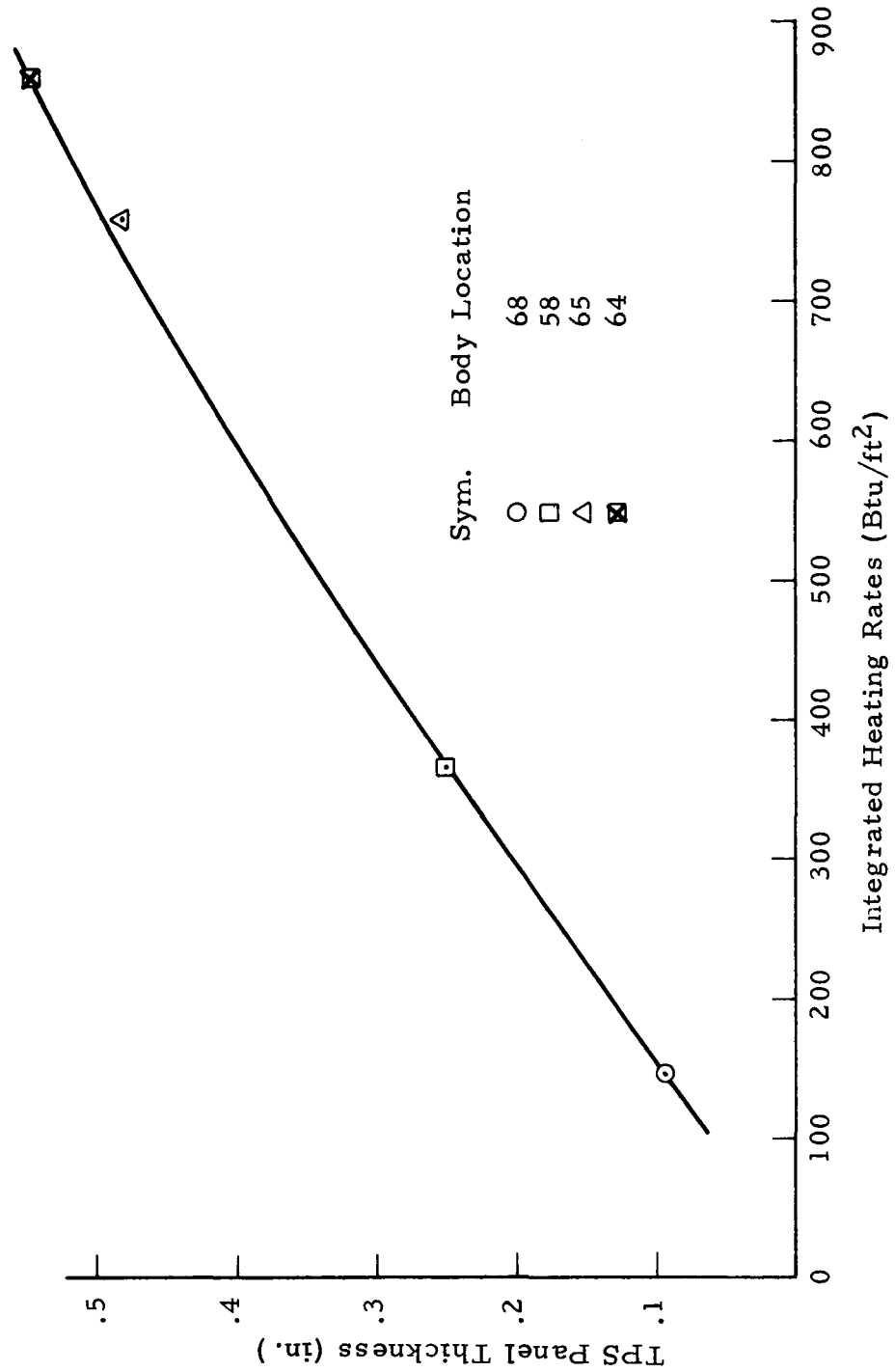


Fig. 44 - Panel Thickness vs Integrated Cold Wall Heating Rate for LOX-RP1 Booster LOX Tank Aluminum TPS Panels

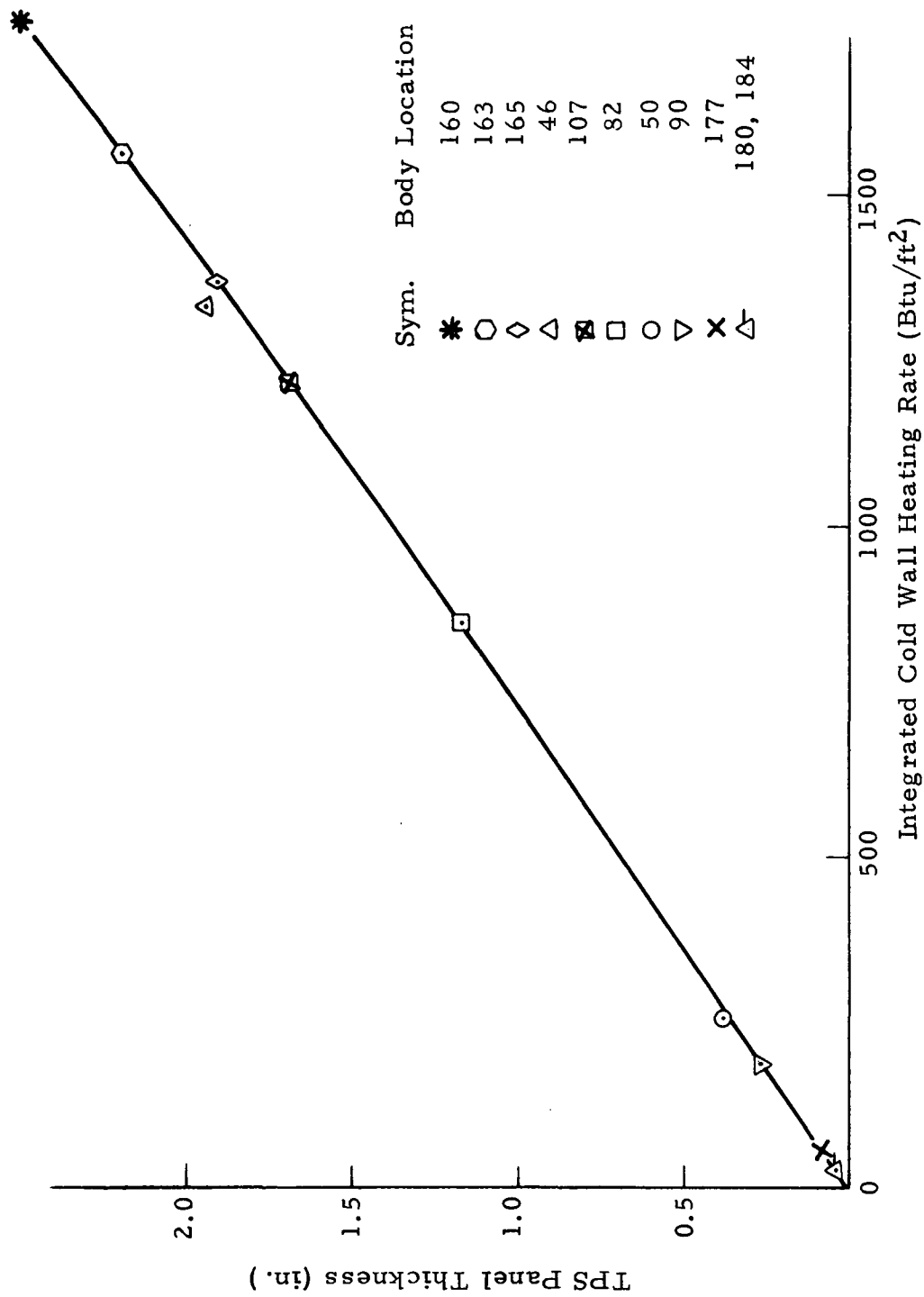


Fig. 45 - Panel Thickness vs Integrated Cold Wall Heating Rate for LOX-RP1 Booster Aluminum TPS Panels

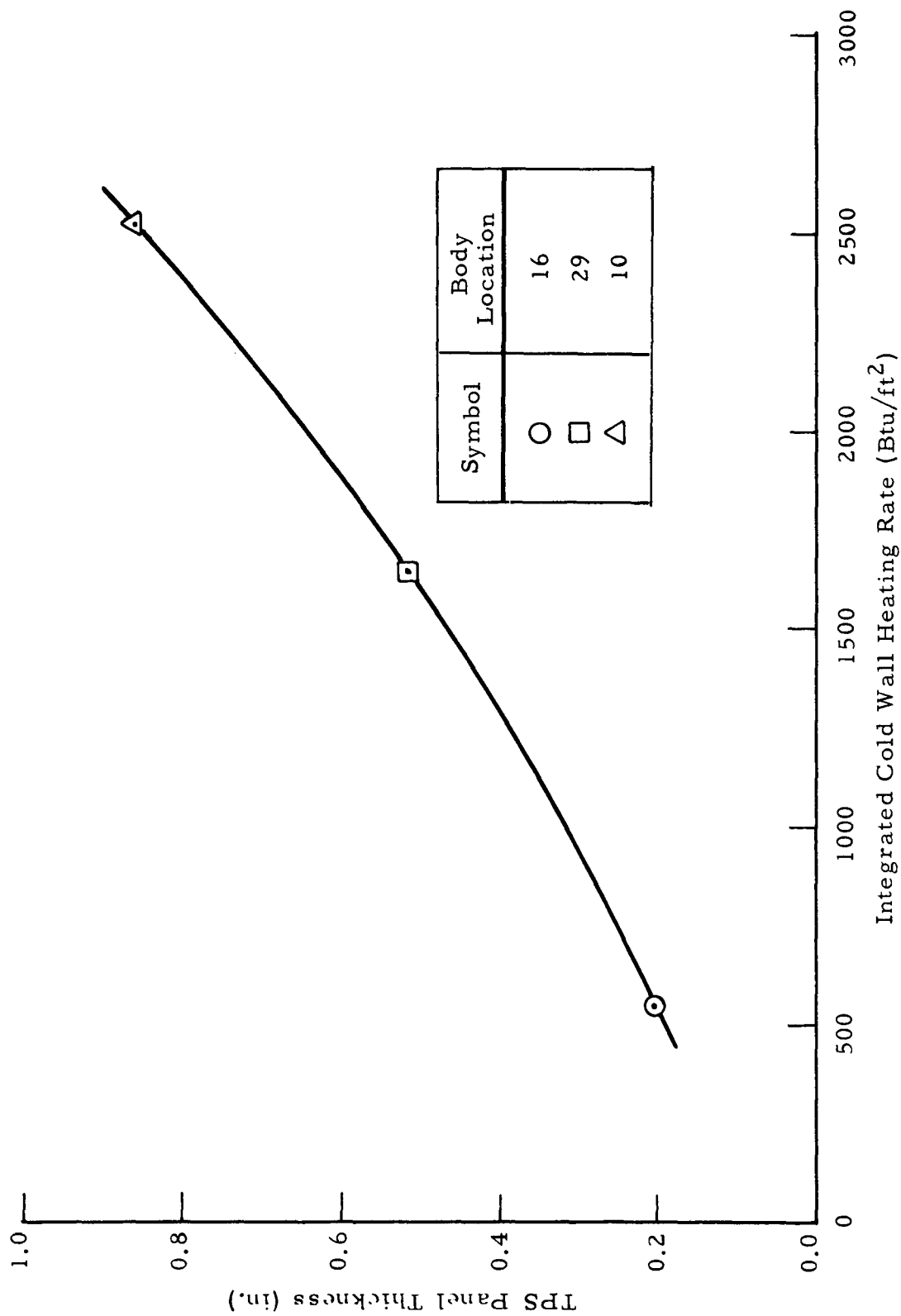


Fig. 46 - Panel Thickness vs Integrated Cold Wall Heating Rate for LOX-RP1 Booster Titanium TPS Panels

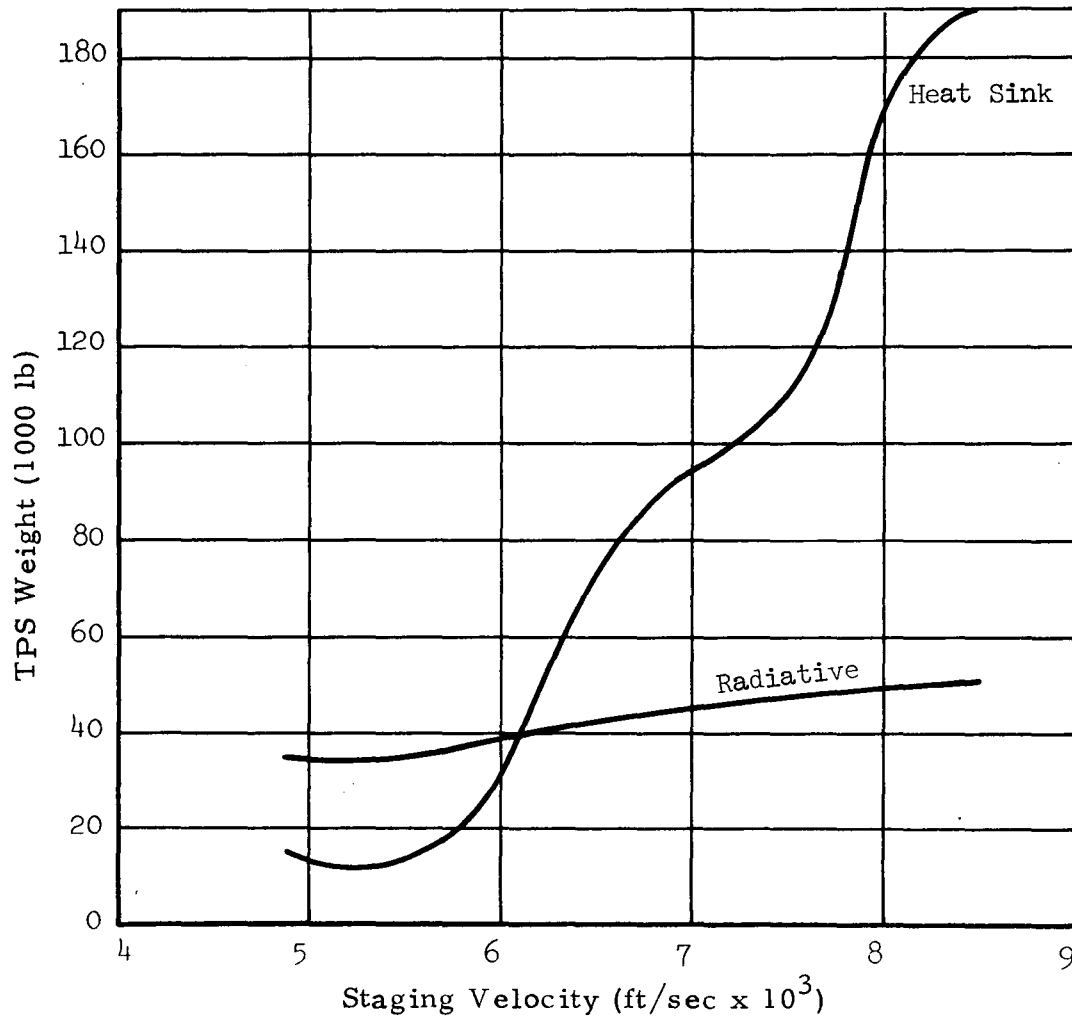


Fig. 47 - Effect of Staging Velocity on Thermal Protection System Weight

Maximum allowable material temperatures used by different contractors vary considerably. TPS requirements for titanium and aluminum as a function of T_{\max} are shown in Figs. 48 and 49.

Several other studies are being conducted which will be documented in the final report as well as a documentation of the TEOP program.

4.2 EFFECTS OF SURFACE RADIATION INTERCHANGE

A re-radiation cooling concept is currently being considered in Space Shuttle concepts to reject large portions of the aerodynamically produced heat flux, which is incident to the vehicle surfaces. Thin-skin radiation equilibrium temperatures have been successfully used in the design of these systems for relatively simple configurations in which the view factors governing the calculations are assumed to be equal to one. This assumption is justified when a point on the surface has an unobstructed view of free space; however, when more complex Space Shuttle configurations are considered, skin panels that are shaded from the surrounding environment do not reject heat as efficiently. Consequently, the vehicle structure at these locations experiences a severe temperature increase.

Two Space Shuttle booster configurations were studied to determine the effect of the shading phenomenon. The McDonnell Douglas-Martin twin-boom booster was one configuration chosen because the side-by-side arrangement of the booster bodies causes considerable shading, aptly demonstrating the increase in temperatures on the interior surfaces between the fuselage booms. The McDonnell Douglas-Martin low crossrange orbiter stacked upon the delta wing booster was the second configuration analyzed because there is a large amount of radiation blockage in the gap between the forward sections of the two mated vehicles. Skin temperature in this region is further increased by high aerodynamic heating attributable to shock impingement occurring in this gap. The booster stage was analyzed to determine the complete aerothermodynamic environment that is experienced from launch to staging and through reentry.

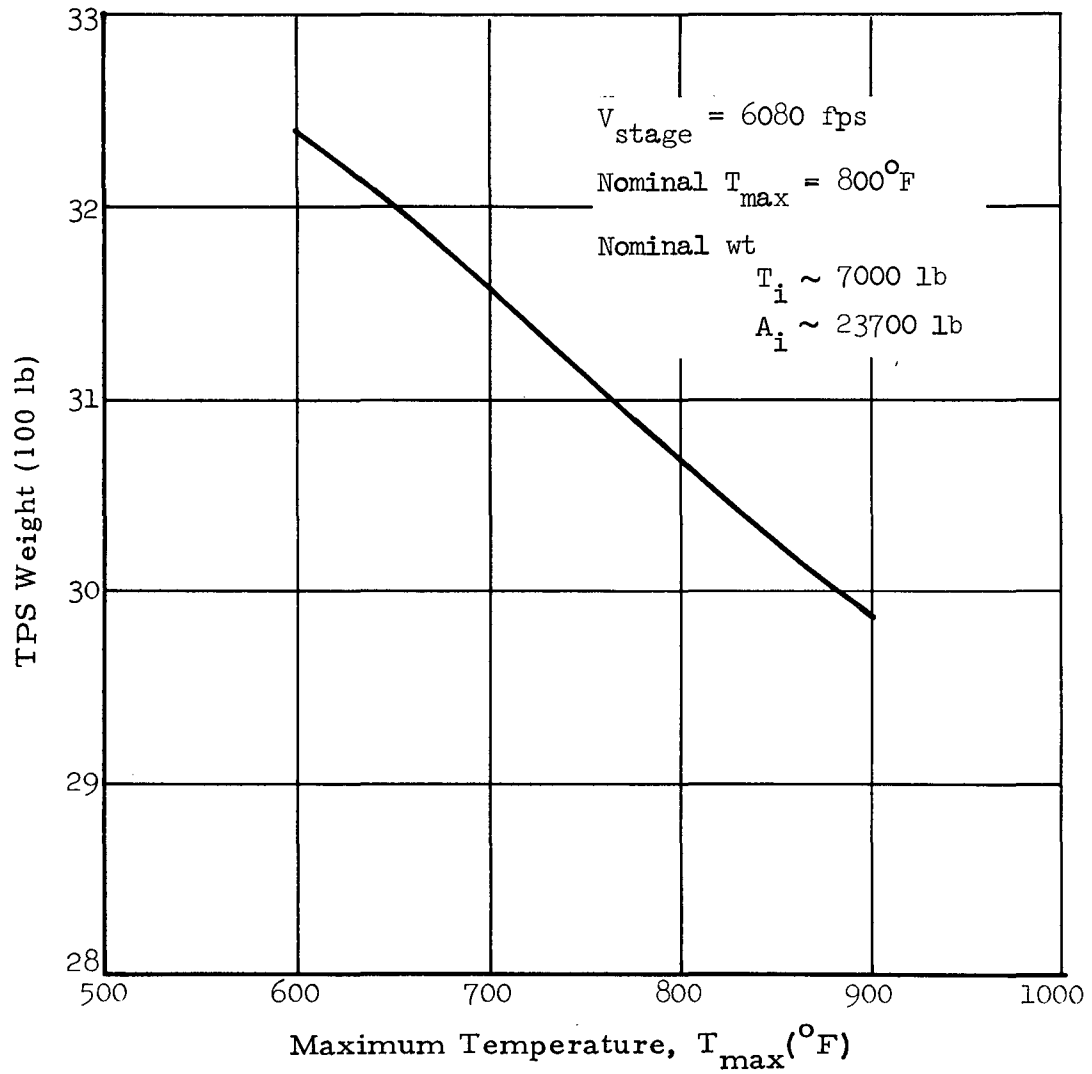


Fig. 48 - LOX-RP Booster TPS Weight Sensitivity to Maximum Titanium Temperature

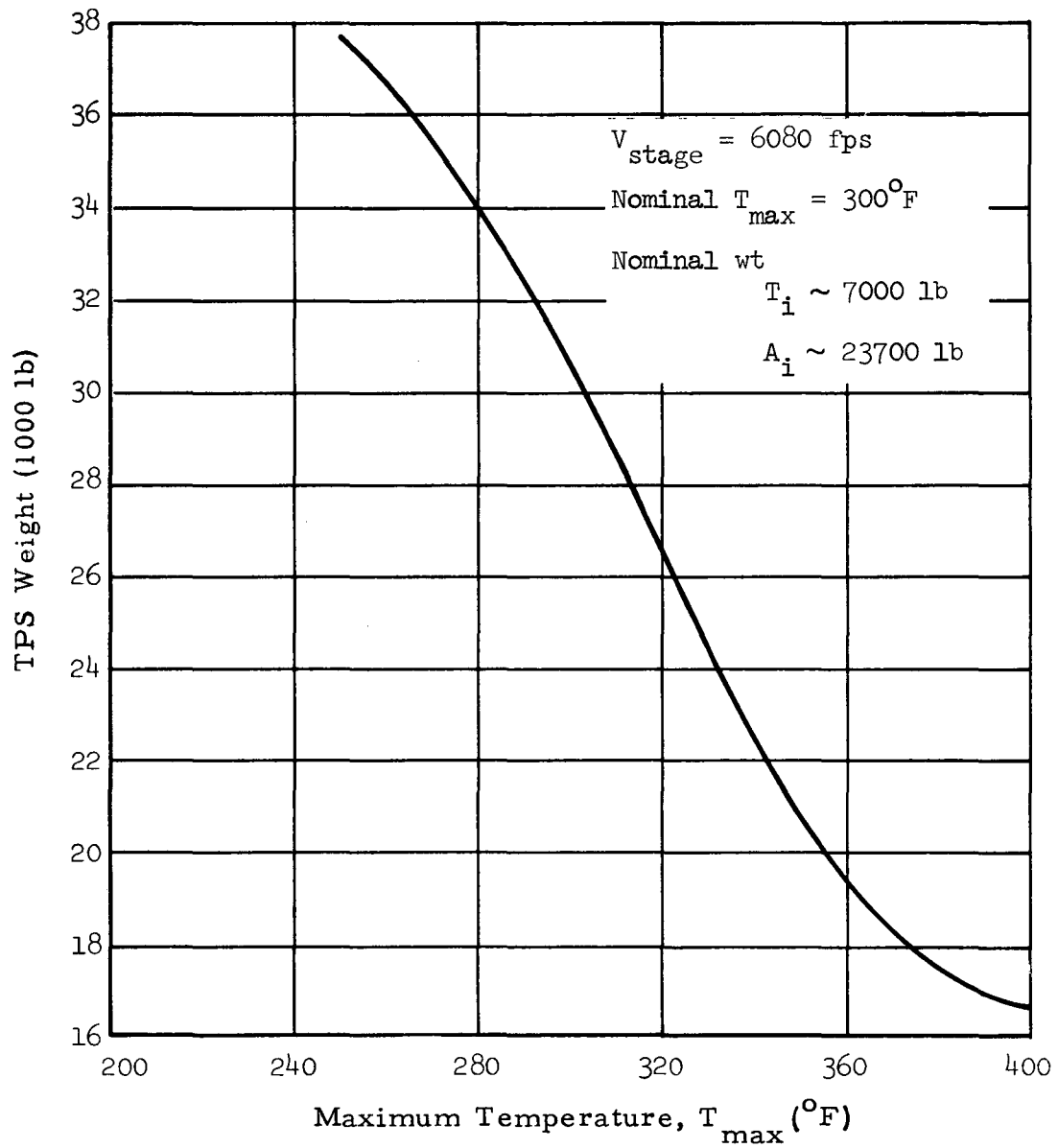


Fig. 49 - LOX-RP1 Booster TPS Weight Sensitivity to Maximum Aluminum Temperature

In each of these studies, the skin panels were considered as segmented areas (nodes), and radiation view factors were computed to other surfaces that a segment could "see." Radiation interchange factors were then calculated between these surfaces and to deep space. Resulting data were used to form the analytic thermal network to which aerodynamic heating rates and material properties were added. The temperature response of the nodal areas for typical trajectories was calculated. These temperatures were computed by assuming no heat transfer to the interior of the vehicle and that there was no lateral conduction in the skin. Resulting temperatures, presented herein, are compared to the conventional radiation equilibrium temperatures obtained by assuming a unity view factor to deep space.

For severely shaded areas of the McDonnell Douglas-Martin twin-boom booster, temperatures that are 290°F higher than those predicted by assuming a unity view factor were found to exist during descent. In some areas the design limit of Rene 41 (1600°F) is exceeded by 200°F when radiant energy exchange is included, but the design limit is not exceeded when unity deep space view factors are assumed. The forebody gap area of the stacked configuration is shaded to such an extent that heat rejection by direct radiation to deep space is almost entirely blocked, allowing these panels to exceed the unity view factor temperature by 750°F during the ascent of this configuration. The effect of removing the radiation blockage on the stacked configuration after staging is examined by continuing the calculations during reentry of the booster.

The results of this study are presented in detail in Ref. 25, and only a selected sample of data is presented herein. The geometry and radiation interchange factors for the twin boom booster is shown in Figs. 50 and 51, and Fig. 52 shows the trajectory and thermal environment for this booster. The temperature-time history for the first four nodes is shown in Fig. 53. Note from this figure that there is significant variation in maximum temperatures, if radiation blockage is accounted for. A summary of the differences in maximum temperatures obtained both assuming radiation blockage and not considering this effort is shown in Fig. 54.

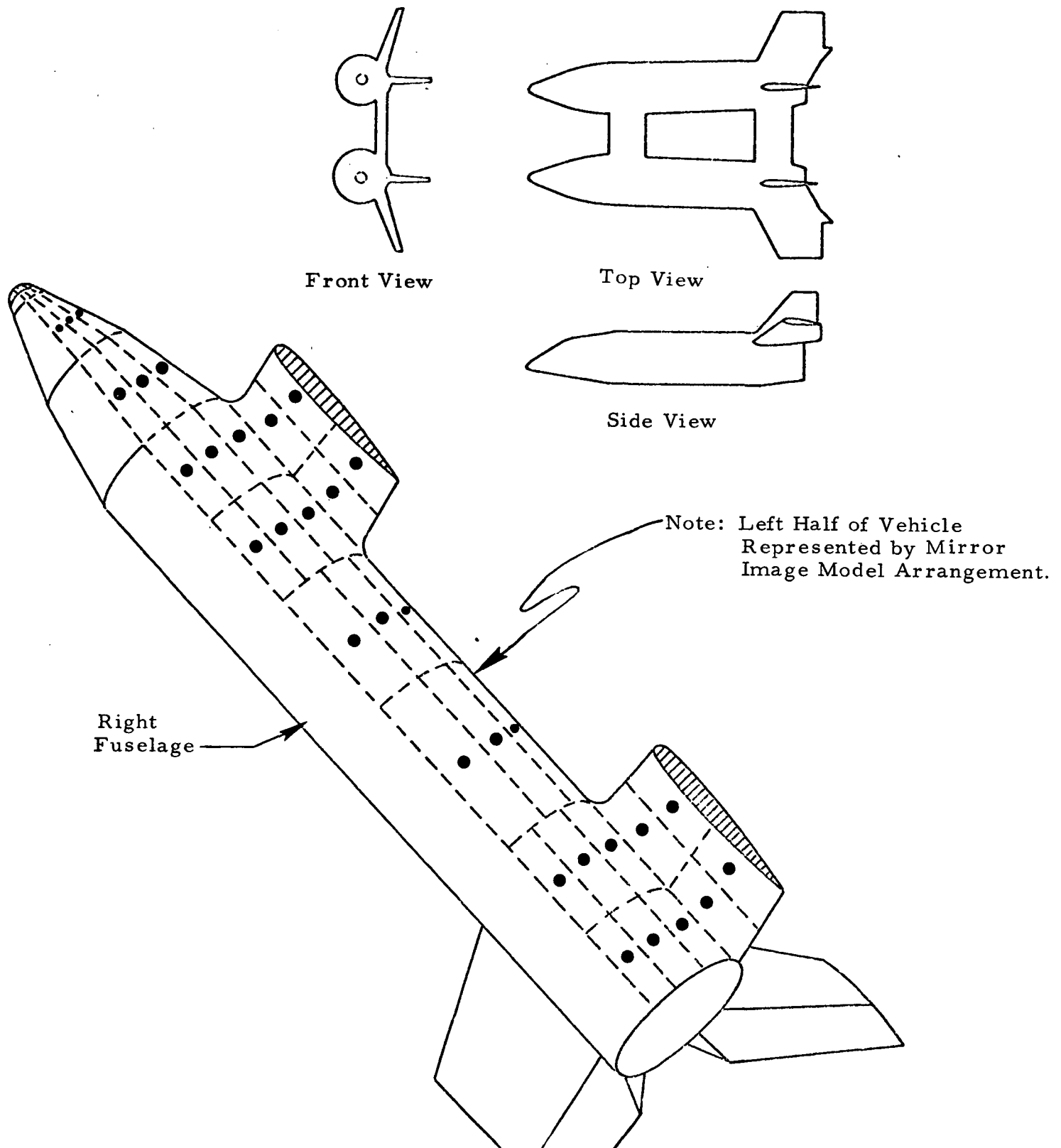


Fig. 50 - Geometry and Nodal Arrangement for Twin-Boom Booster Configuration

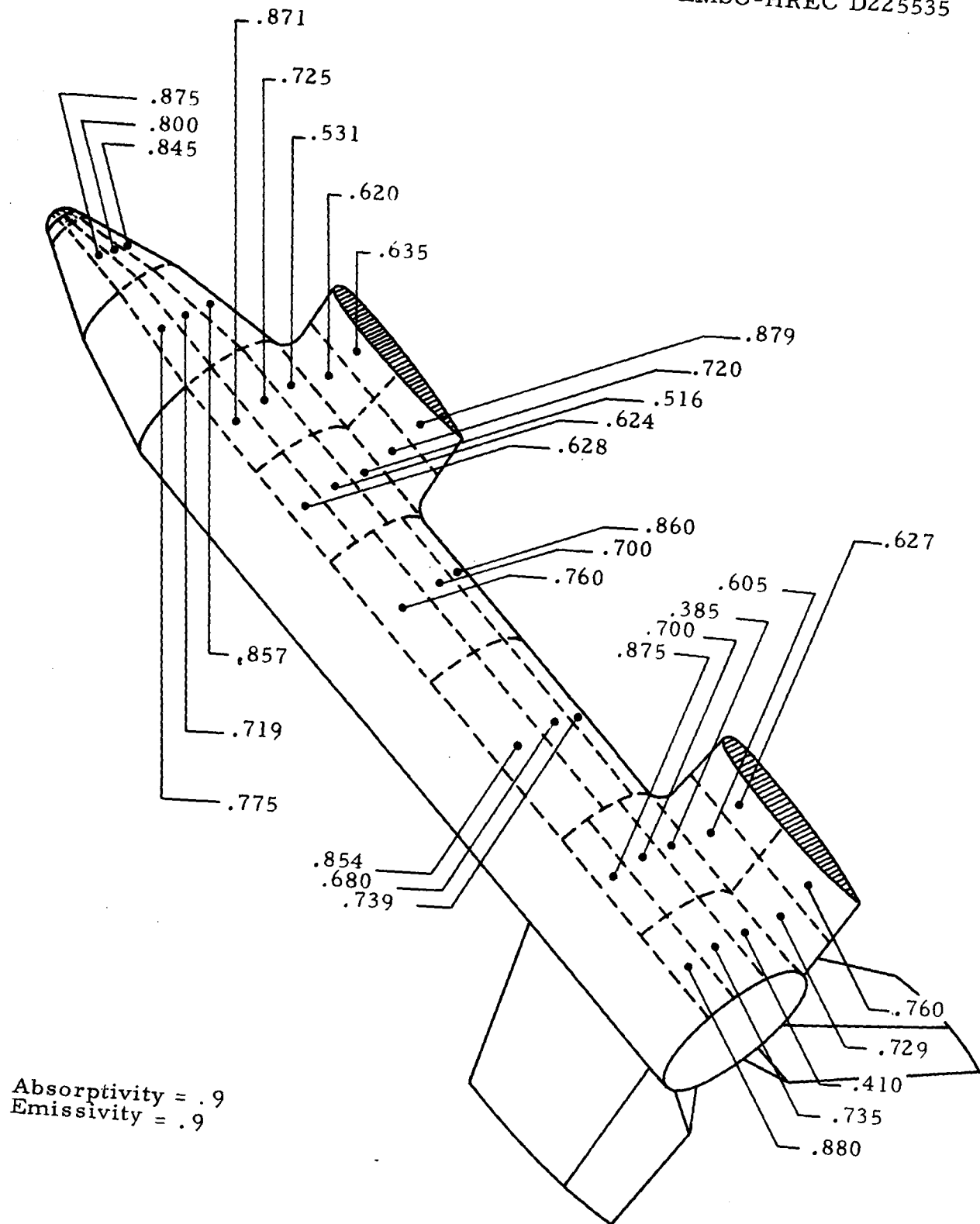


Fig. 51 - Radiation Interchange Factors to Surrounding Environment

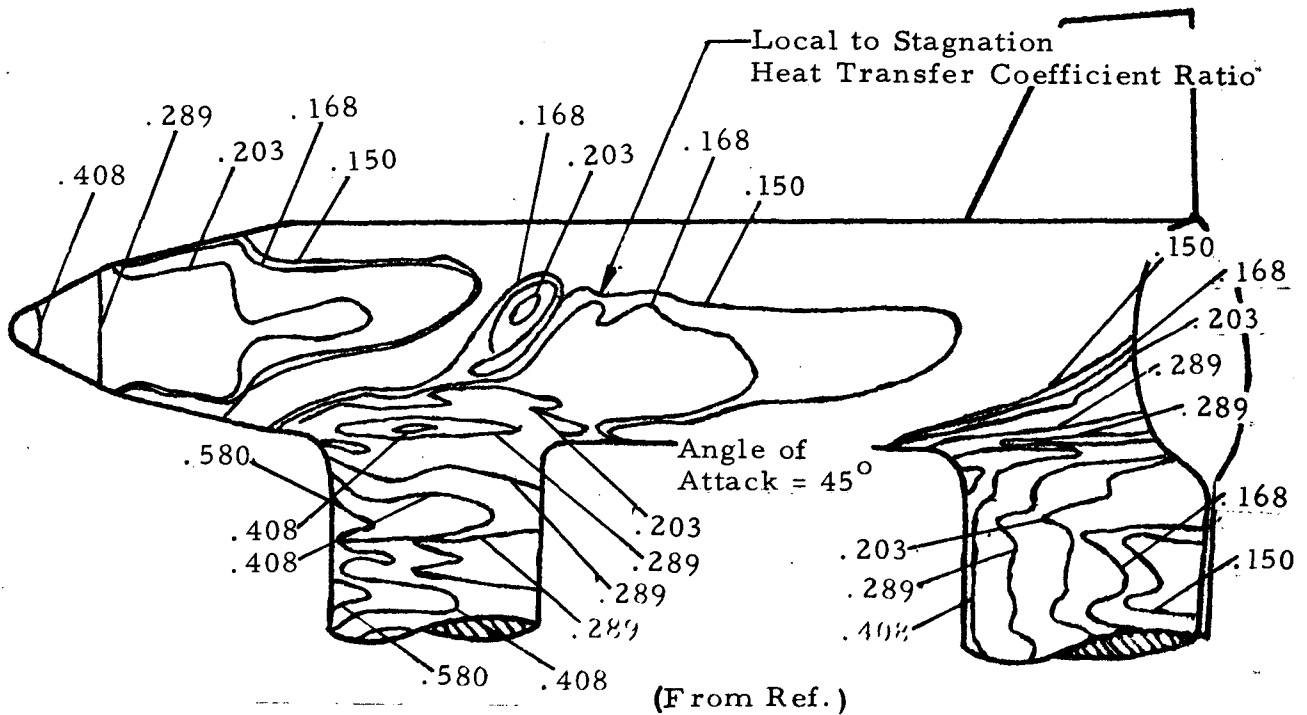
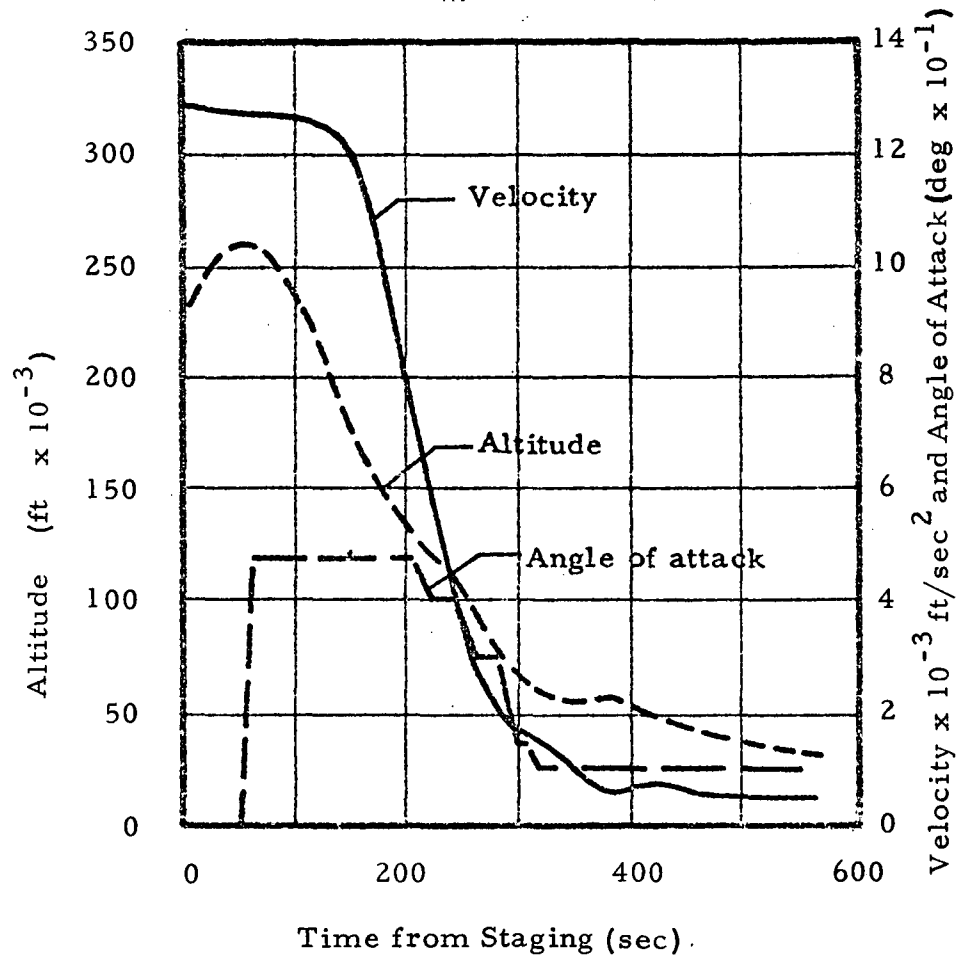


Fig. 52 - Reentry Trajectory and Typical Aerodynamic Heating Distribution for Twin Boom Booster

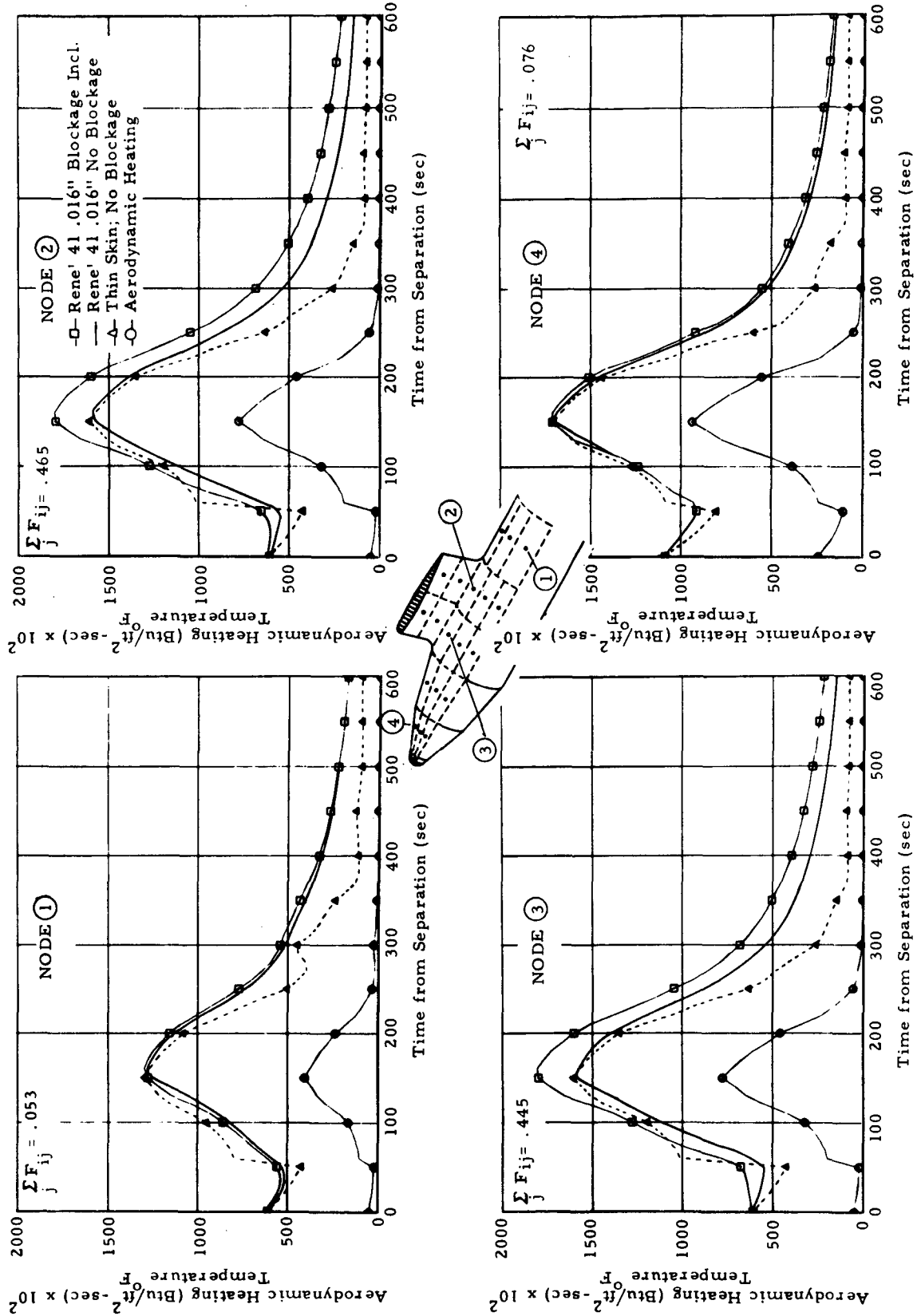


Fig. 53 - Effect of Radiation Blockage on Selected Skin Panels of McDonnell Douglas Twin Boom Booster

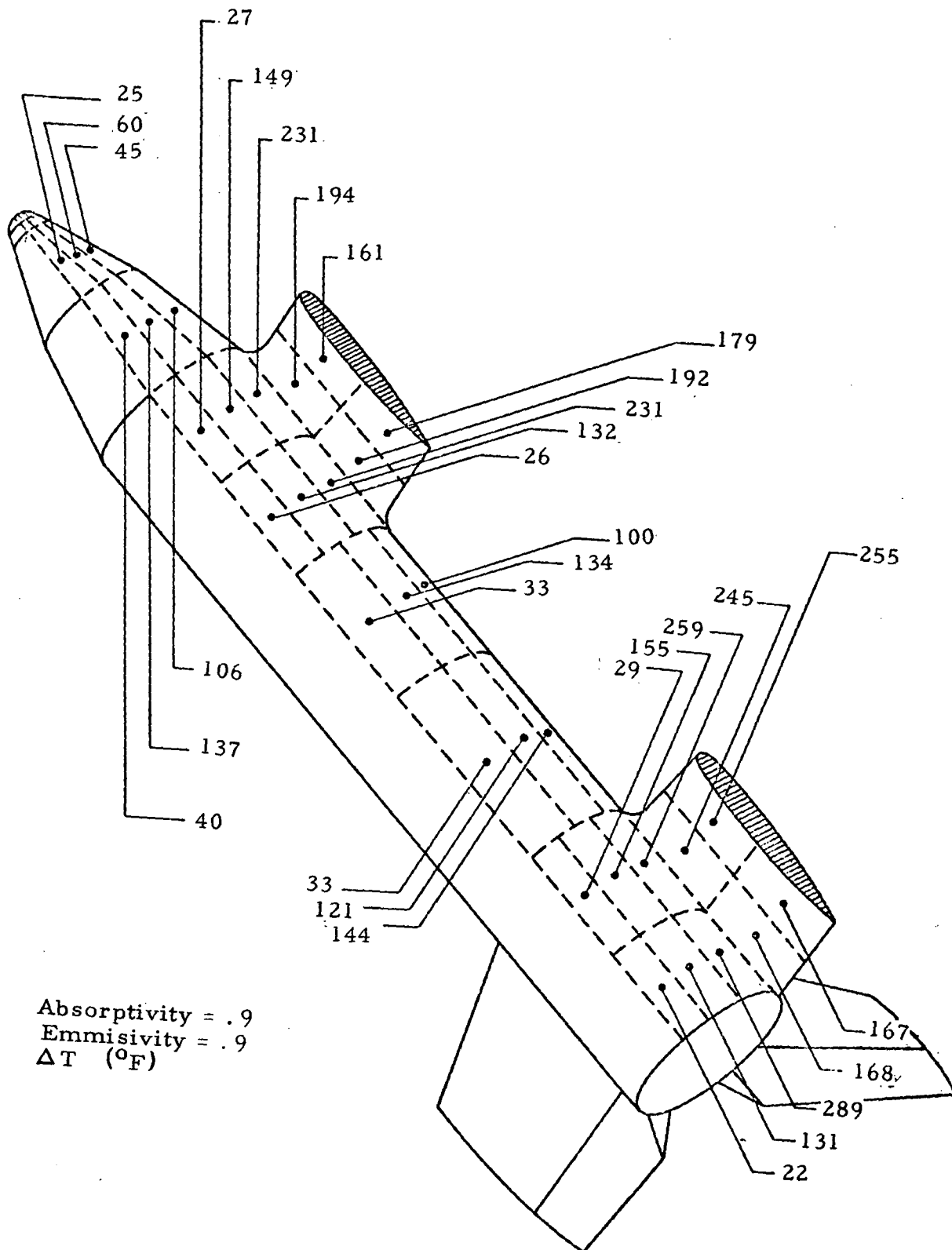


Fig. 54 - Maximum Temperature Increase due to Radiant Energy Blockage and Interchange

REFERENCES

1. Blackledge, M. L., and P. O. McCormick, "Flight Environment from Data - Analytic Definition and Computer Code Description," LMSC-HREC D225048, Lockheed Missiles & Space Company, Huntsville, Ala., December 1971.
2. Connor, L. E., V. W. Sparks and A. G. Bhadsavle, "Heat Transfer Tests of the NASA-MSFC Space Shuttle Booster at Langley Research Center Hypersonic Continuous Flow Facility," LMSC-HREC D162722, Lockheed Missiles & Space Company, Huntsville, Ala., December 1970.
3. Connor, L. E., "Power-Off Base Heating and High Reynolds Number Heat Transfer Tests of the NASA-MSFC Space Shuttle Booster," LMSC-HREC D225153, Lockheed Missiles & Space Company, Huntsville, Ala., June 1971.
4. Blackledge, M. L., J. V. McAnally and P. O. McCormick, "Analytical/Experimental Evaluation of Entropy Swallowing and Heat Transfer Distributions for Delta Wing Space Shuttle Booster," LMSC-HREC D162874, Lockheed Missiles & Space Company, Huntsville, Ala., February 1971.
5. Jacobs, H. R., "Engineering Approximation of the Effects of Blunting on Cones in Laminar and Turbulent Flow," SAMSO TR 68-258, October 1967.
6. Thomas, A. C. et al., "Advanced Reentry Systems Heat Transfer Manual Manual for Reentry Flight," AFFDL TR 65-195, The Boeing Company, Huntsville, Ala., October 1966.
7. Barnett, D. O., "Presentation at Thermal Environment Branch Review of January 20, 1971," NASA-MSFC (Northrop Mission Support) Huntsville, Ala., January 1970.
8. Fannelop, T. K., "A Method of Solving the Three-Dimensional Laminar Boundary-Layer Equations with Application to a Lifting Reentry Body," AIAA J., Vol. 6, No. 6, June 1968, pp. 1075-1084.
9. Cooke, J. C., "An Axially Symmetry Analogue for General Three-Dimensional Boundary-Layers," ARC R4M No. 3200 (London), June 1959.
10. Beckwith, I. E., "Similarity Solutions for Small Cross Flows in Laminar Compressible Boundary Layers," NASA TR R-107, 1961.
11. Vaglio-Laurin, R., "Laminar Heat Transfer on Three-Dimensional Blunt Nosed Bodies in Hypersonic Flow," ARS J., Vol. 29, No. 2, February 1959, pp. 123-129.
12. Lees, Lester, "Laminar Heat Transfer over Blunt-Nosed Bodies at Hypersonic Speeds," Jet Propulsion, Vol. 26, No. 4, April 1956, pp. 259-269 and p. 274.

13. Libby, P.A., "The Laminar Hypersonic Heat Transfer on a Blunt Body According to the Integral Method," Proc. of the 1958 Heat Transfer and Fluid Mechanics Meeting, Berkeley, Calif., June 1958.
14. Pond, J.E., "Space Shuttle Windward Surface Aeroheating by Analytic Streamline Divergence Technique," LMSC-HREC D225206, Lockheed Missiles & Space Company, Huntsville, Ala., July 1971.
15. Hastings, S.M., L. Pasiuck, and A.J. Chones, "The Aerodynamic Heating of Blunt, Axisymmetric Reentry Type Bodies with Laminar Boundary Layers at Zero and Large Angles of Yaw in Supersonic and Hypersonic Air Streams," Presented at the 1961 International Heat Transfer Conference, Boulder, Colo., 28 August 1961.
16. Pasiuck, L., "Comparisons of Experimental and Theoretical Heat Transfer to a Yawed Sphere-Cone Model at Supersonic Speeds," NOL TR 63-208, United States Naval Ordnance Laboratory, White Oak, Md., December 1963.
17. Bushnell, Dennis M., Robert A. Jones, and Jarrett K. Huffman, "Heat Transfer and Pressure Distributions on Spherically Blunted 25° Half-Angle Cone at Mach 8 and Angles of Attack up to 90°," NASA TN D-4792, October 1968.
18. Eckert, E.R.G., "Survey of Boundary Layer Heat Transfer of High Velocities and High Temperatures," WADC Tech. Report 59-624, Wright-Patterson AFB, Ohio, April 1960.
19. Gentry, A.E., "Hypersonic Arbitrary-Body Aerodynamic Computer Program, Mark III Version," Vols. 1 and 2, DAC61552, Douglas Aircraft Co., Inc., Santa Monica, Calif., April 1968.
20. Pond, J.E., "A Small Thermal Analyzer Package with Simplified Input," LMSC-HREC D162533, Lockheed Missiles & Space Company, Huntsville, Ala., October 1970.
21. Almond, James, "Boeing Engineering Thermal Analyzer I," AS-00315, The Boeing Co., Seattle, Wash., 21 August 1970.
22. Almond, James, "Boeing Engineering Thermal Analyzer II,, AS-1917, The Boeing Co., Seattle, Wash., 23 May 1966.
23. Bible, A.E., et al., "Thermal Analyzer Control System for IBM 709-7090-7094 Computer Engineering Utilization Manual," 3-56-65-8, Lockheed Missiles & Space Company, Sunnyvale, Calif., 1 September 1970.
24. Gaski, J.D., "Chrysler Improved Numerical Differencing Analyzer," TN AP-66-15, Chrysler Corp., New Orleans, La., 30 April 1966.
25. Pond, J.E., and M.L. Blackledge, "Effects of Surface Radiation Interchange for Space Shuttle Vehicles," LMSC-HREC D162494, Lockheed Missiles & Space Company, Huntsville, Ala., January 1971.